Targeting Triple Negative Breast Cancer Using Membrane-Derived Nanocarriers for Potential Therapeutic Applications

A Thesis

Submitted in Partial Fulfillment of the Requirements for the award of the degree of

DOCTOR OF PHILOSOPHY

by

Muktashree Saha

(Roll No. - 176106009)

Department of Biosciences and Bioengineering

Indian Institute of Technology Guwahati

Guwahati, 781039, Assam, India

June 2023

Dedicated to My Parents

Declaration

I, hereby, declare that the research embodied in this thesis entitled "**Targeting Triple Negative Breast Cancer Using Membrane-Derived Nanocarriers for Potential Therapeutic Applications"** is the result of investigations carried out by me under the supervision of Prof. Siddhartha Sankar Ghosh, Department of Biotechnology, Indian Institute of Technology Guwahati, India for the award of Degree of Doctor of Philosophy. This work has not been submitted elsewhere for any degree, diploma, etc. of any Institute or University to the best of my knowledge and belief.

Muktashree Saha

Date: 20-06-2023
Place: Guwahati, Assam

Muktashree Saha
Roll No. 176106009

Indian Institute of Technology Guwahati

Department of Biosciences and Bioengineering

Certificate

This is to certify that the thesis entitled "**Targeting Triple Negative Breast Cancer Using Membrane-Derived Nanocarriers for Potential Therapeutic Applications"** being submitted to the **Indian Institute of Technology Guwahati** by **Muktashree Saha** (Roll No. **176106009)** for the award of the degree of **Doctor of Philosophy** in Department of Biosciences and Bioengineering, is a bonafide record of research work carried out by her. The contents of this thesis have not been submitted to any other University or Institute for the award of any degree or diploma.

Date: 20-06-2023
Place: Guwahati

Prof. Siddhartha Sankar Ghosh
(Thesis Supervisor)

Acknowledgment

'Great things are not done by one person. They're done by a team of people.'
–Steve Jobs

I want to use this opportunity to express my heartfelt gratitude to everyone who have played a pivotal role in helping me reach this destination and supported me throughout my journey. At the very beginning I would like to express my deep sense of gratitude to my PhD supervisor, Professor Siddhartha Sankar Ghosh, for giving me a golden opportunity to work in his lab and providing me with all the facilities to carry out my research in a smooth manner. His understanding, encouragement and constant guidance have helped me stay positive and motivated throughout my PhD journey.

I also want to thank my doctoral committee members, Prof. Ranjan Tamuli, Prof. Gurvinder Kaur Saini and Prof. S. Senthilkumar, for evaluating my progress, time and again, and for giving constructive ideas throughout this tenure, which have helped me improve and understand my research work better. I am highly indebted to the Department of Biosciences and Bioengineering, Centre for Nanotechnology, Central Instrumentation Facility, IIT Guwahati and DBT Program Support Facility for providing the support and assistance required to carry out my thesis work. I am also thankful to the faculty, staff and others members of the Department of BSBE and Centre for Nanotechnology.

I sincerely appreciate all my senior and junior lab members for their love and support. I am thankful to them for providing an amicable work environment. I would also like to thank all the members under the DBT program support facility.

'Friends help find the rainbow on a rainy day'.

I have been very fortunate to have found some great friends in my journey of life. I would like to thank Barlina, Pratik and Arupam for being my constant support, my critic, my go to person during this PhD tenure. I would also like to thank Manisha, Minhaz, Urbashi and Sonakshi for always cheering me up and listening to my endless blabbering. My utmost gratitude to Dr. Reshmi and Dr. Sumita who proved that seniors can be friends and family. I would like to thank them for always guiding me,

helping me and motivating me. They proved that 'true friends are never apart, maybe in distance but never at heart'.

No words are enough to thank the love, support and guidance I have received from my parents and elder brother. I am blessed to have Maa, Baba and Dada (Dr. Bedabrata Saha) who struggled to make my path of life journey easier. When everything seemed dark, they helped me see the ray of light and supported me in the most difficult situations. I would like to thank them for their guidance, support and being my inspiration and pillars of strength throughout my life. Last but not the least, I will always remain indebted to the Almighty God for being the guiding light at all times and helping me decide the right path.

It was indeed an experience of a lifetime, a lovely and pleasant stay at this splendid campus of IIT Guwahati.

Muktashree Saha

Table of Contents

Abstract

Among the wide heterogeneity of breast cancer subtypes, triple negative breast cancer (TNBC) is the most aggressive subtype with poor prognosis due to the negative expression profile of estrogen receptor (ER), progesterone receptor (PR) and HER2. Higher expression of EMT markers results in enhanced metastatic behaviour in TNBC which further leads to increased drug efflux, magnified invasive ability and relapse. Lack of proper targets, multitude of crosstalk, aggressive metastatic relapse and resistance to various chemotherapeutic drugs have been observed in patients with metastatic TNBC, thereby, the failure in the development of an effective targeted anti-cancer therapy poses as the main hurdle in efficacious targeted treatment. Considering the challenges, the formulation of a site-directed nano-carrier and targeting the multifaceted regulatory mechanisms with combinatorial therapy was embarked upon, which might result in the obliteration of the metastatic behavior of TNBC.

The present thesis is focused on targeting EMT and MDR dynamics in triple negative breast cancer (TNBC) through site directed delivery of inhibitors via biomimetic nano-carriers, aiming significant cancer signaling pathways involved in these processes to contribute to the development of more effective treatments for metastatic TNBC.

Section 1 contains the **Introduction** and **Review of Literature** of the work, which describes in details the metastasis, progression and relapse of triple negative breast cancer and the various complex molecular processes governed by a cascade of events. The basic molecular mechanisms and prospects of EMT and its role in disease progression and multi-drug resistance have been described in this section. Furthermore, various present day strategic therapies dealing to control metastatic breast cancer have been explicated. Although a wide variety of nano-carriers have been approved by the FDA however, considering their drawbacks, the

requirement of an efficient drug delivery system has become the need in the present day therapeutic strategies which has been accounted elaborately in this section. The objectives of the thesis have been designed to modify EMT dynamics by targeting the multiple signaling networks by site-directed therapy. Finally, the salient features of the thesis have been discoursed.

Section 2 comprises a comprehensive explanation of the **Materials and Methods** and also the details of the protocols used for conducting the experiments in this thesis.

Section 3 describes **Results and Discussions.** For the past few decades, researchers have been trying to unravel the causes of cancer and develop new strategies to deal with it. Amid all the developments in drug-delivery technologies, considerable advances have been made in recent years to develop nanotechnology-based cancer therapeutics for targeted and controlled drug delivery. Several nano-formulations have been designed to improve therapeutic drug delivery; however, the opsonization of these nano-formulations in the bloodstream has ultimately resulted in toxicity and their rapid clearance by the macrophage system. Though the FDA has approved several passive targeting formulations, certain limitations – like recognition as a foreign substance and elimination by the immune system – have led to increased interest in the active targeting of nanoparticles. Tumor-specific nanocarriers are highly desirable because of their targeted drug release and reduced off-target toxicities compared with the passively targeted systems. In recent years, the application of the biomimetic approach by using the cell membranes of various cell types to prepare nano-sized vesicles for targeted drug delivery has gained much importance. These vesicles can evade the immune system, resulting in decreased phagocytic uptake and prolonged circulation in the blood. Additionally, self-recognition of the vesicles by cancer cells also contributes to highly selective tumor targeting *in vivo*. Notably, membranous vesicles continue to retain their inherent properties (e.g., surface proteins, receptors and ligands)

even after the rigorous downstream processing for the synthesis of nanoparticles. Moreover, the nano-vesicles developed from the cancer cell membranes also possess homologous targeting properties which is advantageous for tumor targeted drug delivery. The vesicles derived from the cancer cell membranes carry tumor-specific antigens, receptors and homologous surface adhesion molecules like N-cadherin, galectin-3 and EpCAM, which results in targeted fusion of the membranous vesicles with the homotypic cancer cell. Considering the several advantages of vesicles synthesized from cell membranes, a biomimetic nanoparticle from a breast cancer cell line was developed and this module was used to deliver ammonium pyrrolidine dithiocarbamate (PDTC) – a potent inhibitor of the NF-κB pathway – and the anticancer drug doxorubicin (DOX). Reports suggest that PDTC, when combined with copper, can form a complex, which results in the inhibition of proteasomal activity, decreased cellular proliferation and the induction of apoptosis in a prostate cancer cell line, LNCaP. Chung *et al.* showed that PDTC has a biphasic cytotoxic effect on neuronal cells depending on the concentration of its dose, which also corresponds to the biphasic inhibition of NF-κB. Previous studies with PDTC have shown that it significantly enhances the suppression of breast cancer cell metastasis, cell migration and invasion. In this study, nano-vesicles synthesized from the parent cell of choice were investigated for their self-homing capability and internalization potential. The efficiency of this delivery system was further studied using flow cytometric uptake assays and apoptosis experiments. The mechanism of apoptosis of the cancer cells after treatment with drug-loaded vesicles was confirmed with reactive oxygen species (ROS) measurement assays. Experiments were then carried out on a 3D tumor model.

In the subsequent endeavour, second approach was to incapacitate the invasiveness and modulate the MDR dynamics in TNBC cell line by employing exosomes derived from non-invasive breast cancer cell line, MCF-7 thereby modifying the tumor niche of the metastatic cells. Relapse and resistance to

chemotherapeutic drugs has become the growing concern of researchers in the present scenario of cancer therapy in patients suffering from metastatic breast cancer. On thorough investigation, it has been observed that multidrug resistance (MDR) plays a very significant part in mediating drug resistance in metastatic TNBC cell lines. The upregulation in the expression of ATP-binding cassette (ABC) transporters, primarily ABCB1, ABCC1 and ABCG2, have been majorly involved in MDR in TNBC cell lines. The efflux ability of the ABC transporters contributes in pumping out the therapeutic agents from the cells, thereby, preventing their accumulation, resulting in decreased efficiency of the drugs and leading to drug resistance. Exosomes act as carriers of biologically active molecules across the circulation and assists in intercellular communications. Most of the cells release exosomes and studies have proved that exosome release is higher during stressed or diseased conditions like cancer. As exosomes have the ability to modulate the tumor niche, they were isolated from MCF-7 cells, which are non-invasive breast cancer cell lines and positive for estrogen and progesterone receptors. Considering the above mentioned functional ability of the exosomes, the effect of the exosomes isolated from the non-invasive breast cancer cell line on a metastatic invasive triple negative breast cancer cells was further examined. Interestingly, the exosomes treatment resulted in the transformation of drug resistant triple negative breast cancer cells making them susceptible to chemotherapeutic drugs for effective anti-cancer activities.

In the third part of the thesis, a targeted therapeutic approach was employed by taking into consideration the advantages of both the exosomes and fused nano-system as established in the previous objectives. TNBC is an aggressive neoplasia with no present effective therapy. Although TNBC accounts for ~15-20% of breast cancers, the mortality for women with TNBC is substantially higher than those with other subtypes of tumors, mostly due to the development of metastases. Compared to other subtypes, TNBC is more aggressive and more difficult to treat. TNBC is a heterogeneous group of cancers whose intrinsic subtype analysis

showed ~80% are basal-like and claudin-low tumors. Expression of EMT markers are significantly higher in basal-like and mesenchymal-like subtype of TNBC and are associated with poor outcome. Therefore, targeting EMT is of great interest for developing novel therapeutics for TNBC. Increasing evidence showed that epigenetic mechanisms are involved in the activation of EMT process. E-cadherin expression in repressed by a number of EMT inducers like SNAIL, Slug, ZEB1, ZEB2 and TWIST. The subjugation of E-cadherin by these repressors are associated with histone deacetylase. The reversibility of epigenetic alterations and the importance of DNA methylase and histone acetylation in tumor progression have resulted in the development of pharmacologic inhibitors for epigenetic therapy. Several molecular processes are involved in EMT induction and regulation, including interconnected and independent pathways and signaling molecules. As a result, several extracellular matrix component and growth factors or intercellular signals such as NF-κB and WNT signaling trigger EMT process. The combinatorial use of epigenome modulating drugs along with conventional chemotherapeutic drugs will be required to treat epigenomic alteration driven cancers.

In this study, the HDAC inhibitor, Trichostatin A (TSA) and tyrosine kinase inhibitor, Lapatinib was chosen and determined whether the combinatorial treatment have any anti-tumor effect on the TNBC cells. Using this cell model, the anti-tumor efficacy of HDACi and tyrosine kinase inhibitor was evaluated by varied assays. Literatures have shown that TSA is toxic when it is injected in vivo. For this reason, the HDACi was loaded in the hybrid nanosystem developed by fusing exosomes and membrane nano-vesicles. Taking into consideration the insufficient amount of exosomes or encapsulating efficiency of cargoes into exosomes, the hybrid nanosystem was developed which offers an impressive module in recent therapeutic advancements. This combined system results in harboring the advantages of both the exosomes and the membrane nano-vesicles.

This hybrid nanosystem was developed by fusing exosomes derived from MCF-7 cells and membrane nano-vesicles synthesized from MDA MB-231 cells.

Conclusion and Future prospects in **Section 4** summarizes the crucial findings of the present thesis. The current study gains insight into the complex crosstalk amongst various signaling pathways leading to the progression, relapse and drug resistance in metastatic breast cancer and further explored for the development of a biomimetic site-directed nanosystem thereby effectively targeting TNBC. This thesis contributes towards developing an effective targeted delivery system by efficient homing to the parental cells that reduces the laborious engineering of nanoparticles for specific delivery. Our study showed that targeted co-therapy via the developed biomimetic hybrid nanocarriers played a very substantial role in the site specific delivery of the drugs for a more efficacious outcome. Thus the corroborations of this research might open up new horizons for the curtailment of metastatic TNBC with further validations in *in vivo* system.

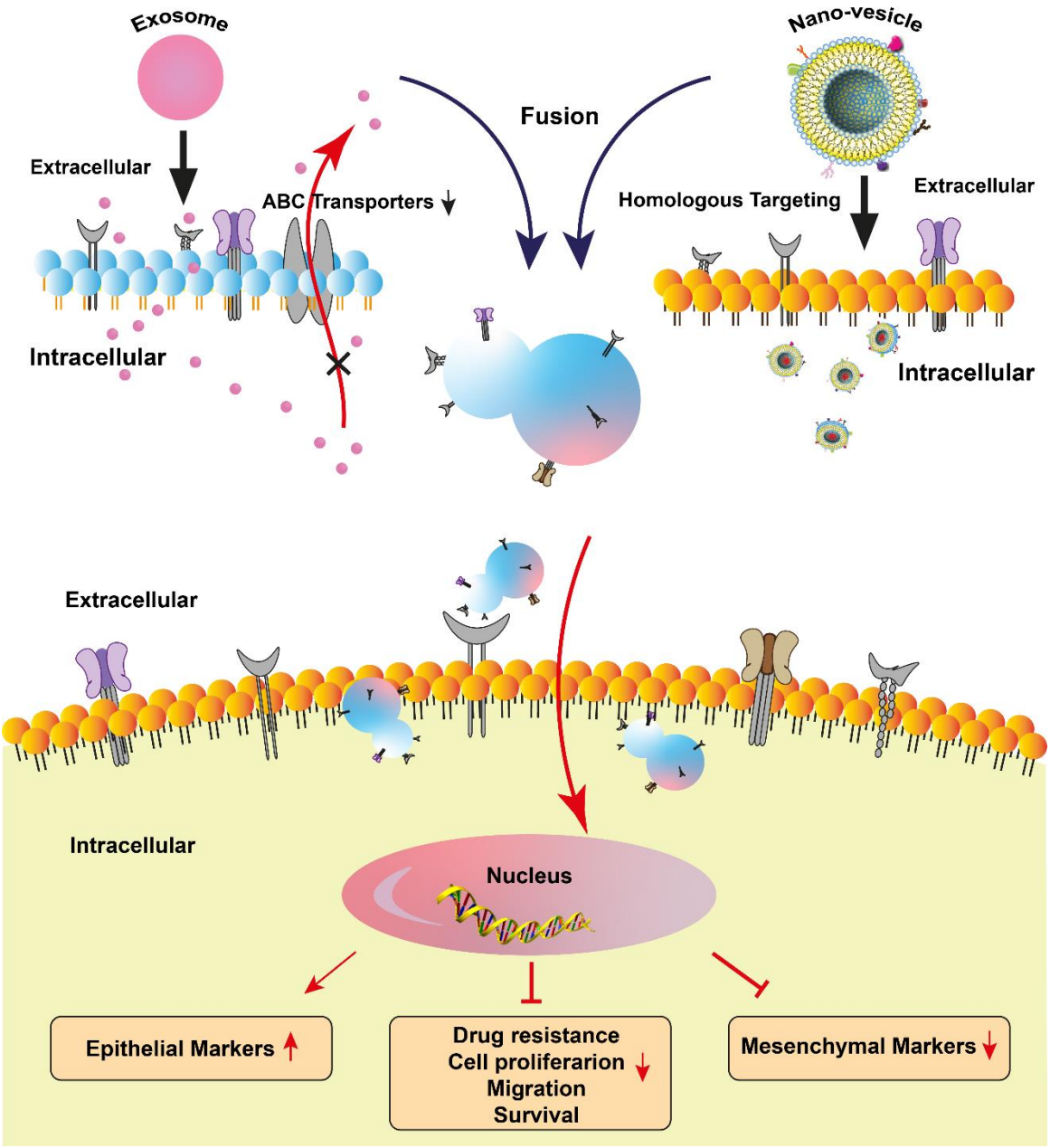

Schematic of the Thesis Work

List of Abbreviations and Acronyms

ABC	ATP-Binding Cassette Transporters
AFM	Atomic Force Microscope
AM	Acetoxymethyl
APS	Ammonium persulphate
ASCT-2	Alanine, Serine, Cysteine Transporter 2
ATP	Adenosine Triphosphate
BC	Breast Cancer
BCA	Bicinchoninic acid
BCRP	Breast Cancer Resistance Protein
BRCA1	Breast Cancer gene 1
BSA	Bovine Serum Albumin
CCCP	Carbonyl Cyanide 3-Chlorophenylhydrazone
CD	Circular dichroism
c-MYC	Cellular Myc
DAPI	4′,6-diamidino-2-phenylindole
DCFDA	Dichlorodihydrofluorescein Diacetate
DLL4	Delta-Like 4
DLS	Dynamic Light Scattering
DMEM	Dulbecco's Modified Eagle's Medium
DMSO	Dimethyl Sulfoxide
DNA	Deoxyribonucleic Acid
DOX	Doxorubicin
ECM	Extracellular Matrix
EDTA	Ethylenediaminetetraacetic Acid
EGF	Epidermal Growth Factor

EGFR	Epidermal Growth Factor Receptor
EMT	Epithelial to Mesenchymal Transition
EPCAM	Epithelial Cellular Adhesion Molecule
ER	Estrogen Receptor
ESCRT	Endosomal Sorting Complexes Required for Transport
EV	Extracellular Vesicle
FBS	Fetal Bovine Serum
FDA	Food and Drug Administration
FESEM	Field Emission Scanning Electron Microscopy
FETEM	Field Emission Transmission Electron Microscopy
FITC	Fluorescein Isothiocyanate
GSK-3β	Glycogen synthase kinase 3 beta
HDAC	Histone Deacetylase
HEK	Human Embryonic Kidney
HER2	Human Epidermal Growth Factor Receptor 2
HES	Hairy and Enhancer of Split
HIF	Hypoxia Inducible Factor
HRP	Horse Radish Peroxide
IC	Inhibitory Concentration
IGF-R	Insulin-like Growth Factor Receptor
IL1β	Interleukin-1β
IM	Immunomodulatory
JC-1	Tetraethyl-benzimidazolylcarbocyanine Iodide
LAR	Luminal Androgen Receptor
MCF	Michigan Cancer Foundation
MCS	Multi Cellular Spheroids
MDA MB-231	M. D. Anderson Metastatic Breast-231
MDR	Multi Drug Resistance

MET	Mesenchymal to Epithelial Transition
MSC	Mesenchymal Stem Cell
MSL	Mesenchymal Stem Like
mTOR	mammalian Target Of Rapamycin
MTT	3-(4, 5- Dimethylthiazol-2-yl)-2, 5-diphenyltetrazolium bromide
MVB	Multi-Vesicular Body
NCCS	National Centre For Cell Science
NF-κB	Nuclear factor kappa-light-chain-enhancer of activated B
OD	Optical Density
PARP	Poly (ADP-ribose) polymerase
PBS	Phosphate Buffer Saline
PBST	Phosphate Buffer Saline with 0.1% Tween
PCR	Polymerase Chain Reaction
PDTC	Pyrrolidine Dithiocarbamate
PEG	Polyethylene Glycol
PI	Propidium Iodide
P1K3CA	Phosphatidylinositol-4, 5- bisphosphate 3-kinase catalytic subunit Alpha
PLGA	Poly(lactic-co-glycolic acid)
PMSF	Phenylmethanesulfonyl fluoride
PR	Progesterone Receptor
PTEN	Phosphatase and TENsin homolog deleted on chromosome 10
PVA	Poly(vinyl alcohol)
PVDF	Polyvinylidene Difluoride
RBC	Red Blood Cell
RIPA	Radioimmunoprecipitation Assay Buffer
RNA	Ribonucleic Acid
ROS	Reactive Oxygen Species

RTK	Receptor Tyrosine Kinase
SAHA	Suberoylanilide Hydroxamic Acid
SDS-PAGE	Sodium Dodecyl Sulphate Polyacrylamide Gel Electrophoresis
SEM	Standard Error of the Mean
SHH	Sonic Hedgehog Protein
TAE	Tris Acetate EDTA
TBST	Tris - buffered saline with 0.1% Tween 20
TEMED	Tetramethylethylenediamine
TGF-β	Transforming growth factor beta
TKI	Tyrosine Kinase Inhibitor
TMB	3,3′,5,5′-Tetramethylbenzidine
TNBC	Triple Negative Breast Cancer
TNF	Tumor Necrosis Factor
TP53	Tumor Protein 53
TSA	Trichostatin A
TWIST1	Twist Family BHLH Transcription Factor 1
VEGFR	Vascular Endothelial Growth Factor Receptor
WNT	Wingless/Integrated
ZEB1	Zinc finger E-box-binding homeobox 1

List of Schemes

List of Figures

Figure 3.3.3 Scratch wound repair analysis of MDA MB-231 cells following inhibitor treatment and in combination after 18 h in comparison to untreated cells.

Figure 3.3.4 Scratch wound repair analysis of EMT induced MDA MB-231 cells after inhibitor treatment and in combination after 18 h in comparison to cells which were not treated (Scale bar- 50 μm) show slowest wound healing capacity when treated with targeted combination of inhibitors.

Figure 3.3.5 Assessment of cell viability upon treatment of MDA MB-231 cells with inhibitors and in combination.

Figure 3.3.6 Assessment of cell viability upon treatment of EMT induced MDA MB-231 cells with inhibitors and in combination reveals an efficient induction of cell death with a much lower concentration of inhibitors required in targeted co-therapy, as indicated by the IC_{50} values.

Figure 3.3.7 Induction of cell death by inhibitor treatment in monolayer cells. Live- dead cell imaging of MDA MB-231 monolayer employing Calcein AM/PI dual staining. Green fluorescence depicts live cells stained by Calcein AM and the red fluorescence indicate dead cells by PI after treatment with IC50 values of free TSA (ii) , lapatinib (iii), nano-system loaded TSA(iv), free TSA+ lapatinib (v) and nano-system loaded TSA+ lapatinib (vi) for 48 h.

Figure 3.3.8 Induction of cell death by inhibitor treatment in monolayer cells. Live–dead cell imaging of EMT induced TNBC monolayer employing Calcein AM/PI dual staining. Green fluorescence depicts live cells stained by Calcein AM and the red fluorescence indicates dead cells by PI after treatment with

IC50 values of free TSA (ii), lapatinib (iii), nanosystem loaded TSA (iv), free TSA+ lapatinib (v), and nanosystem loaded TSA + lapatinib (vi) for 48 h. Decreased green fluorescence and increased red fluorescence in nanosystem loaded TSA+ lapatinib at a much lower concentration explicates the efficient induction of cytotoxicity by targeted co-therapy.

Figure 3.3.9 Induction of cell death by inhibitor treatment in spheroids. Live- dead cell imaging of MDA MB-231 spheroids employing Calcein AM/PI dual staining. Green fluorescence depicts live cells stained by Calcein AM and the red cells indicate dead cells by PI after treatment with free TSA (2 μM) (ii), lapatinib (30 μM) (iii), nano-system loaded TSA (800 nM) (iv), free TSA+ lapatinib (20 μM) (v) and nano-system loaded TSA+ lapatinib (10 μM) (vi) for 72 h.

Figure 3.3.10 Induction of cell death by inhibitor treatment in spheroids. Live–dead cell imaging of EMT induced TNBC spheroids employing Calcein AM/PI dual staining. Green fluorescence depicts live cells stained by Calcein AM and the red fluorescence indicates dead cells by PI after treatment with (ii) free TSA (1 μM), (iii) lapatinib (20 μM), (iv) nanosystem loaded TSA (800 nM), (v) free TSA+ lapatinib (10 μM), and (vi) nanosystem loaded TSA+ lapatinib (8 μM) for 72 h. The increase in red fluorescence and decrease in green fluorescence after treatment with nanosystem loaded TSA + lapatinib at a much lower concentration indicates the increased efficiency of targeted co-therapy in a 3D tumor model.

Figure 3.3.11 Evaluation of apoptosis in MDA MB-231 treated cells. **(A)** Flow cytometric evaluation of apoptosis in treated cells. Annexin V–

FITC–PI-based flow cytometric determination of apoptosis in MDA MB-231 cells treated with IC50 doses of free and targeted inhibitors singly and in co-therapy module.

Figure 3.3.12 Evaluation of apoptosis in EMT induced TNBC treated cells. (A) Evaluation of treated cells for apoptosis by flow cytometry. Annexin V–FITC–PI-based flow cytometric detection of apoptosis in MDA MB-231 cells treated with IC50 doses of free and targeted inhibitors singly and in the co-therapy module reveals more efficient apoptosis when treated with targeted combination of inhibitors.

Figure 3.3.13 DCF-DA assay to sense ROS generation following treatment of MDA MB-231 cells with IC_{50} of the inhibitors after 6 h.

Figure 3.3.14 DCF-DA assay to sense ROS generation following treatment of EMT induced MDA MB-231 cells with IC50 reveals almost similar generation of ROS in targeted co-therapy with a comparatively lower concentration of inhibitors in comparison with untargeted co-therapy after 6 h.

Figure 3.3.15 Flow cytometric evaluation of mitochondrial membrane potential using JC-1 staining of MDA MB-231 cells.

Figure 3.3.16 Flow cytometric evaluation of mitochondrial membrane potential employing JC-1 staining of EMT induced MDA MB-231 cells indicates higher concentration of cells undergoing mitochondrial depolarization in targeted co-therapy.

Figure 3.3.17 Analysis of cell cycle of MDA MB-231 cells following 48 h treatment with inhibitors.

Figure 3.3.18 Analysis of cell cycle of EMT induced MDA MB-231 cells following 48 h of treatment with inhibitors indicating an increase in S-phase.

Figure 3.3.19 Graphical elucidations of alterations in gene expression conforming to treatment with inhibitors quantitated by qRT-PCR analysis. Findings are represented as mean of relative gene expression level w.r.t β-actin ± SEM of three autonomous trials.

Figure 3.3.20 Graphical elucidation of alterations in gene expression conforming to treatment with free and loaded inhibitors and in the combination module quantitated by qRT-PCR. Findings reveal an increase in epithelial markers and a decrease in mesenchymal markers and are represented as mean of relative gene expression w.r.t. *β*-actin ± SEM of three autonomous trials.

Figure 3.3.21 Western Blot representatives showing levels of β- catenin, ZEB1, Vimentin, Sp1, c-myc, Akt, Gsk3β, HDAC4 and β-actin in MDA MB- 231 cell extracts which were treated with IC50 values of the inhibitors for 48 h. β-actin acts as a loading check. Graphs elucidates the alterations in the expression levels compared to untreated samples. The expression levels were derived from the blots employing ImageJ software.

Figure 3.3.22 Western blot representatives showing levels of *β*-catenin, ZEB1, Akt, Gsk3*β*/ pGsk3*β*, Slug, Vimentin, c-myc, HDAC4, Sp1, and *β*-actin in EMT induced MDA MB-231 cell extracts that were treated with IC_{50} values of the inhibitors for 48 h. *β*-actin acts as a loading check. Graphs elucidates the alterations in the expression compared to untreated samples. Expression scores were derived from the blots employing ImageJ software.

List of Tables

Table 3.3.17 Fold change in the expression of c-myc, HDAC4 and Sp1 following treatment of induced MDA MB-231 cells with different inhibitors.

Section 1

Introduction and Review of Literature

Introduction and Review of Literature

Breast cancer is a majorly diagnosed malignancy with the most prominent mortality rate within the female population, with roughly 2.3 million freshly recognized events in 2020 [1]. Amidst the wide variety of breast cancers, triple negative breast cancer (TNBC) is a highly heterogeneous and most aggressive subtype delineated by the lack of estrogen receptor (ER), progesterone receptor (PR) and HER2. Several studies have exhibited the enhanced expression of EMT markers resulting in high metastatic ability of TNBC cells which further contributes to increase in drug resistance, increment in the invasiveness and relapse in patients. Due to the dearth of specific targets, several interdependent signaling networks and resistance to therapeutic agents, development of an efficacious targeted therapeutic module poses as a significant obstacle for successful treatment of TNBC. Taking the various factors into contemplation, the development of an efficient nano-carrier and targeting the multitude of regulatory pathways involved in the progression of TNBC employing combination therapy, is the elementary requirement for annihilation of metastatic TNBC.

1.1 Triple Negative Breast Cancer: Triple Negative Breast Cancer or TNBC accounts for ~15% of the women with breast cancer. It has a negative expression of the ER, PR and HER2 which makes its prognosis difficult [2]. TNBC has been divided into six major subtypes- Basal like 1 (BL1) which is characterized by cell cycle and DNA damage pathway, Basal Like 2 (BL2) which results in increase in growth factor signaling and metabolic pathway, Luminal Androgen Receptor (LAR) which is involved in hormone regulation and metabolism pathways, Mesenchymal (M) involved in cell motility, cell differentiation pathways and EMT, Mesenchymal Stem Like (MSL) which has the characteristics of M-subtype along

with low claudin expression and Immunomodulatory (IM) involved in the process of cell immunity [3] [4] [5]. TNBC has become a very significant area of research because of its heterogeneous nature, poor prognosis factor, resistance to therapeutic drugs and recurrence in patients. BRCA1 mutation and enhanced instability of PIK3CA and TP53 are some of the crucial factors associated with TNBC [6]. Although several clinical trials are on the go for the treatment of TNBC [7], however, chemotherapy still stands as the only conventional option.

1.2 EMT and TNBC: Epithelial-to-Mesenchymal Transition is a biological process which allows the polarized epithelial cells, normally interacting with the basement membrane, to undergo several biochemical changes that enables it to have a mesenchymal cell phenotype which includes enhanced migratory capacity, elevated resistance to apoptosis and increased production of extracellular matrix (ECM) components. In normal conditions, EMT helps in embryogenesis, generation of mesoderm, organ development, wound healing, etc. However, improper induction of EMT may lead to adverse effects, which in cancer cells, leads to the progression of carcinoma to a metastatic stage resulting in enhanced invasive and migration ability to a distant site. Expression of EMT markers are found to be significantly elevated in these cell lines and are affiliated with poor prognosis [8]. The molecular processes that the cells undergo for EMT includes transcription factor activation, expression or change in expression of various of cell-surface proteins, miRNA, proteins of the cytoskeleton and reorganization and synthesis of extracellular matrix degrading enzymes [9]. Since EMT results in cells which has increased migratory and invasive functions, it has great implications in cancer. Whilst there is high level of expression of E-cadherin in the epithelial cells and are compactly bound by tight junctions, there is upregulation in the expression of vimentin, fibronectin and N-cadherin in the mesenchymal cells with less tight junction. The phase transition from epithelial phenotype to mesenchymal

phenotype is induced by TGF-β, EGF, Wnt/β-catenin, Hedgehog, Notch, RTK mediated signaling pathways which, in return, are activated by several external stimuli from the cellular microenvironment [10]. They alter their shape, phenotype like down-regulate EPCAM, express high levels of Snail, Zeb-1, TWIST and increase their motility rate.

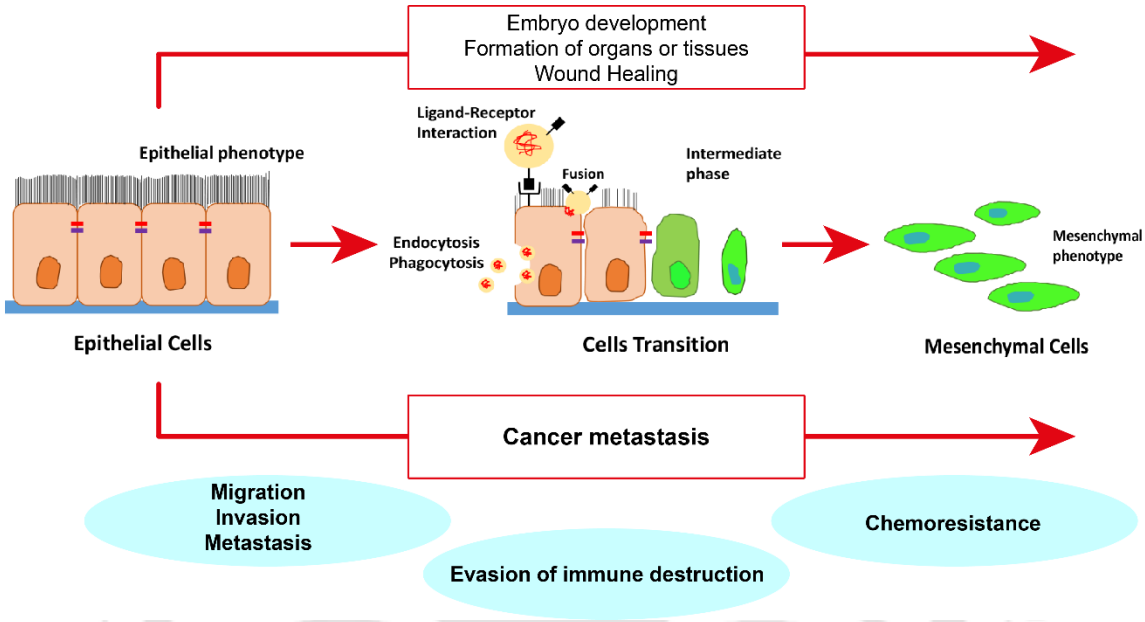

Schematic 1.1. A brief view of epithelial-to-mesenchymal transition (EMT) during normal and unregulated condition. The progression from epithelial to mesenchymal phenotype is marked by the loss of tight junctions and connectivity of the cells from the basal membrane [Conceptualized and illustrated].

1.3 Drug Resistance and TNBC: Metastatic TNBC is considered as one of the most aggressive subtype among breast cancers with very few options for its treatment due to its high heterogeneous character. Several therapeutic strategies have been developed for regulation of TNBC, the conventional ones being chemotherapy, radiation therapy and combination treatment [11]. However, relapse and resistance towards chemotherapeutic drugs have been observed in patients [12]. Although various mechanisms contribute towards the development of chemoresistance like activation in the DNA repair pathway, drug target modification or decrement in the uptake of drugs [13] [14], however, on thorough

investigation, researchers have observed that multidrug resistance (MDR) plays a very significant part in mediating drug resistance in metastatic TNBC cell lines. MDR mechanism stands as a substantial hurdle in the achievement of a successful and efficient mode for cancer therapy for TNBC [15] [16] governed by alterations in several interdependent signaling pathways [17] [18]. Increased expression of the ATP-binding cassette (ABC) genes resulting in the active efflux of drugs contributes significantly towards the development of chemoresistance in the invasive TNBC cells [19] [20]. The drug efflux mechanism of the ABC transporters results in pumping out the chemotherapeutic drugs from the cells, thereby, precluding the accretion of drugs and lowering its efficacy resulting in drug resistance [21]. Several ABC transporters are involved in multi-drug resistance in solid tumors [22], however, the upregulation in the expression of ABC transporters, primarily MDR1 (ABCB1), MRP1 (ABCC1) and BCRP (ABCG2), have been majorly involved in MDR in TNBC cell lines [12] [23]. Britton *et al.* have observed that the downregulation of ABCG2 by inhibiting the growth hormone receptor resulted in the sensitization of the metastatic TNBC cells towards chemotherapy [24]. Guestini *et al.* exhibited that treatment of TNBC via neoadjuvant chemotherapy resulted in the increased protein expression of ABCC1 thereby leading to resistance towards this mode of therapy [25]. It has been observed that cells having mesenchymal phenotype with increased invasive and migratory properties are more resistant towards drugs as compared to the cells with epithelial phenotype, thereby indicating that EMT induced breast cancer cells have higher chemoresistant ability than other subtypes of breast cancer [26] [27].

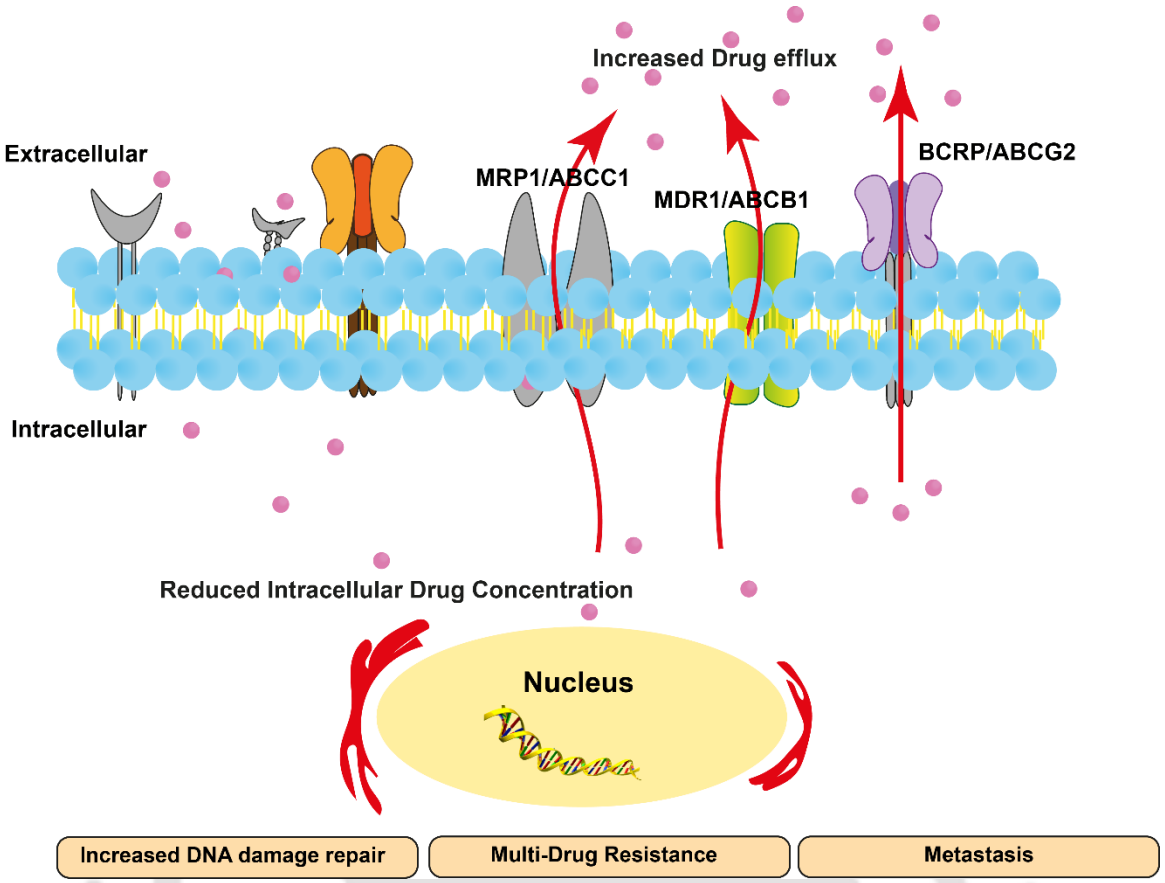

Schematic 1.2. Schematic representation of the role of ABC transporters towards the development of multi-drug resistance leading to enhanced metastasis [Conceptualized and illustrated].

1.4 Pathways involved in the interplay among EMT, MDR and TNBC: Several molecular processes are involved in the induction and regulation of EMT leading to enhanced invasion ability, migration ability, recurrence and drug resistance. These molecular processes include interconnected and independent pathways and signaling molecules. As a result, several extracellular matrix components and growth factors or intercellular signals such as NF-κB, Hedgehog, WNT signaling and epigenetic modulations trigger EMT process [10]. Therefore, the elucidation of the molecular mechanisms responsible for the resistance ability of the TNBC cells towards chemotherapy is of great importance.

Hedgehog signaling pathway has been found to be involved in the metastasis and invasion ability of cancer. It has also been implicated that this signaling pathway

also results in the resistance of the tumors towards therapeutic drugs and relapse of cancer after therapy [28]. The increment in the expression of Shh has been found to be liable for the poor prognosis of patients suffering from TNBC [29]. SHH leads to the unregulated and uncontrolled proliferation of the metastatic tissues resulting in the migration and invasion of tumor to distant tissues and organs [30] [31].

Notch is another signaling pathway which is pertinently involved in the proliferation and poor prognosis of metastatic TNBC cells [32]. The overexpression of its receptor and ligands are responsible for the metastasis of TNBC [33] [34]. Due to the increase in expression of its downstream signaling molecules, it results in poor prognosis in patients. Studies have shown an increase in cell proliferation and decrement in the induction of apoptosis due to enhancement in the expression profile of Notch pathway ligands, HES, HEY-L and DLL4 [35] [36].

Chromatin remodelling or epigenetic modulation is another cause of cancer due to histone modification. Increasing evidences have showed that epigenetic mechanisms are involved in the activation of EMT [37] [38]. The repression in the expression of epithelial markers in EMT are associated with histone deacetylases or methyl transferases [39] [40] [41]. This results in the expression of genes responsible for cancer or suppression of tumor suppressor genes. HDACs is one of the components that results in de-acetylation of the histones and could either repress tumor suppressor gene expression or regulate the oncogenic cell-signaling pathway via modification of key molecules [40]. Treatment of the tumor cells with HDACi can either lead to apoptosis of the tumor cells through intrinsic/extrinsic pathway or it can enhance the susceptibility of tumor cells to apoptosis. The reversibility of epigenetic alterations and the importance of DNA methylation and histone acetylation in tumor progression have resulted in the development of pharmacological inhibitors for epigenetic therapy.

Wnt signaling pathway has been found to play a very significant role in metastatic TNBC with its dysregulation leading to the propagation and invasion of tumor and resistance development towards various anticancer agents [42] [43]. Wnt pathway builds a crosstalk between several signaling pathways and growth factors with β-catenin being the main downstream effector molecular [44].Evidences have shown that there is increase in the expression of EGFR in metastatic TNBC cells. Gene expression studies have exhibited the association of EGFR and Wnt signaling in patients suffering from TNBC. EGFR can result in the phosphorylation of β-catenin thereby destabilizing the interaction between E-cadherin and β-catenin, resulting in transition of the epithelial phenotypic cells to mesenchymal phenotype and subsequent spread of tumor to a distant site [45]. PI3K/Akt/mTOR gets activated by the EGFR conferred by Wnt signaling thereby leading to the localisation of β-catenin and EGFR target genes in the nucleus resulting in increase in the expression of genes responsible for invasion and proliferation [46]. It has been observed by Mccubrey *et al.* that negative regulation of the Akt signaling pathway impacts the tumor suppressor gene, PTEN, subsequently leading to enhanced metastatic phenotype of TNBC mediated by the localization of β-catenin in the nucleus [47]. Studies have also shown the involvement of Wnt5A/ROR1 pathway in the progression of TNBC. A number of kinases mediate the suppression of the apoptotic signalings via ROR1 phosphorylation contributing to the activation of the Akt/mTOR and NF-κB pro-survival signaling pathways thereby exhibiting enhanced migration, proliferation and resistance to therapeutic agents [48] [49].

Deregulation in the Wnt/β-catenin signaling pathway results in effecting the important RTKs in TNBC like EGFR, TGFβ-R, VEGFR and IGF-R thereby leading to unresponsiveness towards its inhibitors during TNBC therapy [50] [51]. Xu *et al.* observed that knockdown of β-catenin resulted in re-sensitization of the TNBC cells to drugs like cisplatin and doxorubicin leading to apoptosis, thereby

suggesting that β-catenin correlates with resistance of TNBC cells towards drugs [52]. Several studies have shown that CSCs are highly resistant to TNBC therapies causing recurrence of metastatic cancer. c-MYC, a target gene of Wnt pathway, synergistically interacts with HIF-1α thereby resulting in the attenuation of the cancer cells' response towards the drugs. HIF-1α leads to the enhancement in the expression of Wnt/β-catenin signaling subsequently effecting the stabilization of β-catenin and increment in the expression of the transcription genes of CSCs [53].

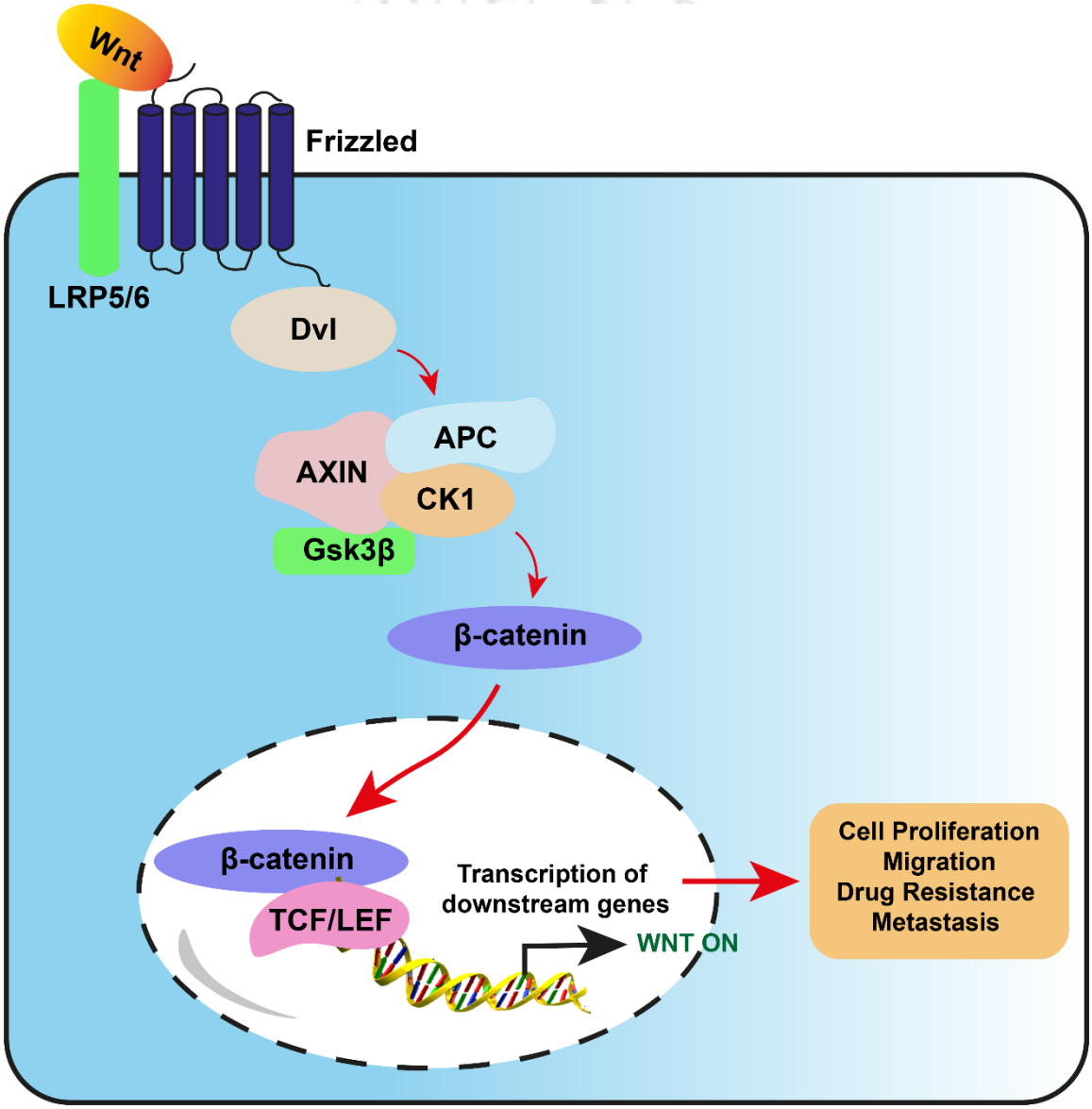

Schematic 1.3. Schematic representation of the Wnt/β-catenin signaling pathway contributing to the progression of cancer [Conceptualized and illustrated].

Thus, considering the heterogeneous nature of TNBC and its interaction with Wnt signaling pathway and several other molecular signaling leading to development of drug resistance to various therapeutics, it is important to better understand the diverse mechanisms and develop targeted and combinatorial cancer therapies against TNBC.

1.5 Conventional and advanced treatment strategies for TNBC: In spite of the discovery of several biochemical and metabolic pathways responsible for tumor metastasis, treatment of TNBC is very crucial due to its poor survival rate as compared to other breast cancer subtypes, rapid relapse and lack of specific targets. Several therapeutic strategies have been developed for the successful subduing of TNBC. The conventional ones being neoadjuvant chemotherapy, surgery and radiotherapy. However, these have been found to be associated with various side effects and relapse in patients have been observed. Some of the alternatives discovered for treatment of TNBC were gene therapy and protein therapy. Nevertheless, since TNBC is caused by several interdependent pathways, these therapeutic strategies have failed to achieve their expected goal. Considering the heterogeneous nature of TNBC, it is crucial to develop targeted therapeutic agents which would markedly improve the treatment module of patients suffering from both early and advanced stage TNBC.

Lately, the use of PARP inhibitors have been found to show promising results in several clinical trials. PARP is a crucial enzyme involved in the repair of DNA breaks via base excision repair pathway induced by several chemotherapeutic drugs and alkylating agents. PARPi blocks the two isoforms- PARP1 and PARP2, thereby leading to inhibition of DNA repair and resulting in apoptosis and cell cycle arrest [54] [55].

Since TNBC is negative for ER, PR and HER2, various significant signaling processes were looked into and it exhibited that enhancement in the immune response levels result in better clinical outcome. TNBC cells exhibit high

expression levels for TILs and results in enhanced response towards chemotherapy [56]. Studies have shown that immunotherapeutic agents when treated in combination with chemotherapy or epigenetic modulating agents have significantly increased the effectiveness of immunotherapy [57] [58] [59]. Atezolizumab was approved in combination with nab paclitaxal for the therapeutic treatment of metastatic TNBC positive for PDL1. It is the only immunotherapeutic drug approved for the treatment as it binds to PDL1, thereby acting as an inhibitor in the immune checkpoints [60].

Epigenetic modulation is another cause for the progression of cancer as histone modifications like histone deacetylation and methylation are involved in various gene regulation. Histone deacetylases contribute in the removal of acetyl group, resulting in the suppression of chromatin structure, thereby inhibiting the transcription of various genes responsible for tumor suppression [61]. The levels of HDACs have been found to be increased in TNBC [62]. Therefore, the use of HDAC inhibitors serve as a promising strategy for treatment of hormone-negative TNBC [63] [64]. Several HDACi like panobinostat, vorinostat, belinostat has been approved by the FDA for the treatment of metastatic TNBC [40]. HDACi have the ability to regulate the metastatic behaviour and angiogenesis of TNBC. They trigger multiple pathways like impairing the homologous recombination repair pathway, upregulation of the tumor suppressor genes, diminution in the activity of MMP9, decrement in the expression of FOXA1, thereby exhibiting anti-tumor effects [65] [66].

Since several signaling pathways are involved in the progression of TNBC acting in an interdependent manner, combination therapy is requisite to improve the therapeutic efficacy of TNBC. PARPi in combination with immunotherapy have proved to show significant anti-tumor activity [67]. Combination of tyrosine kinase inhibitor with PARPi have shown significant suppression of TNBC as inhibition of

PI3K pathway sensitised the cells towards PARPi [68] [69]. The combinatorial use of epigenome modulating drugs along with conventional chemotherapeutic drugs is essential for the treatment of epigenomic alteration driven cancers.

Though several novel therapeutic strategies have been developed for regulating TNBC, however, the main drawback of the aforementioned methods is the delivery of these therapeutic agents and inhibitors to their target sites. So, the development of a suitable nano-carrier is the prerequisite for the therapeutics to work in an effective manner.

1.6 Nano-carrier mediated delivery of therapeutic agents for treatment of TNBC:

For the past few decades, researchers have been trying to unravel the causes of cancer and develop new strategies to deal with it. Amid all the developments in drug-delivery technologies, considerable advances have been made in recent years to develop nanotechnology-based cancer therapeutics for targeted and controlled drug delivery [70]. Several nano-formulations have been designed to improve therapeutic drug delivery; however, the opsonization of these nano-formulations in the bloodstream has ultimately resulted in toxicity and their rapid clearance by the macrophage system [71].

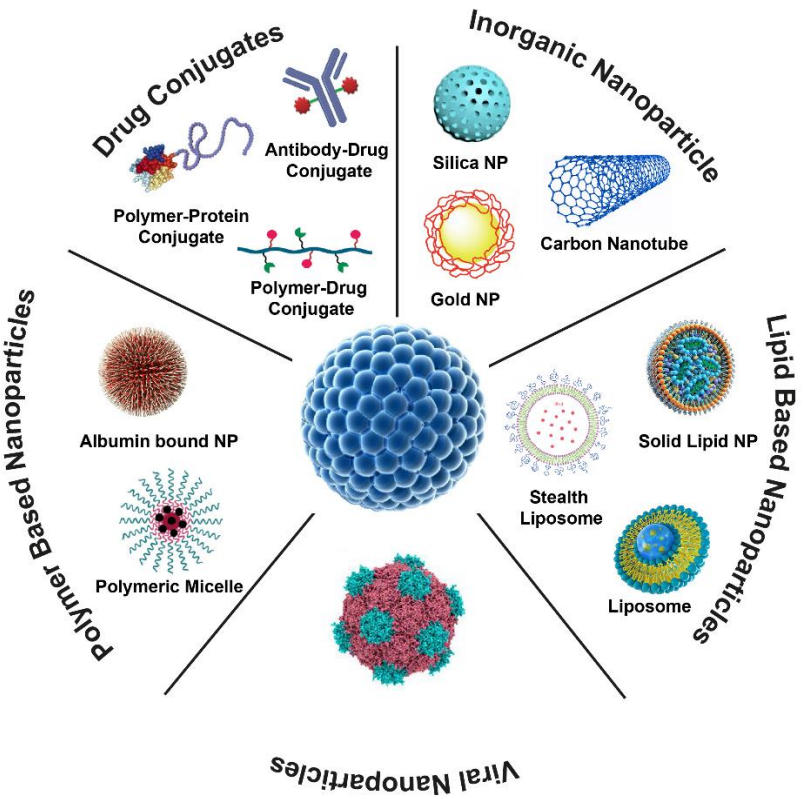

Schematic 1.4. Schematic illustration of various nano-formulations employed for the delivery of therapeutic agents [Conceptualized and redrawn from Ali Aghebati-Maleki *et al*. https://doi.org/10.1002/jcp.29126) [72]].

Though the FDA has approved several passive targeting formulations, certain limitations – like recognition as a foreign substance and elimination by the immune system – have led to increased interest in the active targeting of nanoparticles. Tumor-specific nanocarriers are highly desirable because of their targeted drug release and reduced off-target toxicities compared with the passively targeted systems.

1.6.1 Nano-vesicles: In recent years, the application of the biomimetic approach, by using the cell membranes of various cell types to prepare nano-sized vesicles for targeted drug delivery, has gained much importance [73]. These vesicles can evade the immune system, resulting in decreased phagocytic uptake and prolonged circulation in the blood [74]. Moreover, the biomimetic vesicles are self-recognized by the cancer cells, thereby contributing to an effective *in vivo*

targeting of tumor [75]. The membrane vesicles retain the parental properties like surface receptors, ligands, etc., despite undergoing several downstream processing for their synthesis [76]. The first biomimetic nanoparticle, synthesized by coating the PLGA nanoparticle with RBC membrane, demonstrated enhanced stability, increased circulation time in blood and site-specific delivery [77]. Previous research has documented that platelet-coated nanoparticles have a reduced recognition and cellular uptake by the macrophage system; neither do they cause complement activation in autologous human plasma [78]. Similarly, due to cancer cell membrane-based vesicles' inherent homologous targeting properties, these vesicles can be used for tumor-targeted drug delivery.

The vesicles derived from the cancer cell membranes carry tumor-specific antigens, receptors and homologous surface adhesion molecules like N-cadherin, galectin-3 and EpCAM, which results in targeted fusion of the membranous vesicles with the homotypic cancer cell [79]. Surface adhesion molecules contributes towards the fusion of cancer cells with the healthy cells, thereby resulting in the modification of the cells' microenvironment, leading to the formation of hybridomas. Syncytins are a class of fusogens responsible for mammalian cell-cell fusion mediated by its receptor [80] [81]. Bjerregaard *et al.* showed that breast cancer cell lines, MCF-7 and MDA MB-231, express syncytin, a retroviral endogenous fusion protein which mediate the fusion of the breast cancer cells with endothelial cells, which expresses ASCT-2, a syncytin receptor that are commonly expressed in malignant endothelial cells [82] [83]. Influenced by its inherent homologous targeting properties, cancer cell membranes can be used for tumor targeting and cancer therapy. The presence of the fusogen receptor on the cells facilitate the uptake of the nano-vesicles by the homologous cells, thereby making it more specific for tumor targeting. Thus, membrane derived vesicles can be used as an efficient system for delivering anti-cancer compounds and chemotherapeutic drugs, which helps in attaining a novel therapeutic module.

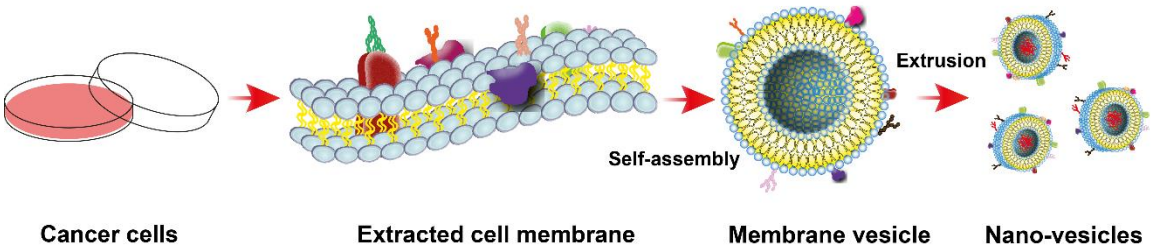

Schematic 1.5. Schematic representation of synthesis of nano-vesicles from cell membranes for homologous targeting [Conceptualized and illustrated].

1.6.2 Exosomes: Exosomes are nano-sized extracellular vesicles (EVs) released by diverse cell variety [84] and were first thought to expel unwanted proteins during reticulocyte maturation like the transferrin receptor [85]. Currently, they are recognized to have a very crucial function in intercellular communication [86]. Based on their biogenesis pathways, EVs are differentiated into three types, exosomes whose size ranges from 30-150 nm are released from the multi-vesicular bodies (MVBs) via exocytosis, micro-vesicles (50-1000 nm), which directly buds out of the cytomembrane and the apoptotic bodies (500-2000 nm) are released by cells experiencing apoptosis [87]. Exosomes are formed in the inter-luminal vessels of the multi-vesicular bodies which fuse with the plasma membrane and is released in the extracellular space by the process of exocytosis. The RabGTPase family of proteins are involved in the fusion of the MVBs with the plasma membrane resulting in the formation of exosomes [88].

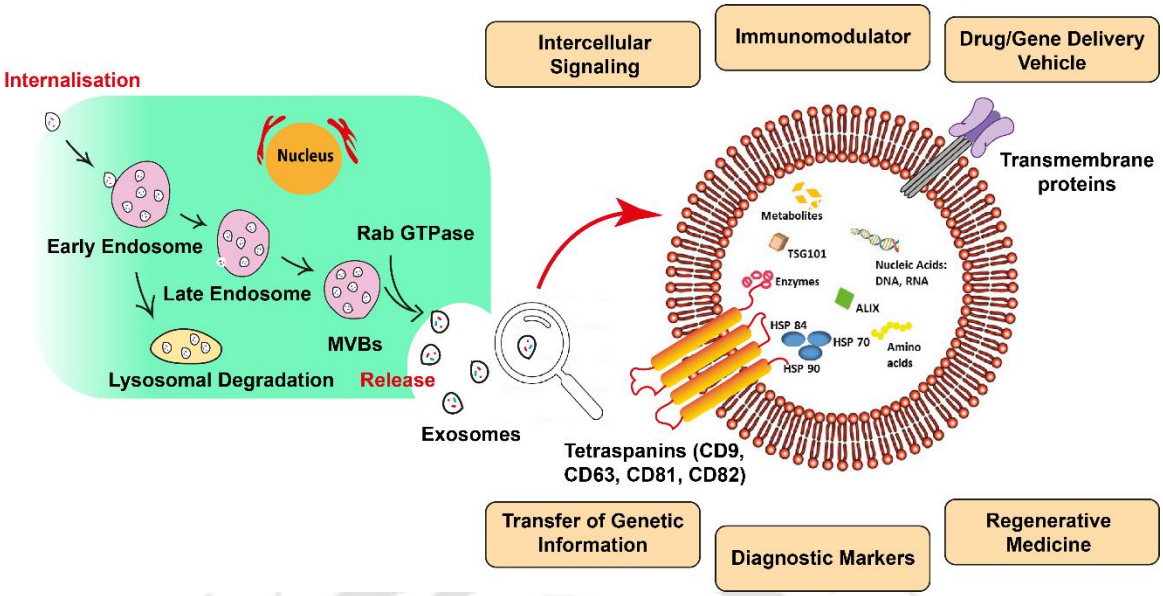

Schematic 1.6. Schematic illustration of the biogenesis of exosomes from cells, its composition and its role in various biological events [Conceptualized and illustrated].

Cell-to-cell communication is very important for the maintenance of cellular signaling and exosomes have emerged as a very important player in the field of intercellular communication [89] [90] [91] [92]. Exosomes are involved in several biological functions like cell-cell communication, acts as an immunomodulatory, is involved in autophagy, cellular homeostasis, transfer of genetic information, acts as a drug/gene delivery vehicle, diagnostic markers and also used in the development of regenerative medicine [93]. In order to achieve coordinated growth and development, the cells must communicate with each other, either directly or indirectly by sending and receiving signals via soluble molecules or by interacting with the target cells. Exosomes have the ability to carry such information carrying cargoes like proteins, lipids, nucleic acids, having the characteristics of the parent cell, and move in circulation, thus, playing a significant role in signal transduction [87] [94] [95]. Various cell signaling pathway proteins like Notch ligand, β-catenin, etc. and intercellular cell signaling mediators like IL1β, TNF-α/β etc. are also carried by the exosomes [96]. Exosomes contain nucleic acids like mRNA, miRNA which regulate gene expression in post-transcriptional

level, ribosomal RNA, long non-coding RNA and some DNA. The exosome content in regulated by various environmental factors which includes cell migration and stress conditions. The mRNAs and miRNAs transferred by exosomes have been proven to be functional in target cells [97]. Exosomes act as carriers of biologically active molecules across the circulation and assists in intercellular communications. Most of the cells release exosomes and studies have proved that exosome release is higher during stressed or diseased conditions like cancer.

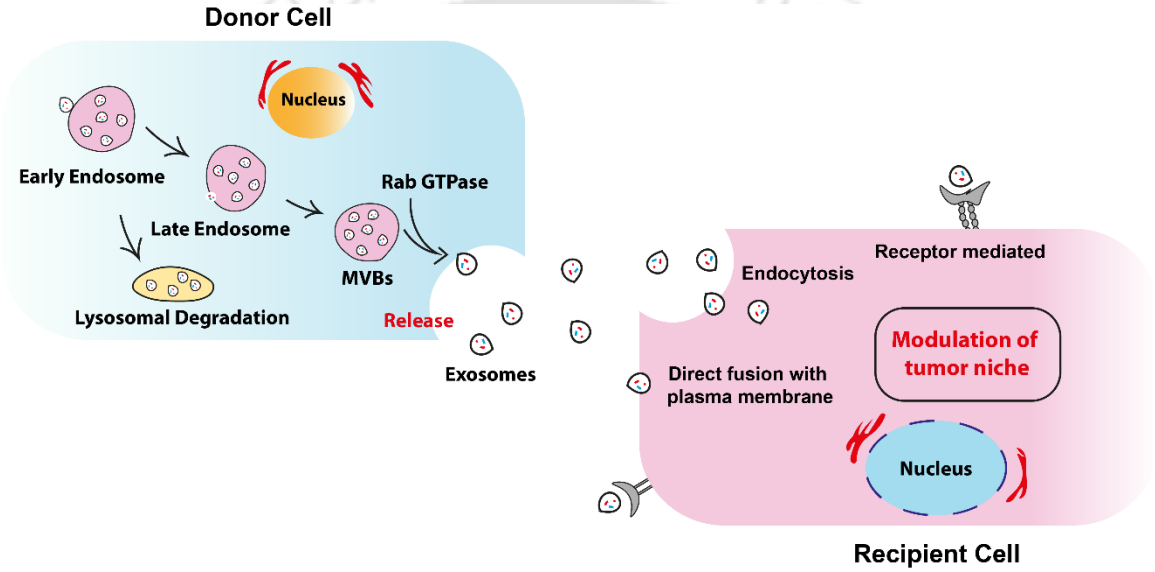

Schematic 1.7. Schematic representation of the role of exosomes in cell-cell interaction thereby contributing to the modification of the cellular environment of the recipient cells [Conceptualized and illustrated].

1.7. Key Features and Scope of Research: The basic comprehension of the interdependent molecular mechanisms responsible for the regulation of EMT can provide better prognosis and treatment of TNBC. The development of a suitable and site-directed nano-carrier can render significant advantage in efficaciously targeting the signaling pathways and attain effective diminution of TNBC. The present research investigation is based on considering the aforementioned facts and the following scopes as potential research areas.

- Developing an efficient biomimetic targeted delivery system that reduces the laborious engineering of nanoparticles for specific delivery and is not evaded by the immune system.
- Assessing the self-homing capability of the synthesised nanosystem for site-directed delivery without causing toxicity towards the non-cancerous or healthy cells.
- Exploring the role of exosomes in the modulation of tumor niche of a metastatic triple negative breast cancer and susceptibility towards therapeutic agents.
- Identification of the significant molecular pathways regulating EMT.
- Evaluating the role of MDR dynamics on the advancement and recurrence in TNBC.
- Exploring the role of Wnt/β-catenin pathway in promoting EMT and further metastasis in TNBC.
- Understanding the role of epigenetic modulation in the progression of EMT and TNBC.
- Co-targeting pathways for the curtailment of EMT and MDR in TNBC.

1.8. Objectives of the current thesis:

- Development of a biomimetic nanocarriers for specific homologous targeting of breast cancer.
- Targeting tumor micro-environment of metastatic TNBC cells via exosomes derived from non-invasive breast cancer cells for MDR inhibition and enhancing drug susceptibility.
- Engineering hybrid nanosystem for homologous targeting of EMT induced triple negative breast cancer cells.

1.9. Salient outcome of the thesis work:

- The first report of utilizing only cell membranes without additional core support for efficient loading and delivery of drug molecules for cancer therapy.
- The membrane derived nano-vesicles were non-immunogenic to macrophage cells and non-hemolytic to RBC, confirming the safety for *in-vivo* applications.
- The nano-vesicles resulted in increased uptake of the drug in 3D multicellular spheroids (MCS) as they have inherent ligand and receptors of the parent cell enabling enhanced uptake.
- The membrane derived nano-vesicles can be used as an excellent module for the delivery of drugs or inhibitors for cancer therapy by specifically targeting the homologous tumor cells *in vivo*.
- The first report of utilizing exosomes from a non-invasive breast cancer cell line, MCF-7 to modulate the tumor micro-environment of a metastatic triple negative breast cancer cell line, MDA MB-231 and enhancing its drug susceptibility.
- The exosomes from non-invasive breast cancer cells successfully downregulated the expression of EMT markers and ABC transporters, ABCB1, ABCG2 and ABCC1 responsible for MDR.
- The study using exosomes can be employed to modulate the tumor niche of metastatic breast cancer and increase susceptibility towards anti-cancer drugs or inhibitors thereby reducing the drug efflux ability or relapse in patients leading to efficient suppression of metastatic breast cancer.
- Additionally, taking the advantages of nano-vesicles and exosomes into consideration, the study is the first to utilize a hybrid nanosystem synthesized by fusing exosomes from non-invasive breast cancer cells and

nano-vesicles from cancer cells to be targeted, for efficient delivery of anti-cancer drugs.

- The targeted combination therapy was efficient in decreasing the migration potential of metastatic TNBC.
- Co-targeting the Wnt/β-catenin pathway and histone deacetylation in site-directed mode, lead to the inhibition of their downstream molecules thereby resulting in the inhibition of progression of TNBC.
- Targeted co-therapy using the hybrid nanosystem incurred an efficient reversal of epithelial to mesenchymal transition (EMT) to mesenchymal to epithelial transition (MET).

The thesis contributes towards developing an efficient targeted delivery system by efficacious homing to the parental cells that reduces the laborious engineering of nanoparticles for specific delivery. The corroborations of this research might open up new horizons for the curtailment of metastatic TNBC for further studies.

Section 2

Materials and Methods

Materials and Methods

2.1. Materials:

BD Biosciences- FITC Annexin V Apoptosis Detection Kit

Bio-rad Laboratories- cDNA synthesis kit, PCR Master mix, SYBR Green Master mix for qPCR

Borosil- Glasswares

Cell Signaling Technology- Antibodies used are listed below (**Table. 2.1**)

SL. No	Antibodies	Catalog No
1	EGFR	4267
2	pEGFR	3777
3	Akt	4691
4	pAkt	4060
5	GSK-3β	12456
6	pGSK-3β	5558
7	Vimentin	5741
8	β-actin	D6A8
9	MDR1	12683
10	β-catenin	9562
11	ZEB1	PA5-28221
12	Slug	PA5-73015
13	c-myc	D84C12
14	HDAC4	D15C3
15	Sp1	D4C3
16	Anti-Rabbit IgG (Alexa Fluor® 647 Conjugate)	4414

Table 2.1. List of antibodies purchased from Cell Signaling Technology.

Corning Inc. – Growth factor reduced matrigel matrix, Boyden chamber transwell inserts

Eppendorf - Cell culture plates

GE Healthcare- Agarose gel and SDS-PAGE running apparatus

Gibco- Antibiotic-Antimycotic solution

HiMedia India – Bovine serum albumin (BSA), Methanol, Ethanol, Cobalt chloride

Promega Corporation– DNase - I

Sigma-Aldrich (USA) – Agarose, Dulbecco's Modified Eagle's Medium (DMEM), Ponceau S, Propidium Iodide (PI), RIPA Buffer, Triton-X-100, Trizma base (Tris) , Tween -20, Tetra methyl ethylene diamine (TEMED), Tri reagent, Ammonium persulphate (APS), Dimethylsulphoxide (DMSO), Sodium pyruvate, Sodium bicarbonate, Epidermal growth factor (EGF), Chemiluminescent reagent, 2',7'-dichlorofluorescein diacetate (DCFDA), DAPI, 3,3',5,5'-Tetramethylbenzidine (TMB), Hydorgen peroxide (H_2O_2), Polyethylene glycol (PEG), Phosphate-buffered saline (PBS), RNAse, Anti-rabbit IgG HRP-linked Antibody, Anti-mouse IgG HRP-linked Antibody, PVDF membrane, Ammonium PDTC, Trichostatin A (TSA), Lapatinib,.

Tarsons Products Pvt. Ltd – Plastic-ware

Thermo Fisher Scientific- Cell culture plates, Protein ladder, Trypan blue, AlamarBlue, Fetal Bovine Serum (FBS), Penicillin-streptomycin, JC-1 dye, Calcein-AM, SYBR Green Master Mix, Anti-ZEB-1 Antibody, Anti-SNAI2 Antibody

Integrated DNA Technologies (IDT) - Primers for all PCR reactions have been listed below (**Table. 2.2**):

Name	Primer Sequence
E-Cadherin	Fwd: 5'- TGAAGGTGACAGAGCCTCTGGAT -3'
	Rev: 5'- TGGGTGAATTCGGGCTTGTT -3'
Vimentin	Fwd: 5'- AGTCCACTGAGTACCGGAGAC -3'
	Rev: 5'- CATTTCACGCATCTGGCGTTC -3'
N-cadherin	Fwd: 5'- CCATCAAGCCTGTGGGAATC -3'
	Rev: 5'- GCAGATCGGACCGGATACTG -3'
Fibronectin	Fwd: 5'- GGTGACACTTATGAGCGTCCTAAA -3'
	Rev: 5'- AACATGTAACCACCAGTCTCATGTG -3'
Twist-1	Fwd: 5'- TGCATGCATTCTCAAGAGGT -3'
	Rev: 5'- CTATGGTTTTGCAGGCCAGT -3'
ABCB1	Fwd: 5'- GGGAGCTTAACACCCGACTTA -3'
	Rev: 5'- GCCAAAATCACAAGGGTTAGCTT -3'
ABCG2	Fwd: 5'- TGGCTTAGACTCAAGCACAGC -3'
	Rev: 5'- TCGTCCCTGCTTAGACATCC -3'
ABCC1	Fwd: 5'- CTGAGAAGGAGGCGCCCTG -3'
	Rev: 5'- GTGTCCGGATGGTGGACTG -3'
β-actin	Fwd: 5'- CTGGAACGGTGAAGGTGACA -3'
	Rev: 5'- AAGGGACTTCCTGTAACAATGCA -3'

Table 2.2. List of primers used for all PCR reactions.

2.2. Cell lines and cell culture conditions:

Human breast cancer cell lines MCF-7, MDA-MB-231, human cervical cancer cell line HeLa and human embryonic kidney cell line HEK-293 were purchased from the National Centre for Cell Science, Pune, India. The cells were cultured in Dulbecco's Modified Eagle's Medium-high glucose supplemented with L-glutamine, sodium pyruvate, 10% fetal bovine serum (FBS), Sodium bicarbonate, 100 units/ml penicillin and 100 µg/ml streptomycin at 37 °C in humidified air containing 5% CO_2.

2.3. Culture Condition for 3D Multicellular Tumor Spheroids: Spheroids of different cell lines were generated using a forced floating method. Briefly, cells were cultured as monolayers up to confluency, trypsinized and re-suspended in DMEM. In the meantime, the 96-well plates to be used for spheroid growth, were made non-adherent by coating the well surface with agarose (1.5% w/v in serum-free medium). Subsequently, cells were seeded in the agarose-coated 96-well plates at a density of 2×10^4 cells per well. Following this, these plates were centrifuged at 700 rcf for 10 min, then incubated for 96 h in a humidified atmosphere at 37°C containing 5% CO_2. The growth of the spheroids was monitored each day with a Nikon Eclipse Ti microscope and after 96 h the generated spheroids were used for further experiments.

2.4. Method Sections:

2.4.1. Methods related to targeting signaling pathways to alter EMT and MDR dynamics of TNBC.

2.4.1.1. EMT Induction: To induce EMT, cells were trypsinized, counted and seeded in appropriate numbers in 6-well plates or 60 mm dishes. Cell were allowed to attach for 24 h in complete media containing 10% serum. After attachment, cells

were starved for 4 h in serum free media. Next, the serum free media was replaced with 0.5 % serum media supplemented with 20 nM EGF. After incubation of 30 min, cells were treated with inhibitors as desired.

2.4.1.2. Determination of Cell Viability: In order to understand the therapeutic potential of the inhibitors alone or in combination, the percent of viable cell was assessed following treatment. Cell viability was evaluated using an AlamarBlue assay. Resazurin, the active ingredient of AlamarBlue, is converted to its reduced form resorufin when entering into living cells. Following treatment for 48 h of monolayer cultures in 96-well plates, 10 µl AlamarBlue was directly added to the wells and incubated for 2 h at 37 °C under 5% CO_2 humidified conditions. In case of spheroids, following treatment for 72 h, 20 µl AlamarBlue was added and incubated for 4 h at 37 °C under 5% CO_2 humidified conditions. After the respective incubations, absorbance was measured at 570 nm with a reference of 600 nm using a microplate reader (Infinite M200 Pro, Tecan, Switzerland). Cell viability (%) was determined using the following formula:

$$\text{Cell Viability (\%)} = \frac{(Abs570 - Abs600)Sample}{(Abs570 - Abs600)Control} \times 100$$

MTT assay was also performed for the determination of cell viability following treatment. The cells were seeded in a 96-well plate, in complete DMEM media, at a density of 5×10^3 cells/well. Following 48 h of EMT induction and treatment with increasing concentrations of inhibitors or drugs, 0.5 mg/mL of MTT in DMEM was supplemented to each well and incubated for 1.5 h. Subsequently, 150 μL of DMSO was also supplemented to each well and the OD was measured at 570 nm for dissolved formazon and readings at 630 nm were taken as reference. Thereafter, cell viability was calculated as follows:

$$Cell\ viability\ (\%) = \frac{(A1 - A2)Sample}{(A1 - A2)\ Control} \times 100$$

Where, $A1$ is the absorbance at 570 nm and $A2$ is the absorbance at 630 nm

2.4.1.3. Drug Combination Assays: The cell viability data was further processed and sigmoidal-dose response curves were plotted using GraphPad Prism software. Further, from the sigmoidal-dose response curves, inhibitory concentration-50 (IC_{50}) values were determined. For combination therapy, the concentration of one of the inhibitors was kept constant to IC_{25} while the concentration of another inhibitor was increased in a dose dependent manner.

2.4.1.4. Determination of Cell Cycle Pattern: To determine the effect of the inhibitors on the progression of cell cycle, a PI (Sigma-Aldrich) based flow cytometry examination was carried out. Cells were seeded in a 6-well plate at a density of 2×10^5 cells. Following attachment, synchronization of cells was carried out before treatment by 24 h of serum starvation. Treatment with the inhibitors and their combination was carried out for 48 h in DMEM media. Thereafter, cells were centrifuged and fixed with chilled 70% ethanol. These were then stashed away in −20 °C until future evaluation as mentioned by Riccardi et al. In brief, chilled PBS was added to the cells and washed. Thereafter, they were incubated with RNase for 1 h at 55 °C. Following RNase treatment, PI was added to the cells and stored on ice in dark until future examination. The samples were evaluated by employing a BD FacsCalibur, and the scorings were examined by employing FCS Express software.

2.4.1.5. Detection of Reactive Oxygen Species: Cellular ROS generation following drug treatment was analyzed using 2′,7′-dichlorofluorescein diacetate (DCFDA) dye. DCFDA is a cell-permeant reagent, and in the presence of hydroxyl,

peroxyl and other ROS activities within the cell, it is oxidized to 2′,7′-dichlorofluorescein (DCF), which gives a green fluorescence. For ROS detection, the cells were first treated with inhibitors or drugs for a required time period. Thereafter, the cells were rinsed with PBS and trypsinized. They were then resuspended in 0.2 μM solution of DCF DA and incubated for 30 min at room temperature. The cells were then centrifuged, washed with PBS and resuspended in 500 μl PBS. Finally, the cells were analyzed in FITC channel using CytoFLEX flow cytometer.

2.4.1.6. Detection of Mitochondrial Membrane Potential: Mitochondrial membrane potential was determined using JC-1 staining. The cyanine dye JC-1 (5,5′,6,6′-tetrachloro-1,1′,3,3′-tetraethylbenzimi-dazolylcarbocyanine iodide) forms red aggregates in polarized mitochondria, whereas it remains as a monomer in depolarized mitochondria. Cells were treated with inhibitors and their combination for 48 h. After completion of the treatment, JC-1 dye (10 μM) was added to each cell culture well for 20 min. For positive control, cells were incubated with 50 μM Carbonyl cyanide 3-chlorophenylhydrazone (CCCP) for 30 min along with the JC-1 dye. After the incubation, the cells were trypsinized and washed with PBS extensively. Finally, cells were resuspended in 500 μl PBS and analyzed using CytoFLEX flow cytometer. Fluorescence intensities were collected in the red and green channels. Positive and negative controls were used to detect depolarized population and for fluorescence compensation.

2.4.1.7. Determination of Apoptotic Cell Population: Early apoptotic, apoptotic and necrotic cell populations were estimated using a FITC Annexin V Apoptosis Detection Kit. Cells were treated for a period of 48 h. Next, cells were trypsinized, washed with chilled PBS and processed according to the manufacturer's instructions. Fluorescence data was collected in green and red

channel using CytoFLEX flow cytometer. Data analysis and fluorescence compensation were performed using CytExpert software.

2.4.1.8. Calcein-AM/ Propidium Iodide (PI) Dual Staining: To visualize the percentage of live and dead cell populations following treatment, cells were stained with Calcein-AM and PI. Calcein AM is a cell-permeant non-fluorescent dye which, after entering inside live cells, is converted to green-fluorescent calcein by acetoxymethyl ester hydrolysis by intracellular esterases. Whereas, PI is a not permeant to live cells, and binds to DNA of dead cells by intercalating between the bases and gives red fluorescence. For imaging live–dead cell populations, monolayer cultures were treated for 48 h, and spheroids were treated for 72 h. Cells were carefully rinsed with PBS thrice. Thereafter, Calcein AM/PI solution was added in the final concentrations of 2 μM and 4 μM followed by a 30 min incubation in dark. After incubation, the stained cells and spheroids were washed thrice with PBS and imaged using a Zeiss LSM 880 confocal microscope in conjunction with Z-stacking analysis.

2.4.1.9. RNA Isolation and Expression Study: Following treatment RNA was isolated from the cells using Tri reagent. From the obtained RNA, cDNA was synthesized using an iScript cDNA synthesis kit according to the manufacturer's instructions. Amplification of the cDNA of interest was performed using a SYBR Green Master Mix and a Rotor-Gene Q (Qiagen) real-time PCR cycler. The data obtained were normalized to β-actin. Further, the normalized data were quantified using the delta-delta CT method. The obtained quantitative RT-PCR (qRT-PCR) data were analyzed using LinReg PCR software.

2.4.1.10. Protein Expression analysis by Western Blot: Following treatment, total protein was extracted from the cells using RIPA lysis buffer. Protein from each sample was quantified using BCA protein assay kit. Equal amount of protein from each sample were subjected to SDS-PAGE. From the resolved gel, protein were subsequently transferred to PVDF membranes. Next, the membranes were blocked using blocking buffer (4% BSA in TBST) and incubated overnight with primary antibodies. Next, blots were extensively washed using TBST. Further, blots were incubated with HRP conjugated secondary antibodies for a period of 2 h at room temperature. Following incubation, blots were rewashed extensively with TBST. Signals were developed using chemiluminescent reagent, and images were acquired using ChemiDoc (BioRad). The images were quantified using ImageJ software. Finally, the data obtained were normalized to β-actin and protein expression data were analyzed.

2.4.1.11. Determination of Migration Potential: Migration was assessed using a scratch wound repair analysis and was carried out employing a method reported by Wu *et al*.. Concisely cells were seeded and raised to ~70-80% confluency in DMEM complete media. For EMT induced cells, the media was substituted by 0.5% DMEM serum media for 12 h. The monolayers were then scratched with an aseptic pipette tip to make "wounds". These were then rinsed with PBS to get rid of cell detritus. Subsequently, the cells were treated with drugs or inhibitors. Thereafter, they were incubated at 37 °C with 5% CO2 in humidified surrounding for an 18 h time duration. Before and after treatment, pictures of the scratch or "wounds" were taken employing a Nikon Eclipse Ti−U microscope and examined employing ImageJ software.

2.4.1.12. Statistical analysis: Statistical evaluations were executed employing GraphPad Prism 6. Obtained scorings were denoted as mean ± standard error of

the mean. One-way ANOVA was employed to examine potential correlations among groups. A *p*-value <0.05 was contemplated as statistically relevant in which *$p < 0.05$; **$p < 0.01$; ***$p < 0.001$; ****$p < 0.0001$, respectively.

2.4.2. Methods employed to study the interaction between EMT, MDR and Wnt/β-catenin signaling pathway to restrain metastatic TNBC.

2.4.2.1. EMT Induction: To induce EMT, cells were trypsinized, counted and seeded in appropriate numbers in 6-well plates or 60 mm dishes. Cell were allowed to attach for 24 h in complete media containing 10% serum. After attachment, cells were starved with 0.5% serum media for 12 h. After serum starvation, media was replaced with 0.5 % serum media supplemented with 20 nM EGF. After incubation of 30 min, cells were treated as desired.

2.4.2.2. Immunofluorescence Microscopy: For the immunofluorescence analysis, MDA MB-231 cells were seeded at a density of 2×10^5 followed by treatment with exosomes for a duration of 48 h. Thereafter, the cells were rinsed thrice with 1X PBS, fixed using 4% formaldehyde and washed again using 1X PBS. In order to avert any non-specific binding of antibody, cells were blocked for a time duration of 2 h using blocking buffer. Subsequently, the MDA MB-231 cells were brooded with 1° antibodies overnight at 4°C and rewashed. Subsequently, they were incubated in the dark at RT with secondary antibodies conjugated with fluorochrome. Following incubation, the MDA MB-231 cells were washed three times with PBS and counterstained with DAPI. The cells were rinsed again and eventually imaging was carried out employing Zoe fluorescence microscope.

2.4.2.6. Western Blotting: Following treatment of the MDA MB-231 cells, total protein from the cells was isolated by RIPA buffer that was supplemented with protease cocktail inhibitor, sodium fluoride, sodium orthovanadate, and phenylmethylsulfonyl fluoride (PMSF) and EDTA. The extracted proteins were then quantitated using a bicinchoninic acid (BCA) assay. A matching quantity of protein was loaded for SDS-PAGE from each sample and proceeded with the Western blot. The resolved proteins were then transmitted to PVDF membranes and blocked using 4% BSA in TBST (blocking buffer) followed by incubating overnight at 4 °C with primary antibodies. The membranes were then rinsed by employing TBST and incubated with secondary antibody for 2 h at RT. Subsequently, the membranes were properly rinsed using TBST and processed. The images were produced using chemiluminescent reagent and ChemiDoc (BioRad) and recorded. Finally, the pictures so obtained were analysed employing ImageJ software (Fiji). Anti-Akt, anti-β-catenin, anti-Vimentin, anti-cMYC, anti-ZEB1, anti-Twist1, anti-GSK3β, anti-phospho GSK3β, anti-Slug, anti-HDAC4 and anti-Sp1 antibodies were used to detect the desired protein expression.

2.4.2.6. Quantitative real-time PCR: After treatment of the cells for 48 h employing Trizol reagent (Sigma), RNA was extracted from MDA MB-231 cells. Thereafter, cDNA was synthesized employing the iScript cDNA synthesis kit (BioRad) as per the manufacturer's protocol followed by the amplification of the cDNA of interest employing PowerUp SYBR Green Master Mix (Applied Biosystems) and Rotor-Gene Q (Qiagen) real-time PCR cycler. The incurred scores were quantitated employing the delta− delta CT method after normalizing it to the housekeeping gene, β- actin. Thereafter, the RT-PCR data was analyzed using the LinReg PCR software.

2.4.3. Synthesis and isolation of biomimetic nano-carriers for targeted delivery.

2.4.3.1. Synthesis of nano-vesicles: The nano-vesicles were prepared from cell membranes of the cells to be targeted. The cells were first seeded and allowed to attain ~80% confluency. They were then harvested by scraping the cells from the plate surface. For lysis and removal of the cell contents, isolated cells were incubated with hypotonic lysis buffer (20mM Tris-HCl, 10mM KCl, 2 mM MgCl2 and EDTA) overnight at 4˚C. Following this, the cells were subjected to homogenization using a hand held Dounce homogenizer (20 passes). The lysis and removal of the cell content were confirmed by observing the cells under the microscope. Subsequently, the homogenized cells were first centrifuged at 650× *g* at 4˚C for 5 min to remove cell debris. Then the supernatant containing the cell membranes was centrifuged at 20,000× *g* at 4˚C for 45 min and the cell membrane pellet was collected in phosphate-buffered saline (PBS). Subsequently, it was proceeded for the synthesis of nano-sized by the process reported by Eylar *et al.*, with slight modification [17]. Briefly, the MCF-7 cell membrane was extruded through a 0.8-μm pore-sized membrane, followed by membranes of decreasing pore size (0.4, 0.2 and 0.1 μm). The prepared vesicles were washed in PBS using centrifugation (20,000× *g*). The pellet thus obtained was then re-suspended in PBS.

2.4.3.2. Isolation of exosomes: Exosomes were extracted from conditioned cell culture media by polymer precipitation method. For this purpose, water-excluding polymer, polyethylene glycol (PEG) was used. MCF-7 cell line was selected for the isolation of exosomes and the polymer used in the isolation process by precipitation method was 50% PEG8000 dissolved in 75mM NaCl. Cells were cultured to 80% confluency in complete DMEM media. Thereafter, the culture media was exchanged with DMEM serum free media and incubated for 24 h. The media was then collected and centrifuged at 2,500g to remove cell debris. The collected supernatant was again centrifuged at 5000g for the removal of small

extracellular components. Subsequently, the supernatant was concentrated and the polymer precipitation solution was added in 2:1 ratio and incubated overnight in 4˚C. Subsequently, the sample was centrifuged at 13,000 rpm for 60 min and the obtained pellet was washed and dissolved in 1X PBS.

2.4.3.3. Synthesis of hybrid nanosystem: Exosomes were isolated from MCF-7 cells by the polymer precipitation method and membrane nano-vesicles were synthesized from TNBC cells, MDA MB-231 by the process of extrusion as described in Saha *et al*.. They were then fused together by the freeze−thaw method. Briefly, exosomes and membrane vesicles were mixed in several proportions, i.e., 2:1, 1:1, and 1:2. They were then frozen in liquid N2 and thawed at 37 °C for 10 min. This was continued for 10 cycles. The fused hybrid nanosystem was then stored in -20˚C for further experiments.

Section 3

Results and Discussion

3.1. Developing Membrane-Derived Nanocarriers for ex-vivo Therapy of Homologous Breast Cancer Cells

Nanomedicine **16(21), 1843–1856 (2021).**

Abstract: The scenario of cancer therapy has changed efficaciously over the last few decades. In the recent past, various new effective approaches has emerged other than surgery or radiotherapy by understanding the molecular features of the tumors and using various nanocarriers for the efficient delivery of drugs. For an active and specific targeting of the cancer cells, camouflaged nanocarriers are the requirement of the era which can achieve specific characteristics like targeted recognition, long time survival in the blood circulatory system and immune evasion.

Herein, the development of a nano-vesicle which cloaks the drug ammonium PDTC to achieve precise targeting of cancer cells as a therapeutic platform was reported. Membrane-derived nano-vesicle was synthesised from breast cancer cell line. The synthesised nano-vesicle was then subsequently checked for its hemocompatibility and biocompatibility to avoid evasion by the immune system. Flow cytometry was used to assess the homologous targeting and cellular uptake mechanism of the nano-vesicles. AlamarBlue assays were used to depict cell viability of the breast cancer cells homologously targeted by pyrrolidine dithiocarbamate (PDTC) loaded nano-vesicles. Flow cytometric analysis was also carried out to detect apoptotic cell populations as well as reactive-oxygen species (ROS) levels following treatment with drug loaded nano-vesicle.

Loading the anti-cancer drug into a nano-carrier developed from the cell membrane of the parent cell source rendered better efficacy for cancer therapy by self-recognition and internalization in the source cancer cells and also by competing with other heterologous cells *in vitro*. The nano-vesicles retained its inherent properties like surface proteins, receptors, ligands etc. even after its downstream processing, which makes it highly specific. As a result of this homologous targeting and functionalization with the cell adhesion molecules of the cancer cell membrane, membranous vesicle loaded ammonium PDTC showed higher uptake by the homologous cells as compared to other cancer cells. It also

exhibited increased anti-proliferative potency against MCF-7 cancer cells despite retaining its biphasic activity with minimal effect on human embryonic kidney cell line, HEK 293. Further, this study was executed in 3D tumor model system, however, higher doses were required for the spheroid system.

This minimally explored avenue of using cell membranes as biological nano-carrier for cancer therapy might pave the path for a potential targeted delivery of anti-cancer drugs even in other types of tumors by the usage of the membrane of the parent cancer cell. It might lead to the development of a potential nano-delivery system for cancer therapy *in vivo* as they can be derived from the patient's own cells.

3.1.1 Results:

3.1.1.1. Characterization of nano-vesicles synthesized from cell membrane of MCF-7: Nano-vesicles were prepared from MCF-7 cell membranes (**Figure 3.1.1**) by the process of extrusion using Avanti Polar Lipids mini extruder set. The synthesized nano-vesicles were characterized using FETEM, FESEM and DLS analysis for their size, shape and morphology. The FETEM images of vesicular membranes revealed that the particles were almost spherical, with an average diameter of 63.11 nm (**Figure 3.1.2A**). The spherical morphology of the vesicular membranes was confirmed by FETEM and FESEM microscopic images (**Figure 3.1.2B and 3.1.2C**). The surface charge of nanoparticles plays a vital role in their cellular uptake. The surface potential of the vesicular membranes was found to be -11.5 mV in PBS (pH 7.4) and -9.6 mV in Dulbecco's modified Eagle medium (pH 7.4), which was similar to the membranes isolated from MCF-7 cells. The average hydrodynamic diameter (*dH*) of the vesicular membrane was estimated to be 156.01 nm by DLS measurements (**Figure 3.1.2D**).

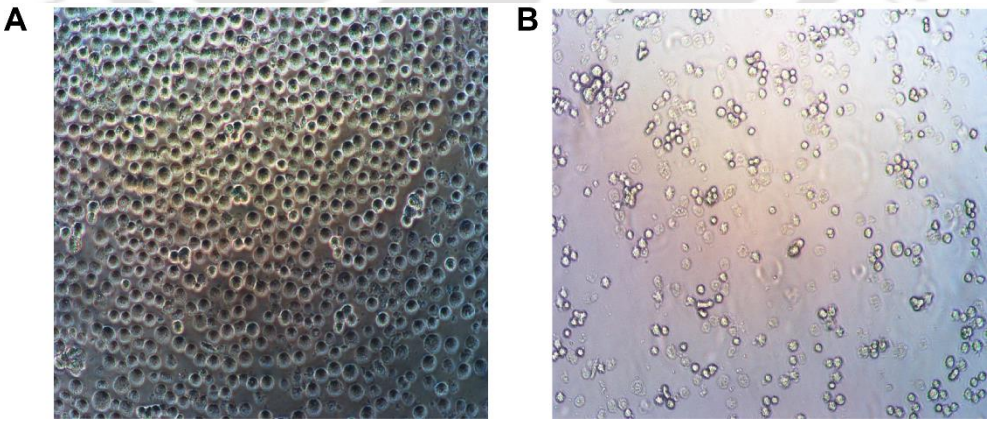

Figure 3.1.1. Microscope image showing **(A)** lysed cells after keeping in lysis buffer overnight at 4°C and subsequently **(B)** sonicated.

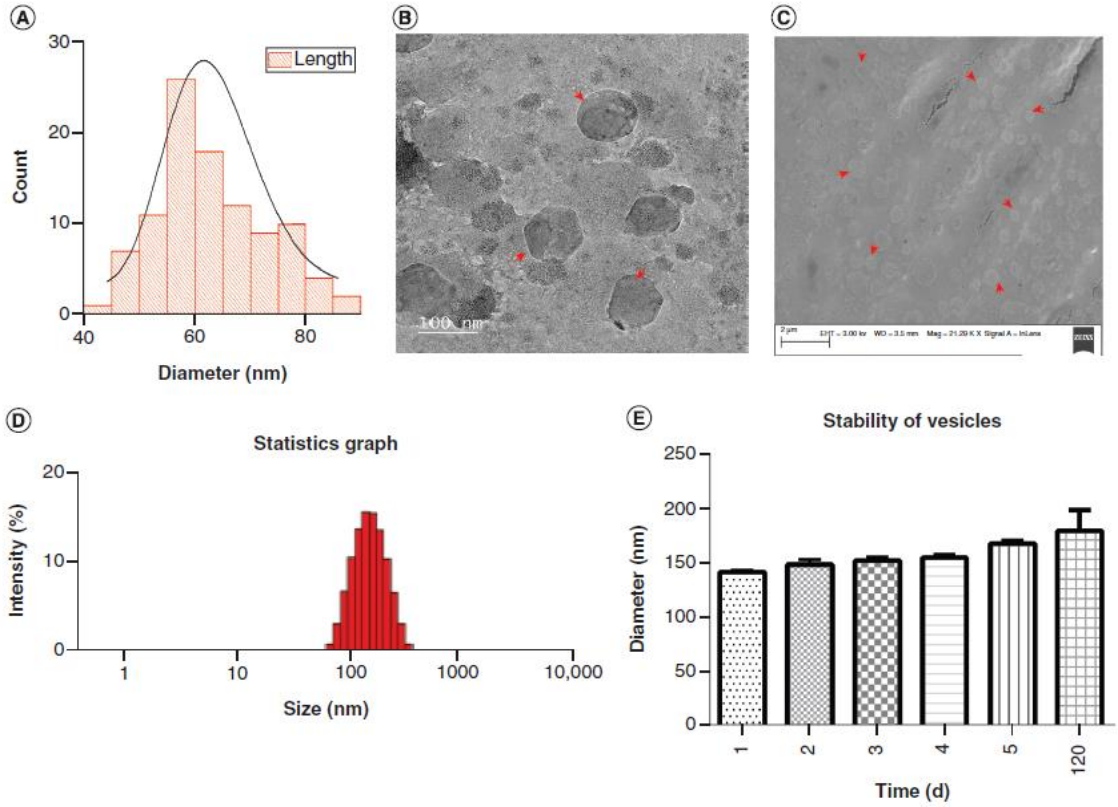

Figure 3.1.2. Characterization of nano-vesicles prepared from MCF-7 cell membrane. (A) Size distribution graph of the nano-vesicles. **(B)** Field emission transmission electron microscopy image of the vesicles (scale bar: 100 nm). **(C)** Field emission scanning electron microscopy micrograph of vesicles (scale bar: 2 μm). **(D)** Dynamic light scattering measurement showing average hydrodynamic diameter of the vesicles to be 156.01 nm. **(E)** Stability study of the nano-vesicles using dynamic light scattering over a period of 120 d.

3.1.1.2. Stability and compatibility study of nano-vesicles for prolonged effect: The stability of the nano-carrier is crucial for it to be bio medically active and efficient. For this reason, the stability of nano-vesicles was studied to check changes in the hydrodynamic size over a period of time. The DLS study results in **Figure 3.1.2E** showed no significant increase in the hydrodynamic diameter of vesicles stored for 120 d. Following this, to confirm whether the membranous vesicles retained their original function and the adhesion molecules were still intact, the protein contents of the membranous vesicles were investigated with SDS-PAGE. **Figure 3.1.3A** shows that the membranous vesicle, MCF-7 cancer cell membrane and MCF-7 cell lysate, all exhibited similar protein profiles. For the nano-vesicles to be efficient for cancer therapy, the nano-assembly should be biologically acceptable.

Accordingly, the viability of the nano-vesicles was examined using the MTT assay, which demonstrated that the vesicular membrane itself had no anti-proliferative activity up to 73 μM treatment, indicating the biocompatible nature of the vesicles (**Figure 3.1.3B**). Studying the interaction of the nano-carrier with red blood cells is essential when the nano-carrier is used in *in vivo* experiments. For this reason, the hemocompatibility of the composite was evaluated. Interestingly, it was observed from the results shown in **Figure 3.1.3C and 3.1.3D** that the designed nano-assembly did not induce any hemolysis. As expected, visible hemolysis was seen in the Triton X-100-treated positive control.

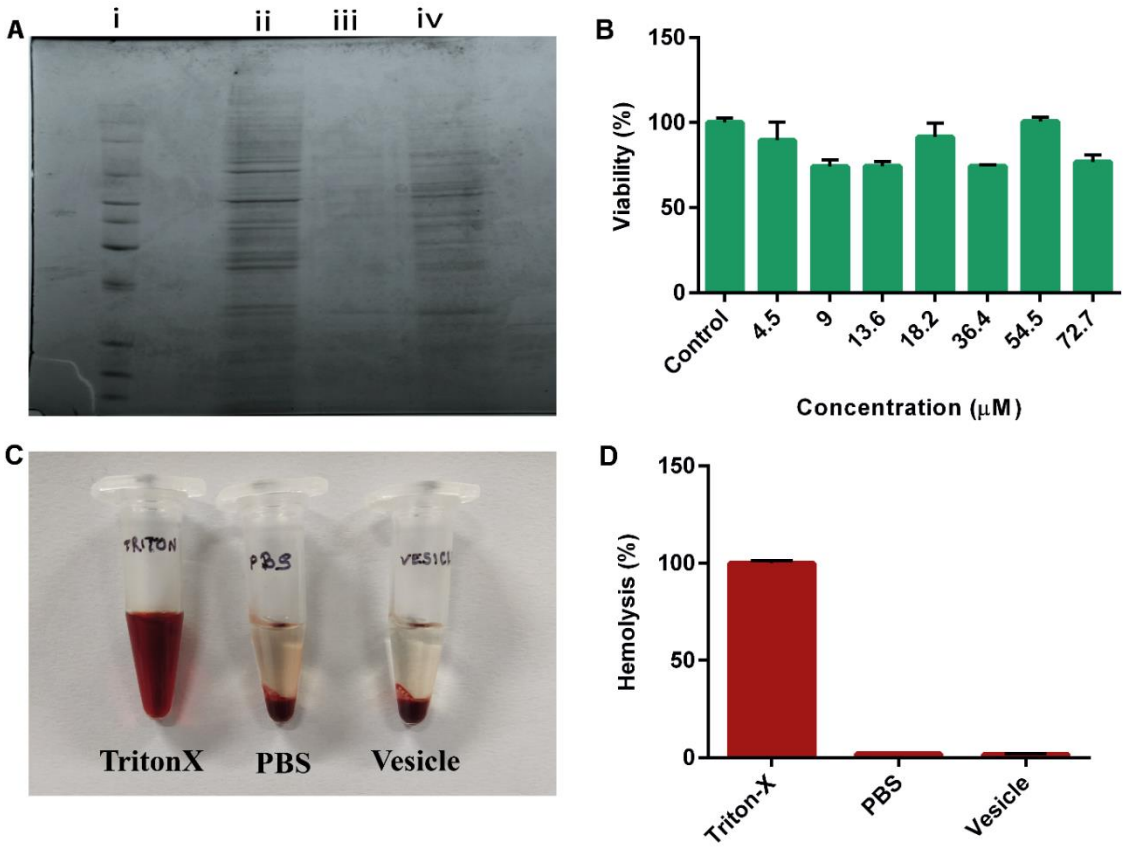

Figure 3.1.3. Stability study of MCF-7 derived nano-vesicles. (A) SDS-PAGE protein analysis of samples stained with Coomassie Blue: (i) marker, (ii) cell lysate, (iii) nano-vesicle and (iv) cell membrane. **(B)** Assessment of biocompatibility of the nano-vesicles on HEK-293 cells. **(C & D)** Assessment of hemocompatibility of the nano-vesicles.

PBS: Phosphate-buffered saline.

3.1.1.3. Homologous targeting & cellular uptake mechanism of the nano-vesicles: To further investigate the specificity of the MCF-7 cell-derived vesicular membrane, HeLa, MCF-7 and HEK-293 cells were incubated with fluorescein dye-

loaded vesicles for 7 h. The flow cytometry histograms in **Figure 3.1.4A** and **3.1.4B** show that MCF-7 has the highest uptake efficiency and fluorescence intensity as compared with HeLa and HEK-293, suggesting specific binding capability of the vesicles to MCF-7 cells. As various non-viral complexes enter mammalian cells via different endocytic pathways, it was necessary to profile the cellular uptake of the vesicular membrane-loaded drugs. The flow cytometric study found that incubation at 4°C and chlorpromazine treatment inhibited the uptake of the nano-vesicles. In contrast, there was no effect on the uptake efficiency after treating with M-β-CD (**Figure 3.1.4C**). The uptake was significantly blocked after the treatment of the cells with chlorpromazine by 48%. Additionally, the internalization of the vesicles was confirmed using confocal microscopy. As shown in **Figure 3.1.4D**, microscopic images of the MCF-7 cells manifested successful internalization of the dye-loaded vesicular membranes by the cancer cells, as evident from the green fluorescence of fluorescein inside the cells. Comparing it with nuclear staining, it was found that vesicles were localized in the cytoplasm after their uptake in the cancer cells. The internalization of the nano-vesicle was further confirmed by performing z-stacking. The green colour on the depth coding scale depicted that the fluorescein-loaded nano-vesicles were taken up by the cells (**Figure 3.1.5**).

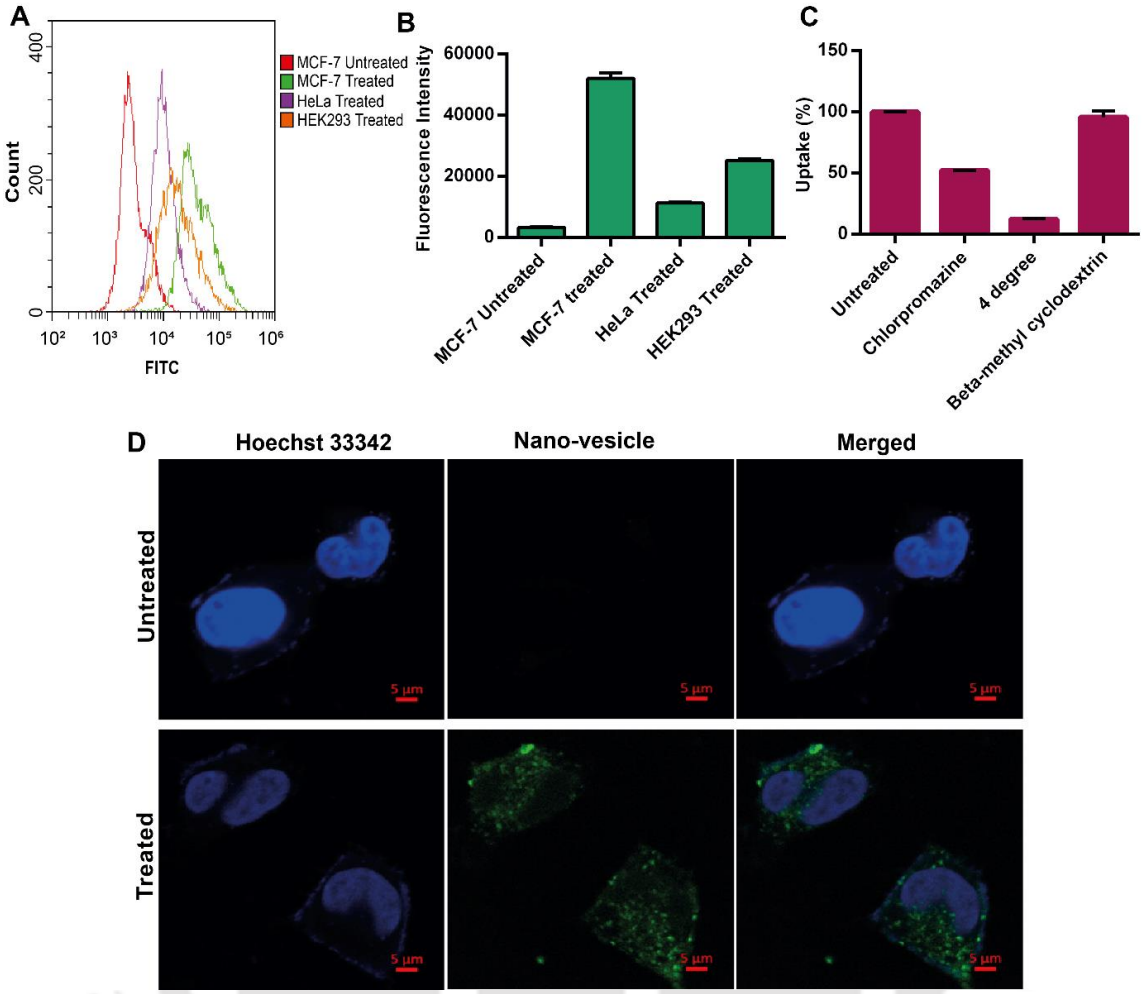

Figure 3.1.4. Uptake study of nano-vesicles. (A) Flow cytometric profiles of three cell lines (MCF-7, HeLa and HEK293) upon 7 h incubation with fluorescein-loaded nano-vesicles. **(B)** Mean fluorescence intensity of different cell lines upon internalization of the nano-vesicles. **(C)** Uptake percentage of fluorescein-loaded nano-vesicles calculated by flow cytometry after treatment of MCF-7 cells with endocytosis inhibitors. **(D)** Confocal images of MCF-7 cells showing successful internalization of nano-vesicles after treatment with fluorescein-loaded vesicles (green). Cell nuclei were stained with Hoechst 33342 (blue).

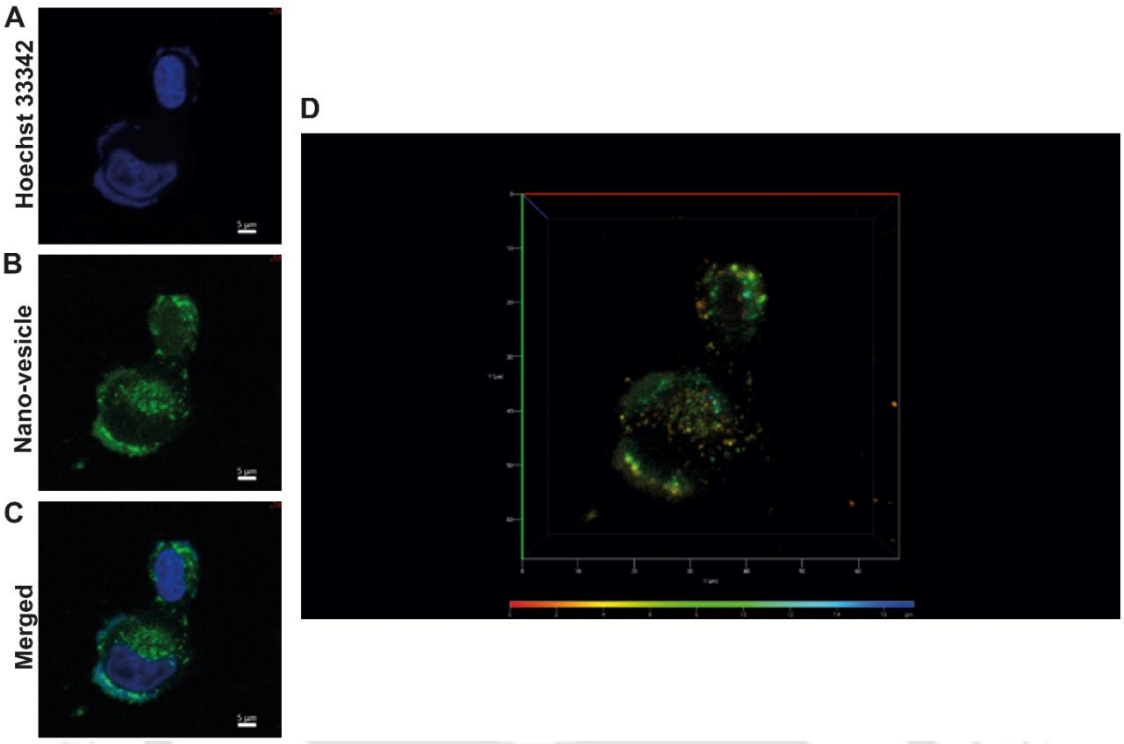

Figure 3.1.5. Confocal microscopy based cellular internalization study of MCF-7 cells treated with nano-vesicles where **(A)** blue fluorescence represents nucleus stained with Hoechst 33342, **(B)** green fluorescence represents fluorescein-loaded nano-vesicles localized in the cytoplasm, **(C)** merged image of the same and **(D)** A z-stack projection of MCF-7 cells incubated with nano-vesicle loaded with fluorescein.

3.1.1.4. Efficient induction of cytotoxicity in monolayer as well as 3D spheroids by drug-loaded nano-vesicles: Ammonium PDTC-loaded vesicles (ves@PDTC) were prepared by extrusion. The loading percentage of ammonium PDTC was found to be 55%. To evaluate the anti-cancer efficacy of ves@PDTC *in vitro*, MCF-7 and HEK-293 cells were treated with increasing concentrations of PDTC and ves@PDTC, respectively. The AlamarBlue assay results in **Figure 3.1.6A & B** reveal that the PDTC, as well as ves@PDTC, exhibited a dose-dependent

decrease in cell viability. The IC_{50} of PDTC was 35.68 µM (**Figure 3.1.6A**), while the IC_{50} of ves@PDTC was found to be 18 µM (**Figure 3.1.6B**).

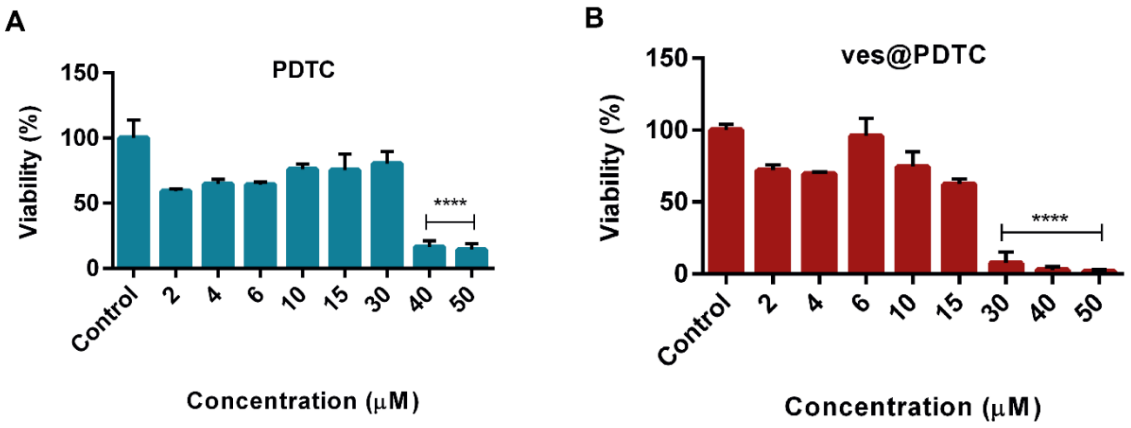

Figure 3.1.6. Assessment of cell viability upon treatment of MCF-7 monolayer cells with **(A)** PDTC and **(B)** ves@PDTC

Similarly, DOX-loaded vesicles (ves@DOX) were also prepared. Additionally, the anti-proliferative activity of DOX and ves@DOX was also analyzed (**Figure 3.1.7A & 3.1.7B**).

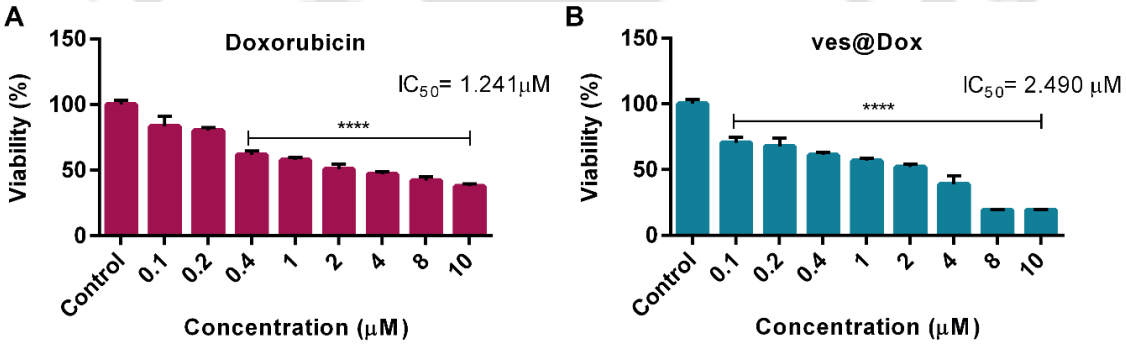

Figure 3.1.7. Assessment of cell viability upon treatment of MCF-7 monolayer cells with **(A)** Doxorubicin and **(B)** ves@Dox

Furthermore, a study conducted on the non-cancerous cells (HEK293 cell line) showed minimal cell death upon treatment with vesicle loaded drugs, which revealed the biocompatibility and stability of the vesicular membrane (**Figure 3.1.8A and 3.1.8B**). The decreased effect of the ves@PDTC on HEK293 cells suggests that the cell membrane vesicles prepared from MCF-7 cells do not have a detrimental effect on HEK293.

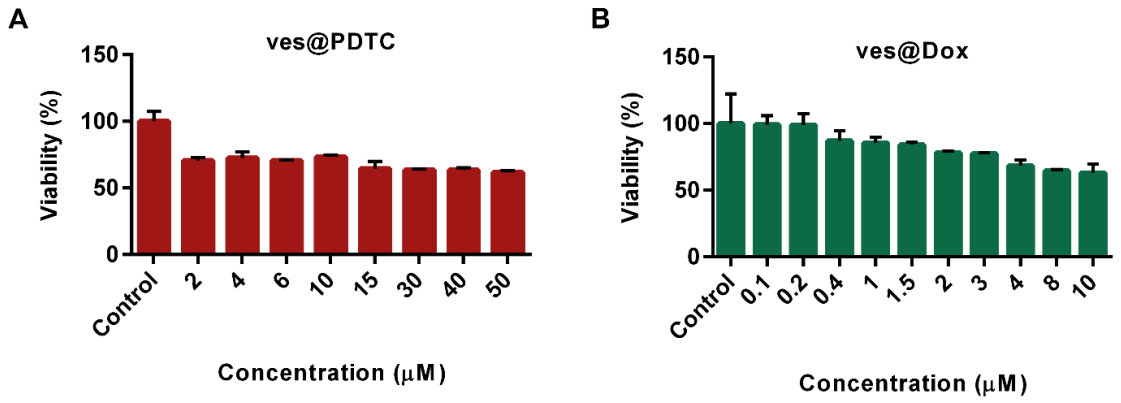

Figure 3.1.8. Assessment of cell viability upon treatment of HEK293 cells with **(A)** ves@PDTC and **(B)** ves@Dox

Because spheroids mimic the tumor micro-environment, 3D spheroids of MCF-7 cells were prepared (**Figure 3.1.9**) and our studies were extended on these models. Upon treatment of the MCF-7 spheroids with increasing concentrations of drugs and drug-loaded vesicles, the spheroids showed dose-dependent reduction in cell viability, with IC_{50} values of 13.17 and 14.25 μM for PDTC and ves@PDTC, respectively, as shown in **Figure 3.1.10A and 3.1.10B**. It was noticed that a significant decrease in concentration was required to achieve a 50% reduction of proliferation in spheroids when treated with ves@PDTC as compared with monolayer culture. This is advantageous as lower concentrations of the ammonium PDTC were required to achieve the IC_{50}.

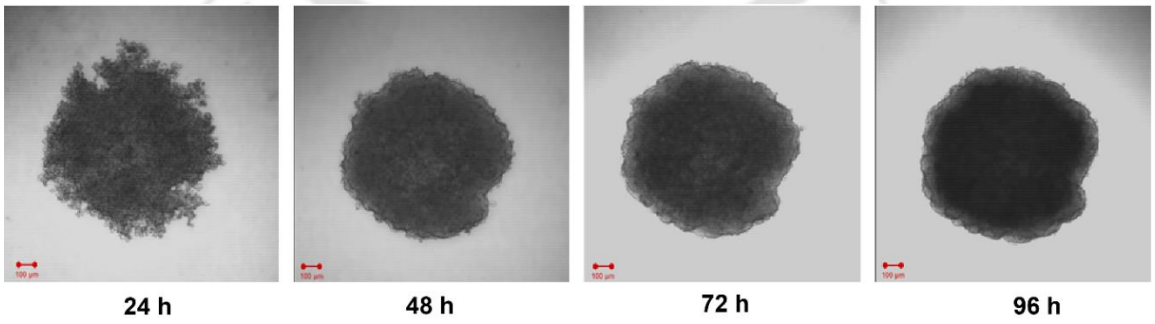

Figure 3.1.9. Microscopic images of spheroids over a period of 96 h, showing the generation of compact structure and a hypoxic core.

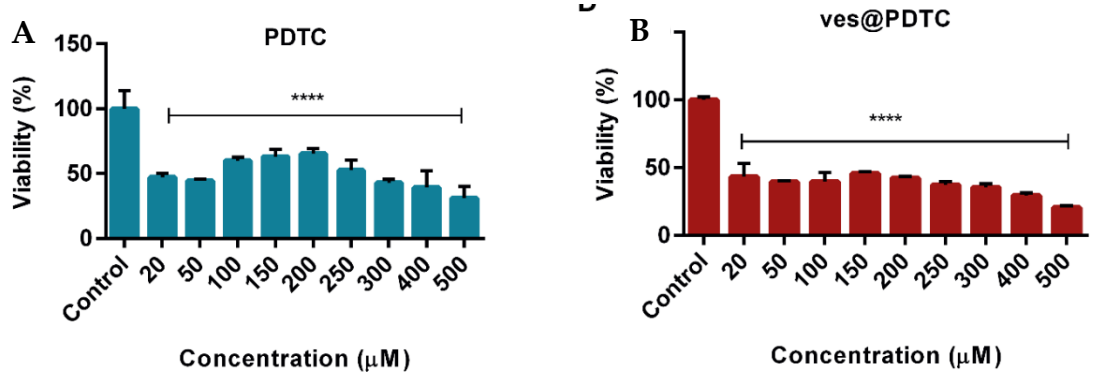

Figure 3.1.10. Assessment of cell viability upon treatment of MCF-7 spheroids with **(A)** PDTC and **(B)** ves@PDTC

The study was also conducted by treating the spheroids with DOX and ves@DOX (**Figure 3.1.11A & 3.1.11B**).

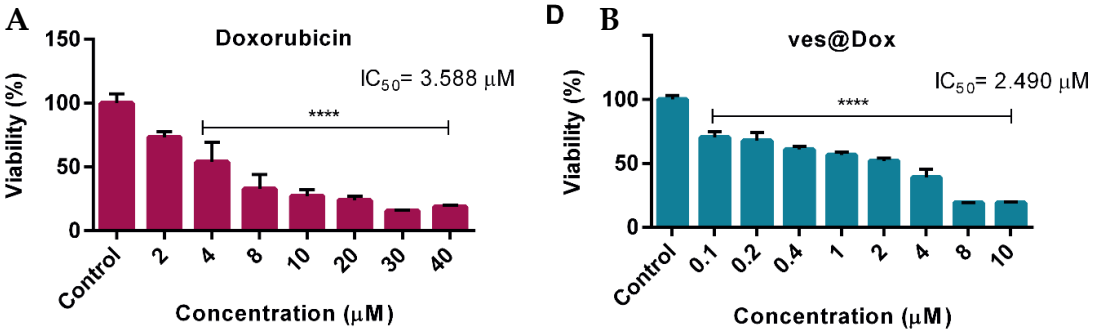

Figure 3.1.11. Assessment of cell viability upon treatment of MCF-7 spheroids with **(A)** Doxorubicin and **(B)** ves@Dox

The live–dead cell imaging of the spheroids following treatment with IC_{50} of ves@PDTC exhibited decreased calcein-AM staining, confirming the increased cell death due to ves@PDTC (**Figure 3.1.12**).

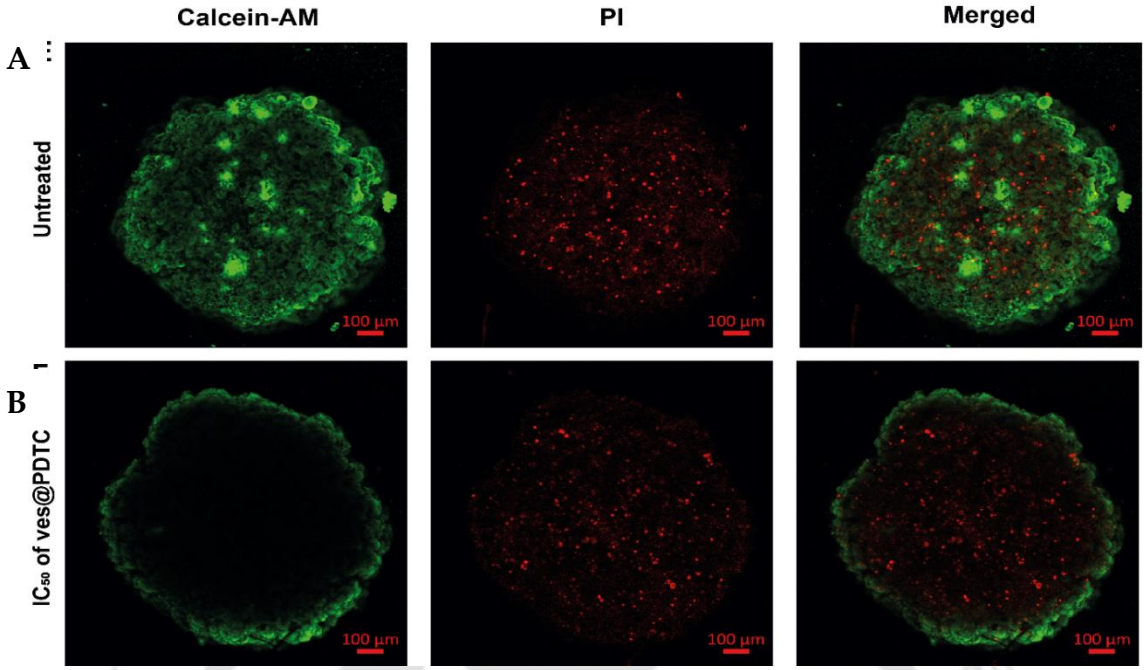

Figure 3.1.12. Live–dead cell visualization of MCF-7 spheroids using Calcein-AM/PI dual staining. Green fluorescence by calcein-AM indicates live cells whereas red fluorescence by PI shows dead cells. **(A)** Untreated spheroids. **(B)** Spheroids treated for 72 h with IC_{50} of ves@PDTC.

3.1.1.5. Induction of apoptosis by drug-loaded nano-vesicles: The viability assays on monolayer and 3D spheroids showed that the vesicles were able to deliver the drug molecules inside the cells, which resulted in a dose-dependent reduction of cell viability. Analysis of Annexin V–FITC–PI stained cells by flow cytometry revealed the efficient induction of apoptosis in approximately 22% of the treated MCF-7 cells (**Figure 3.1.13**). The analysis also exhibited a very low necrotic population (<0.2%) after treatment with PDTC as well as ves@PDTC,

thereby indicating the potential of the nano-vesicles killing the cancer cells without having adverse effects, which is essential for effective cancer therapy.

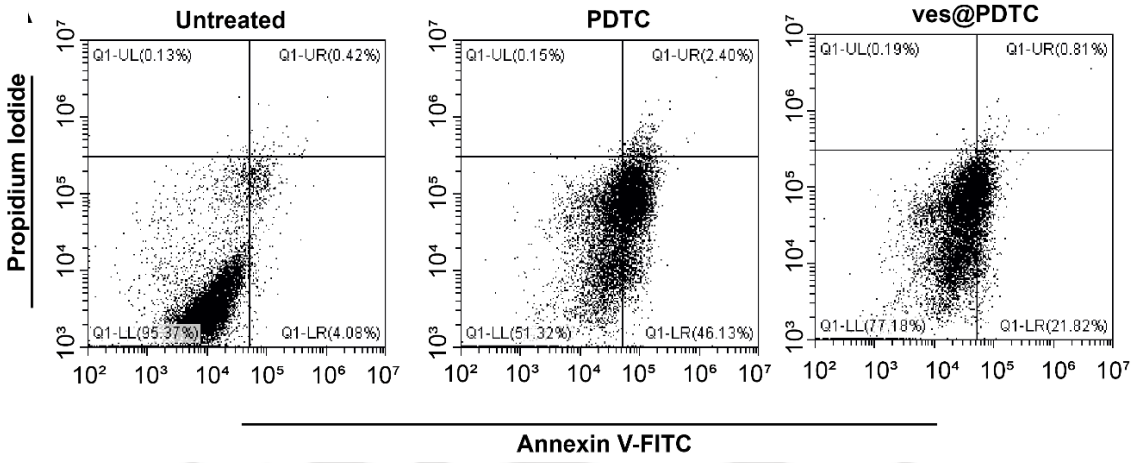

Figure 3.1.13. Flow cytometric assessment of the apoptosis in ves@PDTC treated cells. Annexin V–FITC–PI-based flow cytometric determination of apoptosis in MCF-7 cells treated with IC_{50} concentrations of free ammonium PDTC and ammonium PDTC-loaded nano-vesicles.

FITC: Fluorescein Isothiocyanate; PDTC: Pyrrolidine Dithiocarbamate; PI: Propidium Iodide.

3.1.1.6. Generation of ROS: The DCF-DA assay confirmed the generation of the ROS inside the cells after treatment with ves@PDTC. Cleavage of non-fluorescent DCF-DA by ROS resulted in the production of green fluorescent 2,7-dichlorofluorescein, which indicated a rise in ROS levels, eventuating the mechanism of programmed cell death or apoptosis. Flow cytometric analysis of MCF-7 cells following treatment with IC_{25} and IC_{50} of ves@PDTC showed upregulation in ROS levels compared with untreated cells, triggering apoptosis (**Figure 3.1.14**).

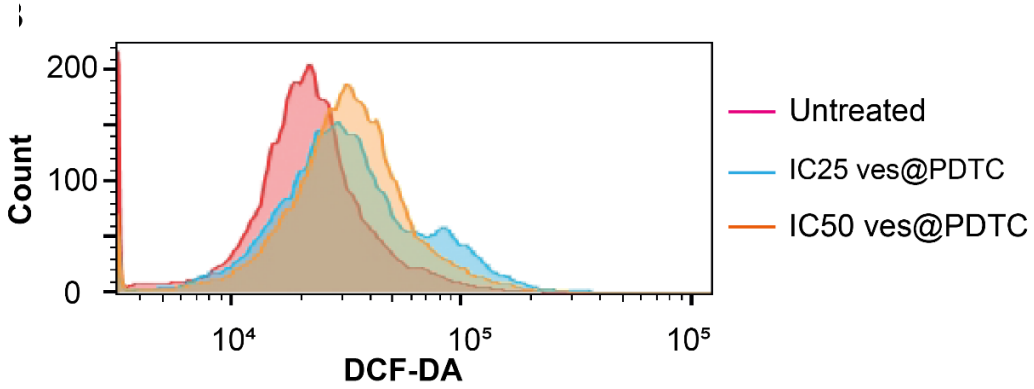

Figure 3.1.14. DCF-DA assay for the detection of generation of reactive oxygen species after treatment of MCF-7 cells with IC_{25} and IC_{50} concentrations of nano-vesicle-loaded ammonium PDTC.

DCF-DA: Dichlorodihydrofluorescein diacetate

3.1.2 Discussion: In this study, a biological nano-carrier for specific targeting and delivery of drugs for cancer therapy was developed. The stability of the nano-vesicles is the aspect that should be of most importance. This paper proposes making nanocarriers from cancer cell membranes that can be used to target the cancer cells due to their homotypic mechanism. Particular attention was paid to making a biocompatible, biodegradable and cancer cell-targeting nano-vesicle without the use of any synthetic materials. As extrusion method was used to make the nano-vesicles from the cancer cell membrane, the ability to make nano-vesicles of the desired size was an advantage over other chemically prepared nanocarriers [98]. The *dH* of the vesicular membranes was higher than the average particle size found in FETEM analysis, which could be due to the formation of a hydration layer at the surface of the vesicular membranes in aqueous dispersion. During the stability studies, it was seen from the DLS measurement that the size of the nano-vesicles did not change immensely even after 120 d of storage. This excellent stability of the vesicles could be due to the liposome-type structure of the bilayer-arranged phospholipids. The surface potentials of the vesicle and intact cell membrane were similar, which confirms that the vesicles retain the proteins from the cell membranes. Our experiments are consistent with previous results, where the reduction of the membrane to a nanometre-sized vesicle does not change the surface potential [99]. Previous studies have shown that the presence of the membrane proteins on the vesicles is essential to incorporate all cell membrane properties into nano-vesicles [100]. The similar protein profile of the nano-vesicles with the cell lysate and membranes confirmed the integrity of the proteins from MCF-7 cells to nano-vesicles (**Figure 3.1.3A**). The results are consistent with the earlier studies reporting that proteins from cell membranes are retained on the surface of vesicles [101]. The presence of the parent proteins and ligands on the surface could help these vesicles to locate the target cells and help in fusing with them for the drug to be delivered [75].

In addition, it was observed that the nano-vesicles were biocompatible (**Figure 3.1.3B**) as well as hemocompatible (**Figure 3.1.3C** and **3.1.3D**). Blood is an essential biological fluid for the transport of nanoparticles to their specific target tissues, with its three constituents – erythrocytes, platelets and leucocytes – playing their respective unique roles. If the synthesized nanoparticles are not hemocompatible, they may pose a detrimental threat to the process of hemostasis [102]. It was observed that our synthesized nano-vesicle is stable, as well as biologically compatible, thereby making it a suitable nano-carrier for further studies. Similar results have been observed in our previous studies with cell membrane-coated nanoparticles [100].

Furthermore, on incubating the fluorescein-loaded nano-vesicles with homologous and heterologous cells, it was observed that the nano-vesicles had a higher affinity towards homologous cells thereby, proving their specificity and efficiency for targeted delivery. In our study, the nano-vesicles were prepared from MCF-7 cells and this was the sole reason that MCF-7 cells showed maximum uptake (**Figure 3.1.4A** and **3.1.4B**). The presence of similar cell adhesion molecules and recognition proteins like N-cadherin and EpCAM on the cellular surface resulted in enhanced homotypic uptake of the nano-vesicles by homologous tumor cells [73]. Owing to the presence of these molecules, homotypic cancer cells tend to aggregate during metastasis and this behaviour plays an important role in the initiation of secondary tumors in distant tissues or organs [74]. Previous studies using cell membranes also showed that when magnetic iron oxide nanoparticles were coated with membranes derived from human squamous carcinoma (UM-SCC-7), they could specifically target the UM-SCC-7 tumor cells in the *in vivo* model [75]. The endocytic pathway study exhibited that the cellular membrane vesicle internalization process was an active (energy-dependent) process. The vesicles were mostly taken up by the clathrin-mediated pathway (**Figure 3.1.4C**). Earlier studies have shown that nano-vesicles synthesized from human bone marrow-derived mesenchymal stem cells (MSC) enter into the macrophages via

clathrin- mediated endocytosis. When dynamin was inhibited, it disrupted the internalization of the membrane-derived nano-vesicles inside the cells [103]. Recent studies showed that a cancer cell membrane coating over a nanoparticle results in targeted delivery of the nanoparticles [104]. Further experiments on the internalization with confocal imaging of the cells treated with loaded nano-vesicles showed that the vesicles were localized in the cytoplasm, confirming the successful uptake of these nanocarriers by their parent cells (**Figure 3.1.4D**).

The cytotoxic study of MCF-7 cells treated with nano-vesicle-loaded drugs (**Figure 3.1.6B**) showed that the delivery of the drug via nano-vesicles results in an increased effect at a much lower concentration as compared with the free drug for monolayers. Although the 2D monolayer cultures are a common and convenient way of testing drugs in *in vitro* culture, they lack cell-to-cell interactions. The functionality of each cell is dependent upon the interaction with its neighbouring cells. 2D cultures lack the tumor microenvironment, which is an essential factor for tumor signaling and drug response. Spheroids are 3D systems, which serve as a model for tumors in their architecture as well as their responsiveness toward drugs [105]. Thus, the cytotoxicity study was carried out in 3D spheroids as well, which also showed enhanced anti-proliferative activity for ves@PDTC (**Figure 3.1.10B**). Although the PDTC shows a biphasic effect on cell viability, as observed by Chung *et al.* [106], the significant anti-proliferative action of the PDTC after loading into vesicles was recorded. This could be ascribed to the increased accumulation of PDTC due to the targeted delivery to the MCF-7 cells, resulting in increased activity. This variation in concentration to achieve 50% inhibition demonstrates the difference in responses between 2D and spheroid cultures; spheroids closely resemble *in vivo* tumors and thus impart biological significance to the findings. The accumulation of the drug due to the targeted nature of the carrier causes biomolecular changes inside the cell. Among these, ROS have a significant role in the induction of apoptosis as well as in various physiological processes [107]. An increase in ROS levels is an indication of damage of proteins and nucleic acids, and

disruption of membranes and various other organelles, resulting in the activation of apoptosis [108]. The increase in ROS levels upon treatment of the cells with drug-loaded nano-vesicles proved the disruption of the cells by programmed cell death (**Figure 3.1.14**), which was further confirmed by apoptosis assay (**Figure 3.1.13**).

Based on the above discussion, it is rational to suggest that the synthesized biomimetic nano-vesicles are highly efficacious for delivering drugs to their specific targets by recognizing their own cell type without being taken up by other heterologous cells.

3.1.3 Conclusion: Development of a membranous nano-vesicle that exhibited excellent biocompatibility and enhanced internalization ability was the main aim of this study. The nano-vesicles synthesised from MCF-7 cells, a breast cancer cell line, exhibited a very efficient self-homing capabilities towards its parental cells *i.e.* MCF-7 cells. The stability of the DOX- and ammonium PDTC-loaded membranous vesicle was also confirmed. Additionally, vesicular membrane-loaded PDTC exhibited anti-proliferative activity at lower doses than free PDTC. Furthermore, a dose-dependent anti-proliferative effect and a biphasic behaviour of the compound (ammonium PDTC) were also observed. Generation of ROS in cells treated with the vesicular membrane loaded with PDTC implied regulated cell death via nucleic acid damage or membrane disruption of the cancer cells. This approach has a wide future application in different cancers. The parent cell-derived membranous vesicle may serve as an excellent self-targeting, tumor-specific nanosystem for potential anticancer therapy *in vivo*.

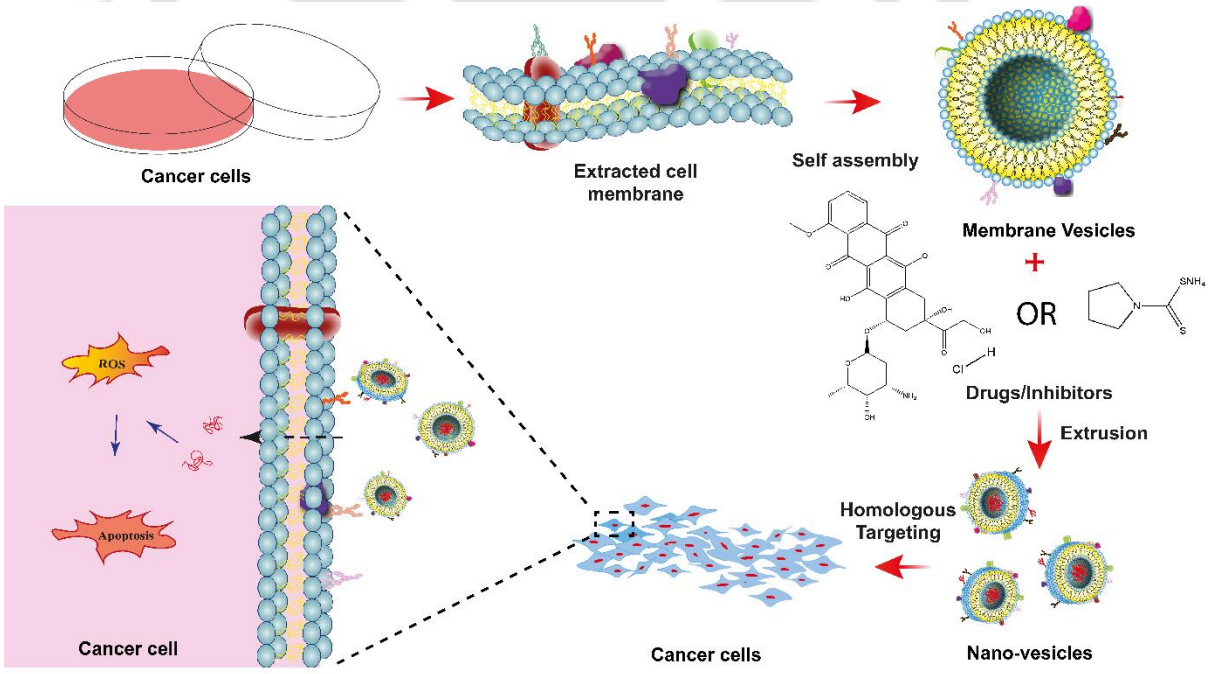

Scheme 3.1: Schematic illustration of self-homing capability of nano-vesicles developed from breast cancer cell line for efficient targeting of parental cancer cells [***Nanomedicine***, *16*(21), 1843-1856, 2021]

3.2. Targeting tumor microenvironment of metastatic TNBC cells via exosomes derived from non-invasive breast cancer cells for MDR inhibition and enhancing drug susceptibility

(Manuscript Under Revision)

Abstract: The current challenging situation in the domain of oncology is to develop an effective targeted anti-cancer therapy. Approximately 15% of the metastatic breast cancer is attributed to TNBC and the main hurdle in its efficacious treatment is the lack of proper targets as they are negative for ER, PR and HER2. Several efforts are being made for the development of drugs, aiming the multifaceted chemoresistance nature of TNBC. Among the various mechanisms leading to drug resistance, transporter mediated drug efflux has been found to be the main driving force. In this study, MDA MB-231, a TNBC cell line was targeted with exosomes derived from MCF-7, a non-invasive breast cancer cell line, to modulate the tumor niche of the metastatic cells. There was ~1.6 fold increase in ROS generation and an S-phase arrest in the cell cycle following treatment with exosomes. Gene expression analysis exhibited that the cargoes and receptors of the exosomes resulted in the down regulation of the MDR receptors with ~0.7 fold decrease in BCRP expression along with the decrement in the expression of the EMT markers like Vimentin and TWIST1 by ~0.7 and ~0.8 respectively. An increase in drug susceptibility in metastatic TNBC cell line following treatment with Lapatinib, a tyrosine kinase inhibitor in combination with exosomes was also observed. The current strategy makes the metastatic breast cancer cells, MDA MB-231 more susceptible to drugs, thereby resulting in effective anti-cancer therapy.

3.2.1 Results:

3.2.1.1. Efficient isolation and characterizations of exosomes: Various methods have been described by the researchers for its isolation with its own pros and cons. Isolation of exosomes using three different methods namely, ultracentrifugation, size-exclusion chromatography and polymer precipitation method was attempted. It was observed that modified polymer precipitation method yielded highest concentration of exosomes with minimal use of high-end equipment or rigorous downstream processing. Exosomes were isolated successfully using polymer precipitation method (**Figure 3.2.1**) which was further confirmed by FETEM and Western Blot analysis. The presence of the surface markers CD9 and Alix confirmed the successful isolation of exosome from MCF-7 cell lines (**Figure 3.2.2A**). The exosomal morphology were supported by FETEM images as shown in **Figure 3.2.2B**. The FETEM analysis of the exosomes revealed that the extracellular vesicles were roughly spherical in shape and have an average diameter of 42.03 nm as analysed by ImageJ software (**Figure 3.2.2C)**. The zeta potential of the isolated exosomes was determined to be -1.8 mV and the average hydrodynamic diameter was found to be 191.1 nm (**Figure 3.2.2D**).

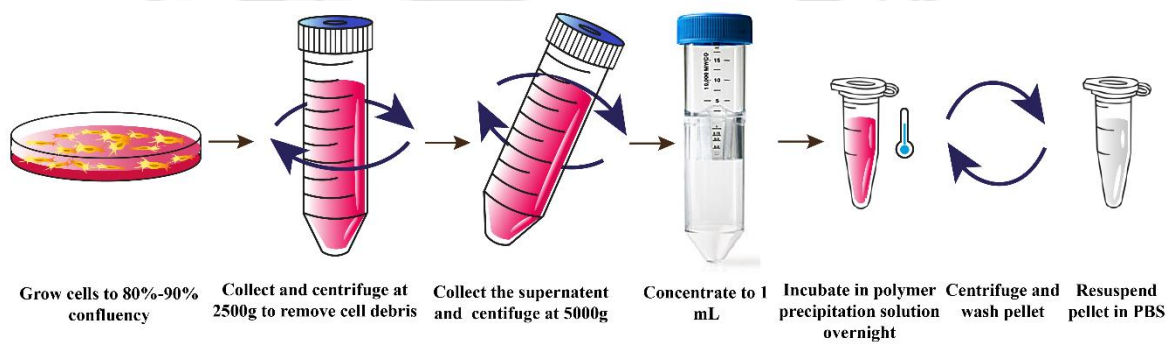

Figure 3.2.1. Isolation of exosomes from cell culture supernatant by polymer precipitation method

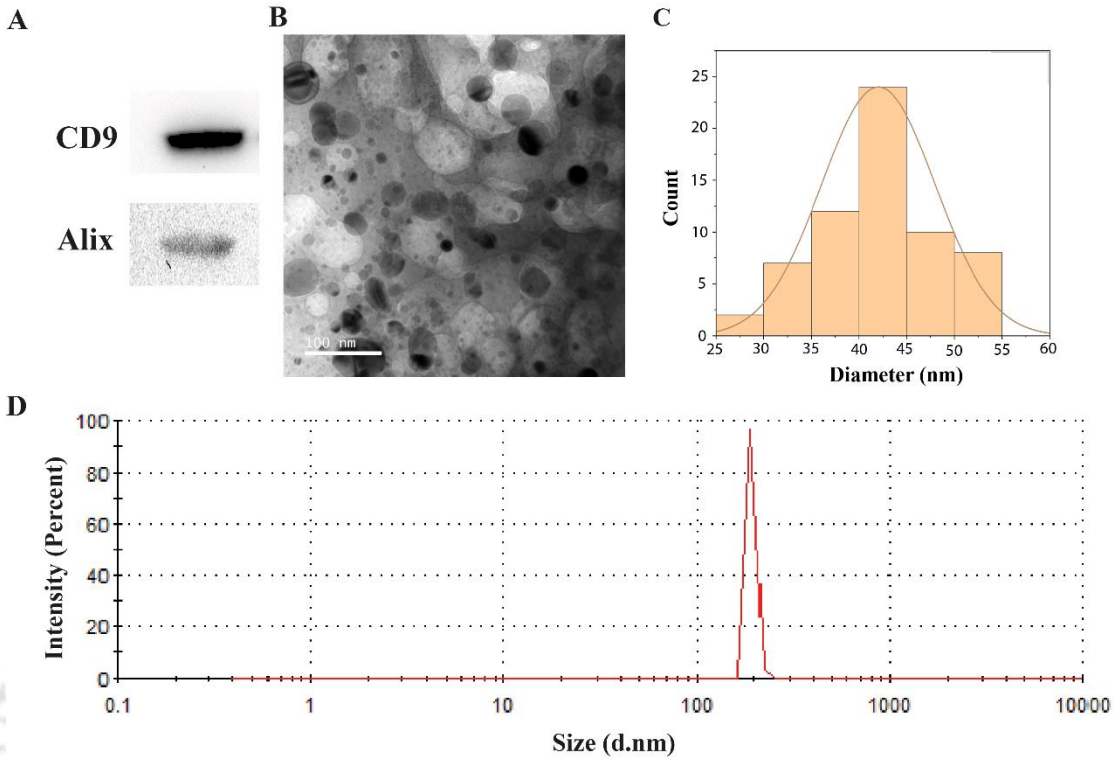

Figure 3.2.2. Characterisation of isolated exosomes **(A)** Western blot analysis proving the presence of the surface markers CD9 and Alix, **(B)** FETEM images showing the spherical shape and size of the exosomes, **(C)** Size distribution graph of the exosomes from FETEM images and **(D)** Dynamic Light Scattering analysis showing the average hydrodynamic diameter of the exosomes.

3.2.1.2. Cytotoxicity index of empty exosomes on TNBC cells: To check the effect of the isolated exosomes alone, uninduced and EMT induced MDA MB-231 cells were treated with exosomes in increasing concentrations. Although no evident cytotoxicity was observed in uninduced MDA MB-231 cells (**Figure 3.2.3A**), however, the empty exosomes exhibited some cytotoxic effect on the EMT induced TNBC cells. Though IC_{50} wasn't obtained even after treatment with the

higher doses, the cells remained ~52% viable following treatment with the upper limit of the exosome concentration i.e 20 µg/mL as depicted in **Figure 3.2.3B**.

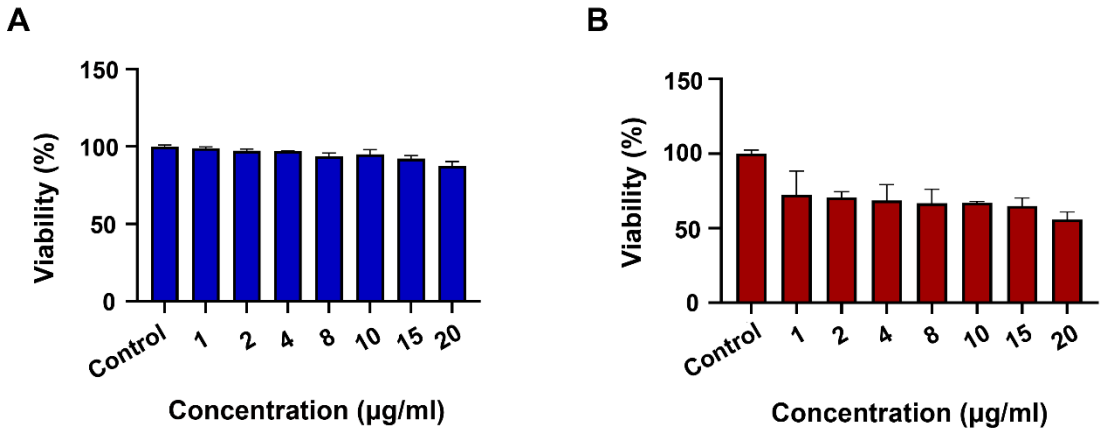

Figure 3.2.3. Cytotoxicity analysis of the **(A)** uninduced and **(B)** EMT induced MDA MB-231 cells following treatment with exosomes revealed decrease in cell viability in EMT induced MDA MB-231 cells.

3.2.1.3. Effect on the wound healing ability of TNBC cells: During the process of epithelial-to-mesenchymal transition, the morphology of the epithelial cells gets transformed into mesenchymal ones, thereby resulting in enhanced migration and invasion ability leading to metastatic behavior. Since the exosomes were isolated from non-invasive breast cancer (nBC) cell lines, the outcome of exosomes on the wound healing ability of TNBC, MDA MB-231 was examined.

Though there was no significant cytotoxicity observed in uninduced MDA MB-231 cells, nevertheless, a slower wound healing ability was detected following

treatment with the highest concentration of exosomes possible as compared to the untreated ones (**Figure 3.2.4**).

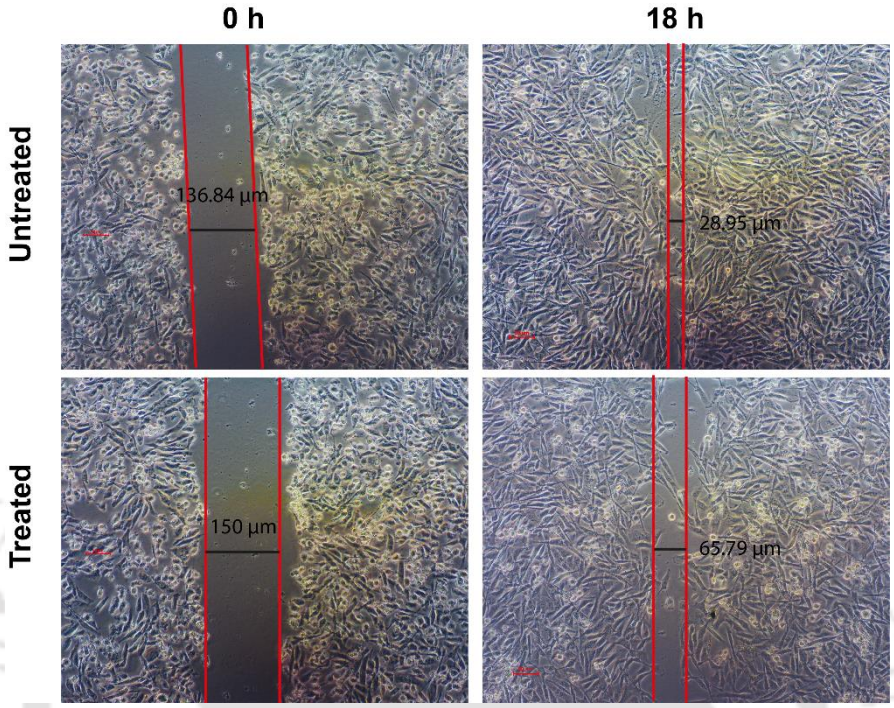

Figure 3.2.4. Scratch wound healing assay showed a decrease in the migration ability of MDA MB-231 cells after treatment.

The EMT induced MDA MB-231 (iMDA MB-231) cells treated with the exosomes derived from MCF-7 cells, resulted in observable diminution in wound repair potential suggesting the exosomes have the ability to reduce the migration capability of the metastatic breast cancer cell lines (**Figure 3.2.5**).

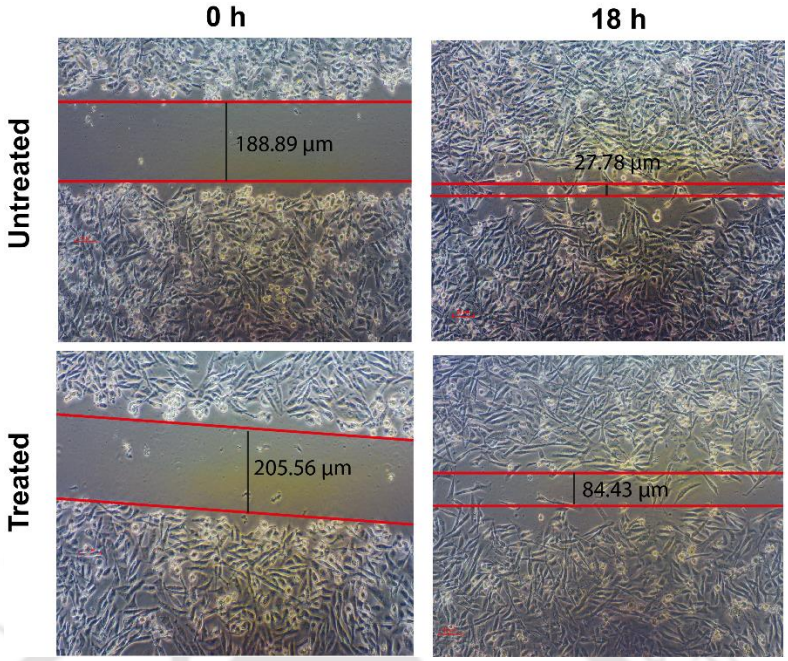

Figure 3.2.5. Scratch wound healing assay showed a decrease in the migration ability of the iMDA MB-231 cells following treatment with exosomes.

Live-dead cell imaging of MDA MB-231 cells showed a very minimum decrease in the green fluorescence (live cells) (**Figure 3.2.6**) in uninduced MDA MB-231 cells after treatment with exosomes isolated from MCF-7 cells, corroborating the observations of cell viability assay (**Figure 3.2.3A**).

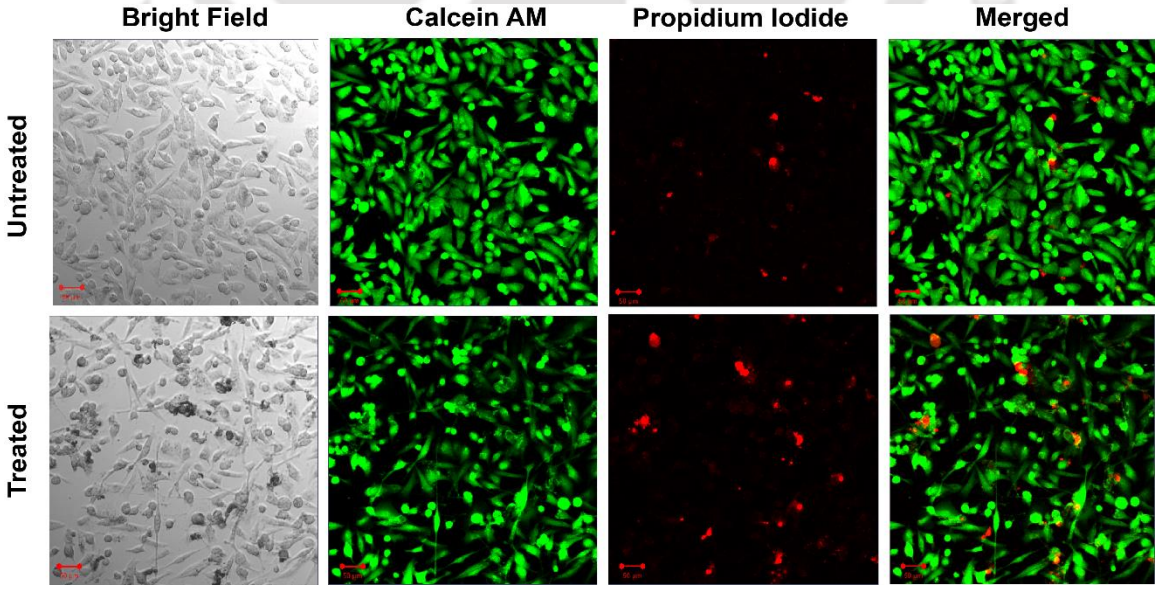

Figure 3.2.6. Live-dead cell imaging demonstrated minimal decrement in green fluorescence (live cells) after 48 h of exosome treatment in MDA MB-231 cells.

After treatment for 48 h time duration, live-dead cell image analysis demonstrated an efficient decrement in the fluorescent intensity of Calcein AM (green) with slight increment in the red fluorescence by PI (**Figure 3.2.7**) in EMT induced MDA MB-231 cells.

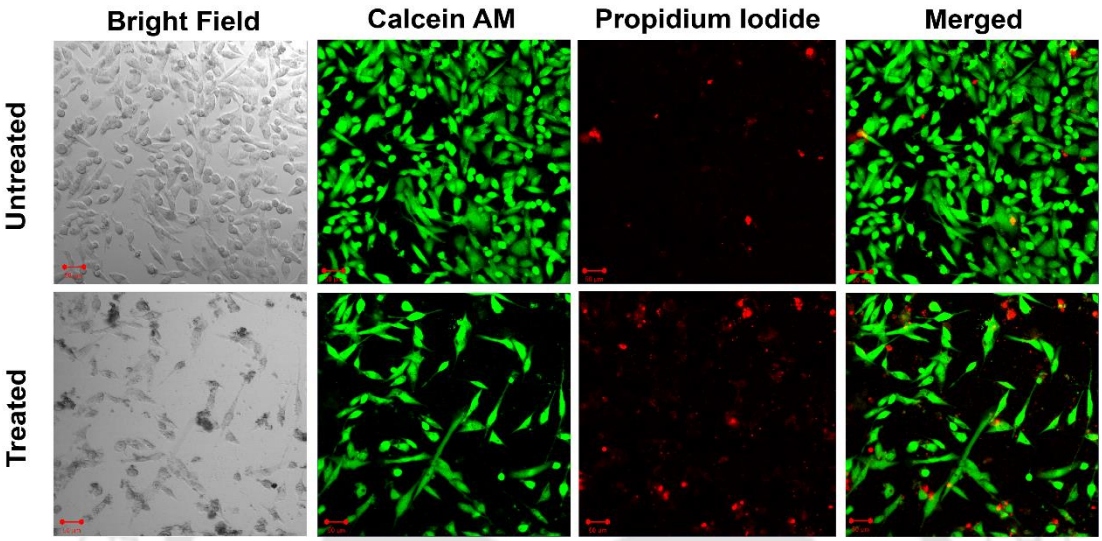

Figure 3.2.7. Live-dead cell imaging demonstrated observable decrement in green fluorescence (live cells) after 48 h of exosome treatment in iMDA MB-231 cells.

3.2.1.4. Reactive Oxygen Species (ROS) generation: Though we didn't observe any evident cytotoxic effect of the exosomes on the uninduced TNBC cell line, MDA MB-231, DCF DA assay was performed in order to explore the effect of exosome treatment on the generation of reactive oxygen species (ROS) by staining the cells with DCF-DA dye and analysing by flow cytometry. Flow cytometric analysis revealed that there was increment in the ROS generation by ~1.2 fold following treatment with exosomes for 6 h (**Figure 3.2.8**).

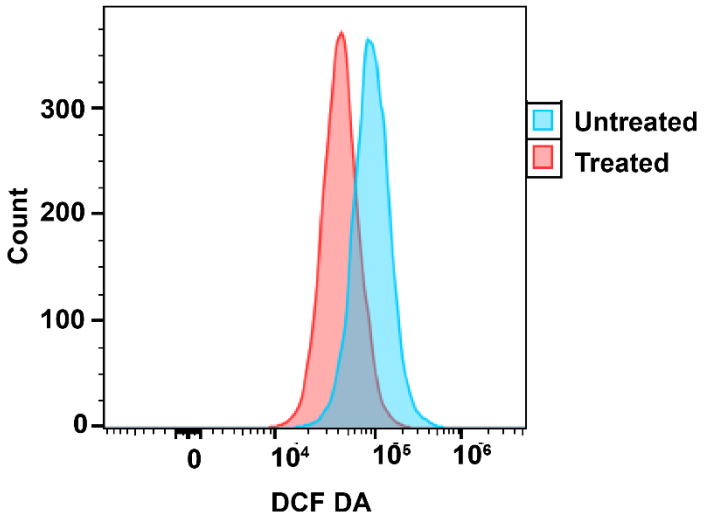

Figure 3.2.8. Evaluation of ROS by DCF DA assay in MDA MB-231 cells showed an increase in the generation of ROS following treatment with exosomes for 6 h.

Evaluation of iMDA MB-231 cells by flow cytometry for the formation of reactive oxygen species exhibited an increase in the formation of ROS subsequent to treatment with the exosomes isolated from MCF-7 cell lines for 3 h. There was almost 1.6 fold increase in the ROS formation in comparison to the untreated cells (**Figure 3.2.9**).

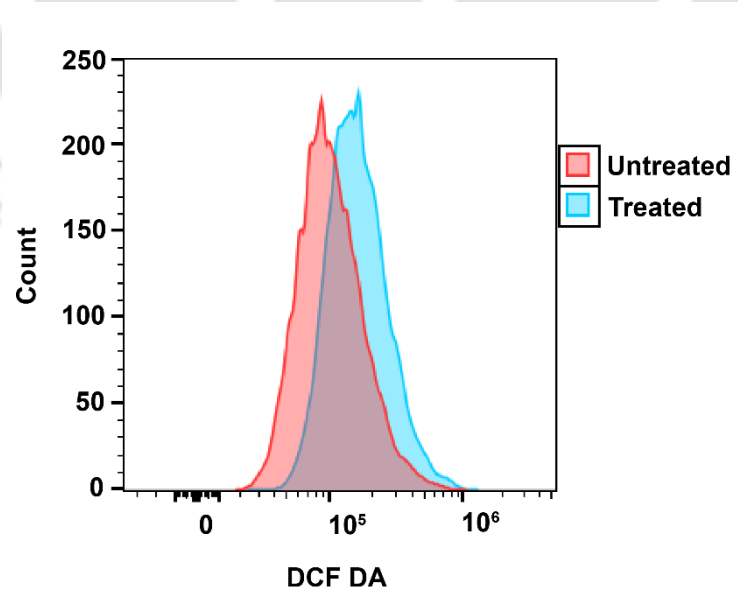

Figure 3.2.9. Evaluation of ROS by DCF DA assay in iMDA MB-231 cells depicted an increase in the ROS generation following treatment with exosomes for 3 h.

3.2.1.5. Cell cycle analysis: To understand the consequence of exosome treatment on TNBC cells, cell cycle analysis was performed for a time duration of 48 h treatment. An S-phase arrest was observed in iMDA MB-231 cells, thereby resulting in decrease in cell proliferation. The percentage of S-phase enhanced by ~21% when the cells were treated with exosomes, whereas, there was a ~37.5% decrease in the G0/G1 phase following treatment as depicted in **Figure 3.2.10**. A small degree of G2/M phase arrest indicating damage of intracellular DNA which is irreparable, was also ascertained. Hence, exosomes result in the alteration in the progression of cell cycle in metastatic TNBC cell line, MDA MB-231 following treatment.

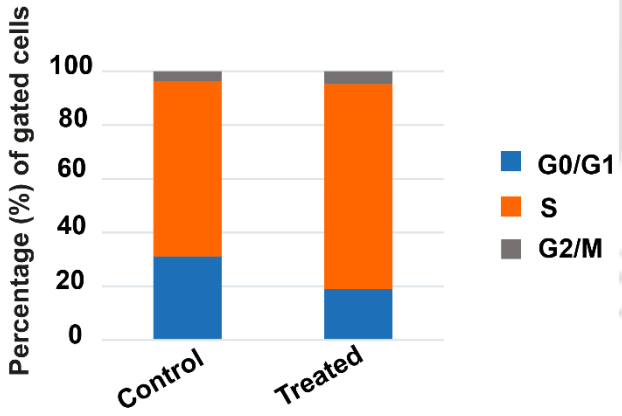

Figure 3.2.10. Flow cytometric evaluation of cell cycle of the iMDA MB-231 cells showed an S-phase arrest after treatment.

3.2.1.6. Alteration in the expression of ABC transporters and EGFR subsequent to treatment with exosomes: The MDR genes like ABC transporters and EGF receptor (EGFR) are usually overexpressed in chemoresistant and drug resistant cells like MDA MB- 231 cells, a metastatic TNBC cell line. The immunocytochemistry imaging showed a decrease in the intensity of red fluorescence for MDR1 (**Figure 3.2.11A**) and EGFR (**Figure 3.2.11B**) following treatment of iMDA MB-231 cells with exosomes from nBC cells thereby depicting a decrement in the expression of these genes.

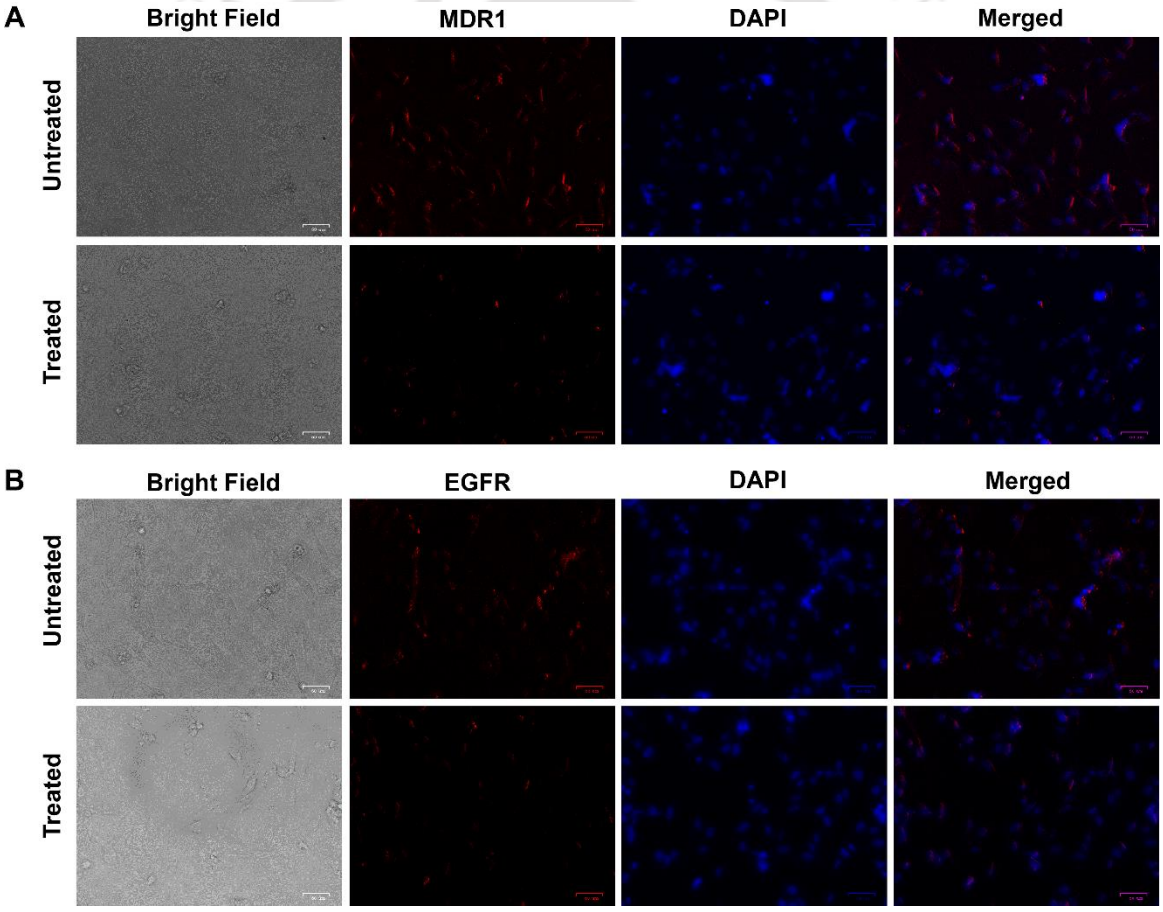

Figure 3.2.11. Immunofluorescence images revealed a decrease in the expression of the **(A)** ABC transporter gene MDR1 and **(B)** EGFR after treatment of the iMDA MB-231 cells with exosomes isolated from nBC cell, MCF-7.

ABCB1, ABCC1 and ABCG2 are the primary transporters affiliated to the multi-drug resistance ability of the metastatic TNBC cells to cancer chemotherapy. The mRNA expression studies, following treatment of uninduced cells with exosomes from MCF-7 cells, demonstrated a decrease in the expression of ABC transporter genes, MDR1 by ~0.7 fold and MRP1 and BCRP by ~0.3 fold each, thereby proposing an efficient effect of the exosomes on the ABC transporter genes (**Figure 3.2.12**). The fold change has been summarized in **Table 3.2.1.**

Genes	Fold change
MDR1	0.7
MRP1	0.3
BCRP	0.3

Table 3.2.1. Fold change in the expression of ABC transporters of uninduced MDA MB-231 cells following treatment with exosomes.

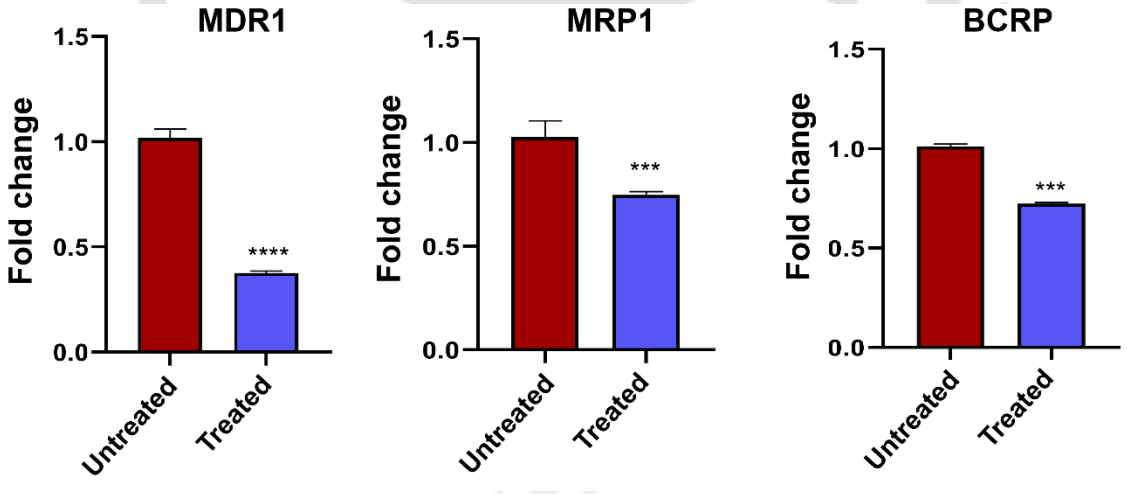

Figure 3.2.12. Graphical representation of the alterations in gene expression reveal a decrease in the ABC transporter genes.

We further observed that upon treatment of the uninduced MDA MB-231 cells with the exosomes, there was downregulation of the EMT markers N-cadherin, vimentin and fibronectin by ~0.4, ~0.3 and ~0.4 fold respectively (**Figure 3.2.13**). There was also an upregulation in the expression of E-cadherin by ~1.5 fold (**Figure**

3.2.13) suggesting suppression of metastatic behavior of MDA MB-231 cells. The fold change exhibited by the EMT markers has been summarized in **Table 3.2.2.** However, we didn't observe any significant change in the expression of TWIST1 and SNAI1 after treatment (not shown), contrary to the observations in EMT induced MDA MB-231 cells (**Figure 3.2.15**).

Genes	Fold change
E-cadherin	1.5
N-cadherin	0.4
Vimentin	0.3
Fibronectin	0.4

Table 3.2.2. Fold change in the expression of EMT markers of uninduced MDA MB-231 cells following treatment with exosomes.

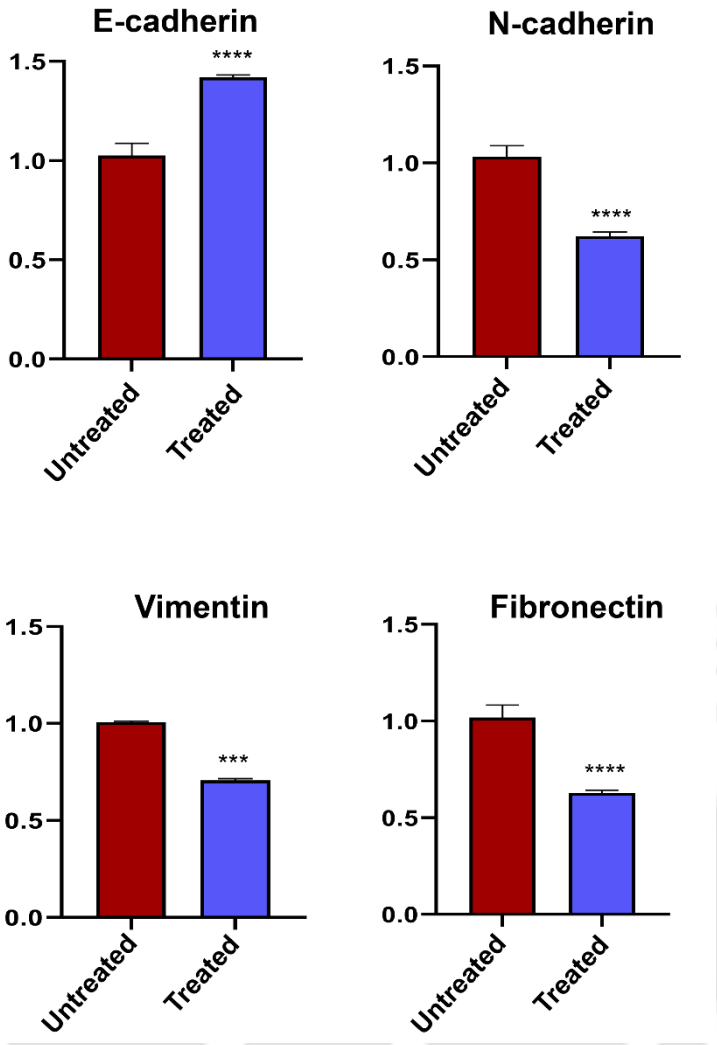

Figure 3.2.13. Graphical representation of the alterations in gene expression reveal an increase in the epithelial marker, E-cadherin, whereas a decrease in the EMT markers, N-cadherin, Vimentin and Fibronectin.

Our mRNA expression studies of iMDA MB-231 cells following treatment with exosomes isolated from non-invasive MCF-7 cell lines have resulted in the decrease in the expression of the ABC transporters. There was ~0.3-fold decrease in the expression of MDR1 and MRP1 each and ~0.7-fold decrease in the expression BCRP (**Table 3.2.3**), thereby indicating the effect of the exosomes on TNBC cells in lowering the drug efflux ability of the chemoresistant breast cancer cell line (**Figure 3.2.14)**.

Genes	Fold change
MDR1	0.3
MRP1	0.26
BCRP	0.7

Table 3.2.3. Fold change in the expression of ABC transporters of iMDA MB-231 cells following treatment with exosomes

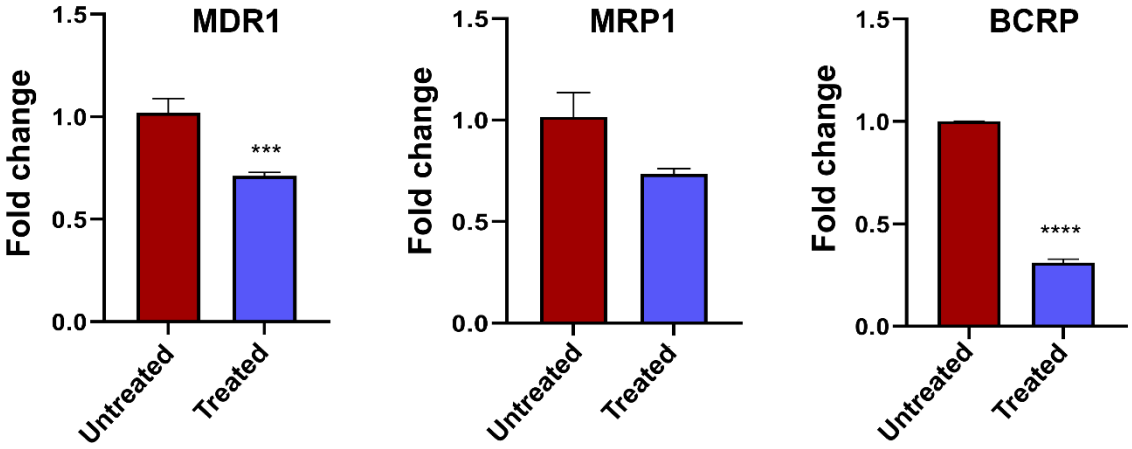

Figure 3.2.14. Graphical representation of the alterations in gene expression reveal a decrease in the ABC transporter genes in EMT induced MDA MB-231 cells.

In addition to the change in expression of the ABC transporters, it was also observed that there was a modest decrease in the expression of the EMT markers, N-cadherin by ~0.2 fold and SNAI1 by ~0.3 fold, and an efficient decrease in the expression of Vimentin and TWIST1 by ~0.7 and ~0.8 fold, respectively (**Figure 3.2.12)**. There was also a substantial increment in the expression of the epithelial marker, E-cadherin by ~2 fold thereby, indicating the reversal of EMT to MET to a significant extent following treatment with empty exosomes (**Figure 3.2.15)**.

Genes	Fold change
E-cadherin	2.2
N-cadherin	0.2
Vimentin	0.65
TWIST1	0.76
SNAI1	0.3
Fibronectin	0.24

Table 3.2.4. Fold change in the expression of EMT markers of iMDA MB-231 cells following treatment with exosomes.

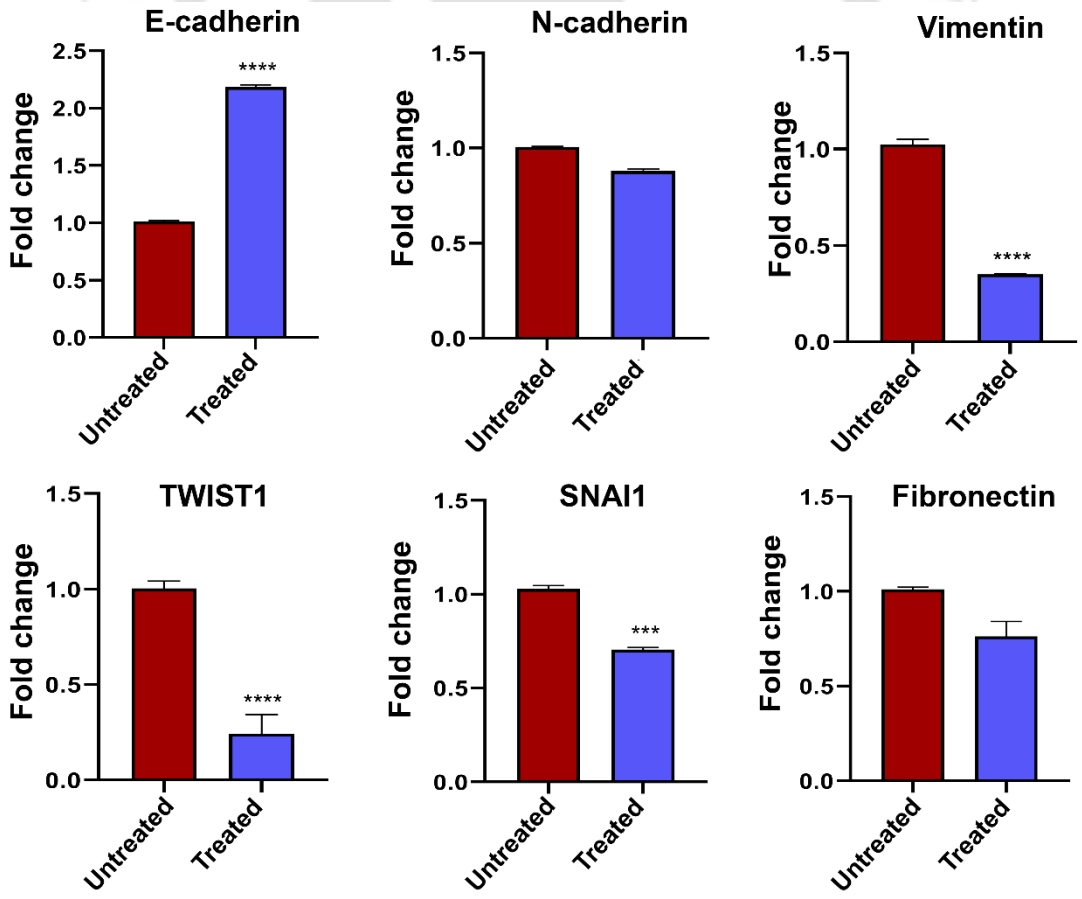

Figure 3.2.15. Graphical representation of the alterations in gene expression of iMDA MB-231 reveal an increase in the epithelial marker, E-cadherin whereas, a decrease in the EMT markers.

3.2.1.7. Exosome treatment increases the drug susceptibility of metastatic TNBC cells: During the process of exosome biogenesis, exosomes are packed with proteins, lipids and nucleic acids. These cargoes are identical to their cell of origin. As exosomes are taken up by the target cells, these cargoes result in the modulation of the tumor niche. In order to evaluate whether the exosomes from nBC cell lines can modify the tumor micro-environment, the metastatic TNBC cells, MDA MB-231 were treated with tyrosine kinase inhibitor, lapatinib along with the exosomes. It was observed that there was decrease in IC_{50} value of lapatinib, when it was treated along with the exosomes (3.499 μM) in comparison to lapatinib alone (5.088 μM) as depicted in **Figure 3.2.16**. The results indicated that exosomes are capable in altering the cellular microenvironment and increase the susceptibility of the metastatic TNBC cells towards anti-cancer drugs.

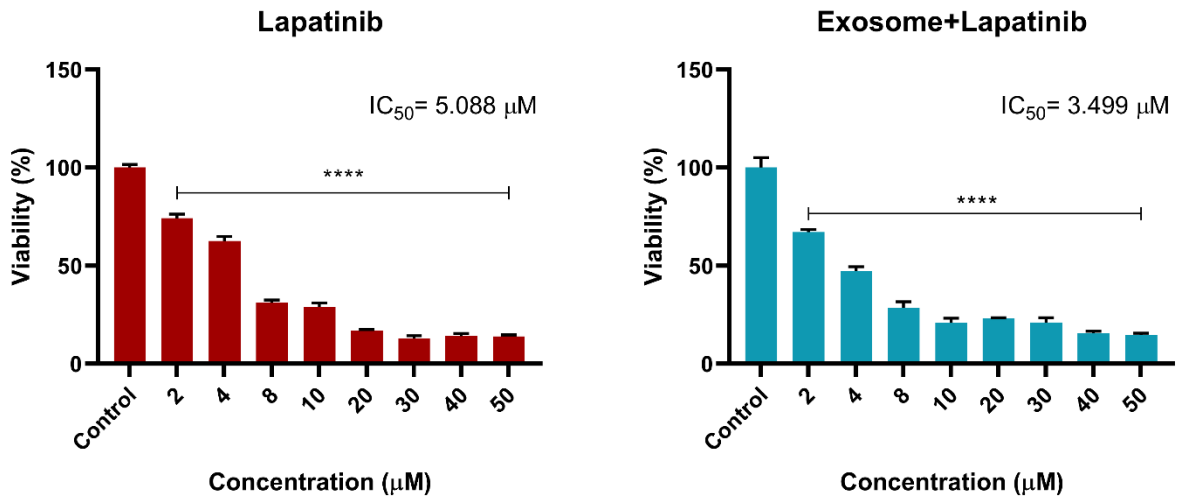

Figure 3.2.16. Analysis of cell viability subsequent to treatment of iMDA MB-231 cells with lapatinib and exosome+lapatinib.

Further, in order to assess the effect of exosomes in combination with inhibitor in the generation of apoptotic and necrotic population of cells, Annexin V-FITC based

apoptosis assay was carried out. The flow cytometric analysis revealed that there was effective induction in the early apoptotic population following treatment with lapatinib in combination with exosomes from MCF-7, a nBC cell line **(Figure 3.2.17).** The immensity of apoptosis following treatment with lapatinib and lapatinib in combination with exosomes is summarized in **Table 3.2.5.**

Sample	% of Apoptosis
Exosome	35.08
Lapatinib	35.66
Exosome+Lapatinib	73.32

Table 3.2.5. Percentage of apoptotic population following treatment with exosome, lapatinib and exosome+lapatinib

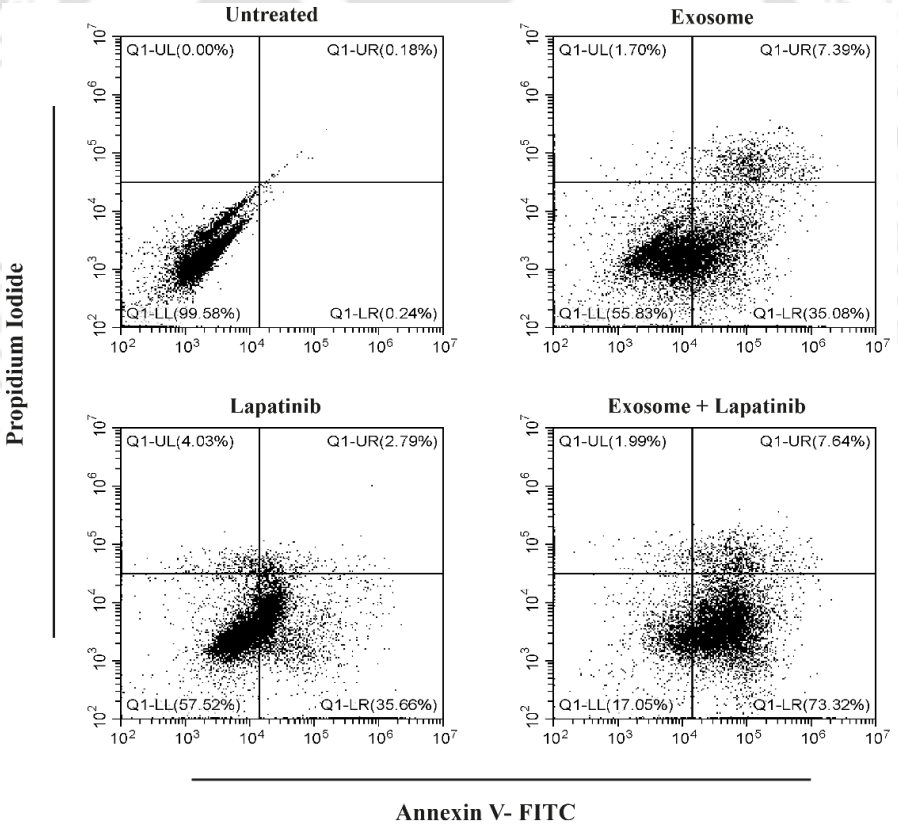

Figure 3.2.17. Annexin V–FITC–PI-based flow cytometric assessment of apoptosis in iMDA MB-231 cells treated with exosome, lapatinib and exosome+lapatinib.

3.2.2 Discussion: Though chemotherapy is considered as the main mode of therapy for metastatic tumors, MDR mechanism stands as a substantial hurdle in the achievement of a successful and efficient mode for cancer therapy. Overexpression of the MDR proteins belonging to the ABC superfamily and acting as drug efflux pumps, results in the outflow of various components and drugs out of the plasma membrane of the cells [15] [16] [109].

Exosomes are extracellular vesicles that are released from the cells and are taken up by the nearby cells thereby resulting in cell signaling [110]. Exosomes affect tumorigenesis by manipulating the tumor microenvironment. Exosomes contain cargoes identical to their parent cells, which modify the domain of the tumor niche [111]. It has been shown that the cargoes are active when they are taken up by the targeted cells. There has been evidences that exosomes isolated from mammary epithelial cells in the primary stage and breast cancer cells lead to increment in ROS generation thereby inducing damage response to the DNA, p53 stabilization and maintenance of cellular homeostasis in epithelial cells [112]. MCF-7 cells were chosen for the isolation of exosomes and treating the TNBC cells because they are tumorigenic in nature but non-metastatic and display lower invasive ability in this study which would lead to the modification of the tumor microenvironment.

The most crucial challenge in the present investigation was the isolation of exosomes in sufficient amount or concentration for it to be used in further downstream signaling. As the exosomes are of endosomal origin, they carry proteins which are required in transport of membrane and fusion, biogenesis of MVBs and also protein families which are affiliated with lipid microdomains, like integrins and tetraspanins. The successful isolation of the exosomes from non-invasive, non-metastatic breast cancer cell line, MCF-7 was confirmed by FETEM for its morphology and Western blotting for the presence of the surface markers like CD9 (tetraspanin) and Alix (protein involved in MVB biogenesis) [113] [114] [115]. The TNBC cell line, MDA MB-231 was selected for treatment with exosomes to comprehend if it could have any effect on the metastatic ability of the TNBC cells. It was observed that the empty exosomes had no significant

cytotoxic effect on the MDA MB-231 cells leading to very minimal decrease in wound healing ability. However, there was significant increase in the ROS production in TNBC cells suggesting modification of the tumor microenvironment. Cell cycle progression is a requisite event which governs the process of cell division and gene duplication [116]. After treatment with the exosomes it was also observed that there was some alteration in the cell cycle. An S-phase arrest was observed in the cell cycle as compared to the untreated group of cells following treatment, thereby suggesting that the exosomes resulted in the prevention of proliferation of metastatic TNBC cells, MDA MB-231.

Drug and chemo resistance plays a very significant barrier in the successful treatment of metastatic TNBC cells. Numerous mechanisms result in drug resistance, the most common among them being the transporter mediated drug efflux. Various ABC transporters are strongly involved in the resistance, especially, ABCB1/MDR1, ABCC1/MRP1 and ABCG2/BCRP [117] [118]. After the treatment of the metastatic breast cancer cells, MDA MB-231 with the exosomes, significant downregulation in the expression of the ABC transporters was observed. Our exosome therapy also ensued in the increment in expression of E-cadherin and reduction in the expression levels of Vimentin, SNAI1, N-cadherin and TWIST1, the markers of EMT, thereby inhibiting metastasis in the TNBC cell line. It also exhibited an increase in susceptibility towards anti-cancer inhibitor when treated in combination.

Hence, the exosomes from a nBC cell line can serve as an efficient mode in modulating the micro-environment of the target cell thereby, suppressing the drug resisting nature and metastatic behavior of the TNBC cell lines and making it more susceptible to anti-cancer drugs contributing to its efficient therapy.

3.2.3 Conclusion: In the recent years, exosomes have been discovered to pave new avenues in the development of immunotherapeutic modules. The employment of exosome-based therapies has been rapidly increasing towards cancer treatment as they have the ability to carry components from their parent cell resulting in the modification of the niche of the recipient cells. Metastatic TNBC cells exhibit poor prognosis and is considered as the most aggressive subtype with magnified invasive ability. Considering the metastatic nature and chemoresistant behavior of TNBC cells due to overexpression of MDR genes, the possibility as to whether and how exosomes from a nBC (MCF-7 cells) could affect the tumor microenvironment of a metastatic TNBC cell line (MDA MB-231) was looked upon. It was observed that the exosomes not only resulted in halting the DNA replication of the metastatic TNBC cells by undergoing an S-phase arrest, but also resulted in substantial downregulation in the gene expression of ABC transporters as well as EMT markers. These findings delineated the effect of exosomes in the modification of the tumor niche, thereby lowering the drug resistance ability and making it susceptible towards targeted and efficient anti-cancer therapy.

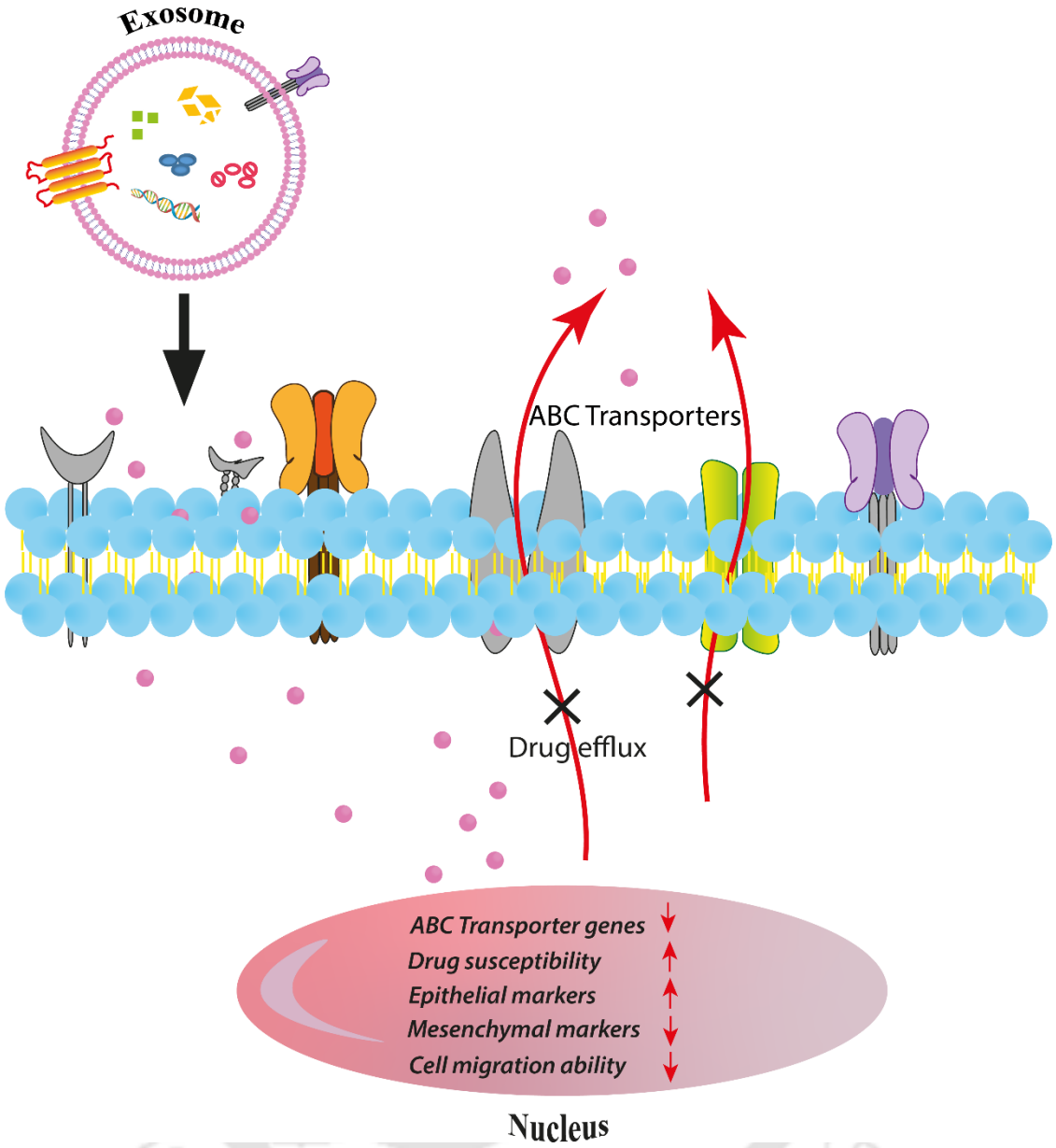

Schematic 3.2. Modulation of tumor micro-environment of metastatic TNBC cells via exosomes.

3.3. Engineered Hybrid Nanosystem for Homologous Targeting of EMT Induced Triple Negative Breast Cancer Cells

ACS Applied Bio Materials **6(2), 681–693 (2023).**

Abstract: The increased mortality rate due to metastatic breast cancer with poor prognosis has raised concern over its effective therapy. Though various therapies and anticancer drugs have been approved, there is still a lack in the targeting of metastatic triple negative breast cancer (TNBC). Considering these factors, a hybrid nanosystem was developed that was synthesized by fusing exosomes from MCF-7 cells and nanovesicles from the MDA MB-231 cells that would be targeted. The developed nanosystem was characterized by various techniques like Western blotting, AFM, FETEM, DLS, CD, and fluorescence spectroscopy. The hybrid system was used for the delivery of an HDAC inhibitor, Trichostatin A (TSA), in combination with lapatinib (a tyrosine kinase inhibitor) for cotherapy of epithelial to mesenchymal transition (EMT) induced TNBC. This targeted cotherapy module had higher efficiency and effectivity in the reduction of metastatic ability and proliferation of EMT induced MDA MB-231 cells as compared to free inhibitor treatment or untargeted cotherapy.

Reduction in the expression of the Wnt/β-catenin signaling pathway molecules like β-catenin (by 0.7 fold), Gsk3β (by 0.6 fold), and pGsk-3β (0.3 fold) was observed upon treatment. This subsequently resulted in the suppression of EMT markers, thereby resulting in reversing EMT to MET and suppressing metastatic breast cancer.

3.3.1 Results:

3.3.1.1. Characterization of Exosomes and Nano-vesicles: Exosomes from non-invasive breast cancer cells and nano-vesicles from the cells to be targeted were isolated and synthesised to develop a fused nanosystem for targeting metastatic TNBC. The exosomes and nano-vesicles were characterized by FETEM (**Figure 3.3.1**) before proceeding for fusion for the development of the hybrid nanosystem. The FETEM images showed that the exosomes and nano-vesicles had a spherical morphology with an average diameter of 42.03 nm and 67.84 nm respectively.

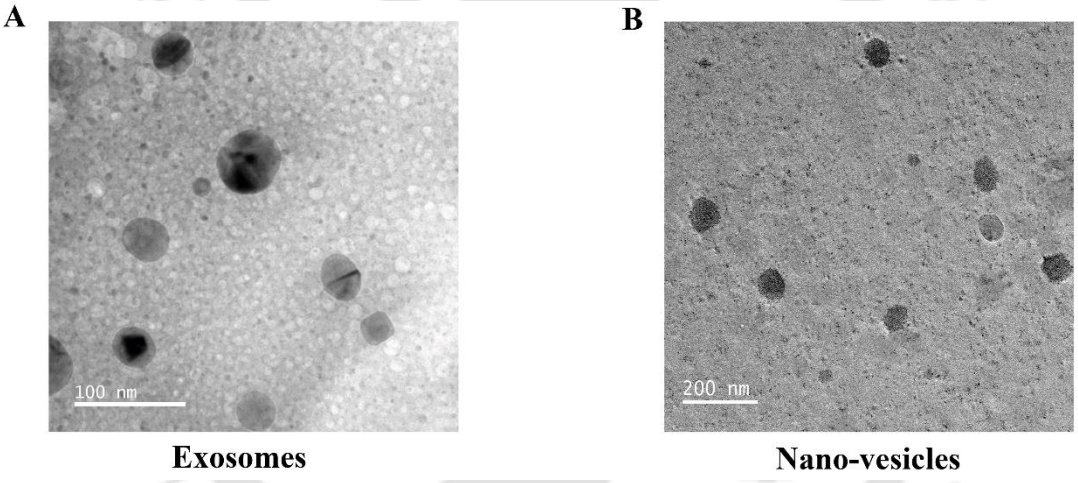

Figure 3.3.1. Characterization of exosomes and nano-vesicles. **(A)** FETEM image of exosomes depicting a spherical morphology with an average diameter of 42.03 nm and **(B)** FETEM image of nano-vesicles having an average diameter of 67.84 nm.

3.3.1.2. Characterization of the Fused Nanosystem Exhibited Successful Fusion between Exosomes and Membrane Nanovesicles: The presence of the surface markers of both exosomes and nanovesicles in fused nanosystem was

confirmed by Western blot analysis. It was seen that CD9, and Alix and EGFR are present in the exosomes and nanovesicles respectively as well as in the fused nanosystem, however, the sample containing 2:1 exosome:vesicle showed the best fusion result (**Figure 3.3.2A**). So, hereafter, the succeeding experiments of synthesizing the fused nanosystem was continued in a 2:1 exosome:vesicle ratio.

The CD spectral analysis showed that there was an evident decrease in the beta secondary structure when exosomes and membrane vesicles were fused via freeze–thaw cycle thereby, corroborating the efficient occurrence of fusion between them (**Figure 3.3.2B**). **Table 3.3.1** represents the change in the secondary structures of the nanosystem after fusion in 2:1 exosome:nanovesicle ratio.

	Exosome	**Vesicle**	**Fused**	**Unfused**
Helix	17.2	23.6	30	24.3
Beta	41.2	23.3	**3.7**	17.4
Turn	17.8	26.7	35.9	27
Random	23.9	26.4	30.3	31.3

Table 3.3.1. Secondary structural analysis data of exosome, nano-vesicle, fused nanosystem and unfused samples.

The surface potential of nano-sized particles has a very crucial part in the uptake by the cells. The surface potential of the fused nanosystem was detected to be −0.9 mV. The average hydrodynamic diameter (*d*H) of the exosomes was found to be 144.7 nm, that of nanovesicles was found to be 176.3 nm, and that of the fused nanosystem was detected to be 391.2 nm by dynamic light scattering measurements (**Figure 3.3.2C**). The average *d*H of the exosomes, nano-vesicles, and nanosystem was found to be higher as compared to FETEM analysis owing to the presence of a hydration layer at the surface in aqueous solution. The fluorescence spectra of the fused nanosystem showed a change in the intensity of the fluorescence (**Figure 3.3.2D**); however, the sample containing unfused exosome and vesicle mixed in a 2:1 ratio showed similar fluorescence spectra as compared

to exosomes. This observation represents that there is a conformational change after the exosome-plus-vesicle mixture was passed through a freeze–thaw cycle, thereby confirming fusion.

AFM analysis revealed a fused morphology between spherical structures with an average diameter of 149.7 nm. The FETEM pictures of the fused nanosystem disclosed that the particles have an average size of 98.56 nm as analysed by the ImageJ software. The fused morphology of the nanosystem was affirmed by AFM and FETEM microscopic pictures as shown in **Figure 3.3.2E and Figure 3.3.2F**, respectively.

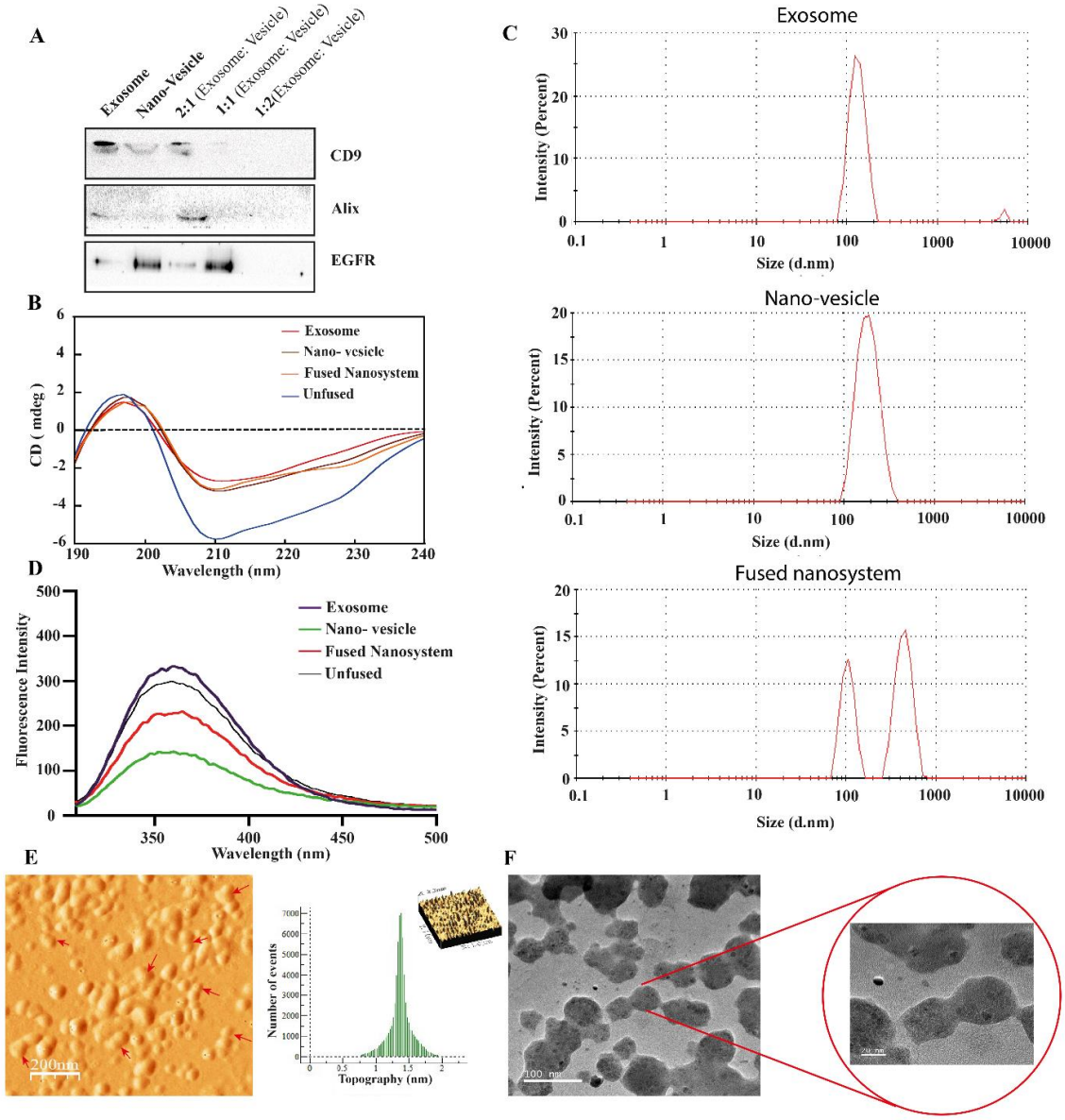

Figure 3.3.2. Characterization of fused exosome and nano-vesicle (nanosystem). **(A)** Western Blot analysis revealed the successful fusion of exosome and nano-vesicle after freeze-thaw cycle by the presence of the surface markers of both nano-vesicles and exosomes. The best results were shown by the fusion ratio 2:1. **(B)** CD spectral analysis showed a decrease in β-sheets after fusion of exosome and nano-vesicles in 2:1 ratio. **(C)** Dynamic Light Scattering (DLS) measurement depicting average hydrodynamic diameter of the synthesized hybrid nanosystem. **(D)** Fluorescence spectrometric analysis of Tryptophan showing change in fluorescence intensity after fusion. **(E)** AFM and **(F)** FETEM images showing fused morphology of the nanosystem.

3.3.1.3. Reduction in Cell Migration Ability: On the course of epithelial-to-mesenchymal transition, epithelial cells change over their cytology into mesenchymal cells, thereby acquiring enhanced capabilities for migration and intrusion, which might ultimately lead to metastasis. Because the Wnt/β-catenin signaling pathway is entailed in the movement and encroachment of TNBC, the consequence of free TSA, lapatinib, nanosystem loaded TSA and their combination on the migration and intrusion of MDA-MB-231 cells was investigated. Movement was evaluated by employing a wound-repair scratch analysis, wherein the cell migration in the direction of the wounded area was ascertained. It was observed that the cells treated with lapatinib, free TSA, loaded TSA, and their combination depicted tedious wound repair potential when compared to cells that were not treated in both uninduced MDA MB-231 cells (**Figure 3.3.3)** as well as EMT induced MDA MB-231 cells (**Figure 3.3.4)**. The pace of migration of the cells was observed to be most depleted in the combination therapy with nanosystem loaded TSA and lapatinib thereby suggesting the targeted co-therapy to be more effective.

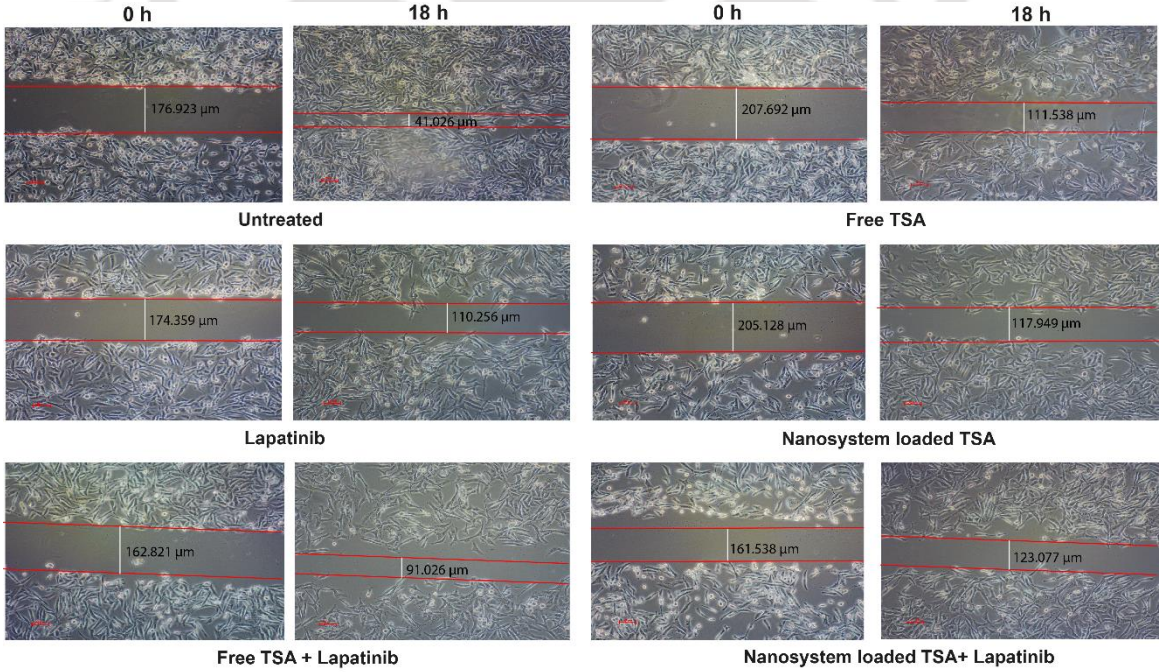

Figure 3.3.3. Scratch wound repair analysis of MDA MB-231 cells following inhibitor treatment and in combination after 18 h in comparison to untreated cells.

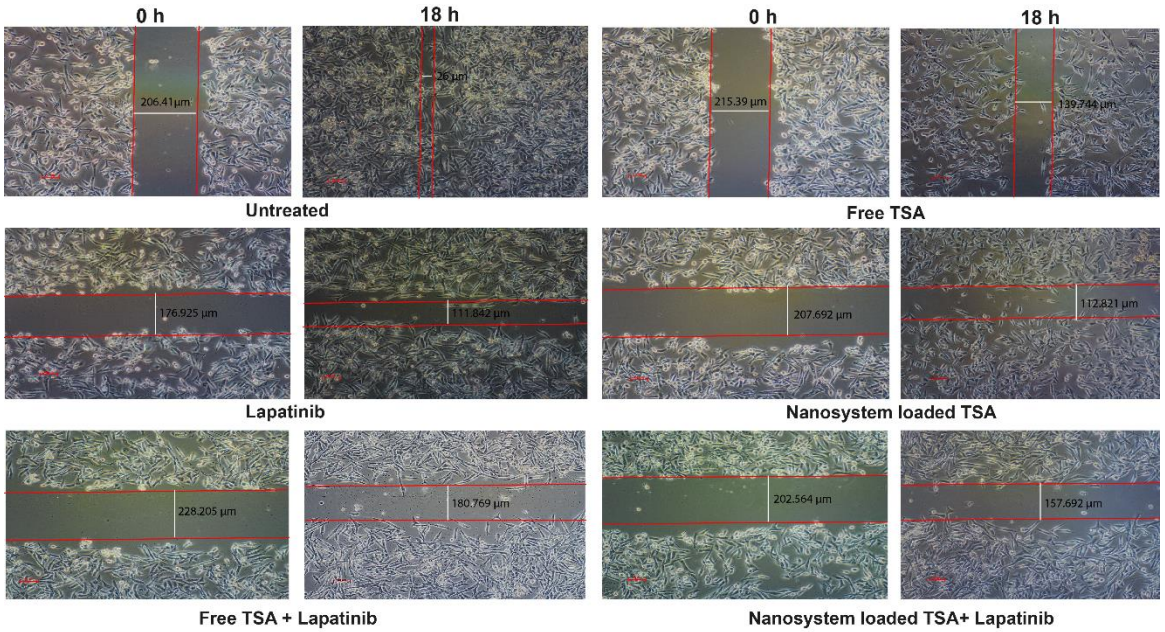

Figure 3.3.4. Scratch wound repair analysis of EMT induced MDA MB-231 cells after inhibitor treatment and in combination after 18 h in comparison to cells which were not treated (Scale bar- 50 µm) show slowest wound healing capacity when treated with targeted combination of inhibitors.

3.3.1.4. Efficient Induction of Cytotoxicity by Fused Nanosystem Loaded Inhibitors: To check the consequence of the inhibitors and the combination module in EMT induced MDA MB-231 cells, EMT was induced with EGF and treated with the above-mentioned free, loaded, and combination of inhibitors. The uninduced MDA MB-231 cells were also taken into consideration. It was observed that the inhibitors showed better effect on the EMT induced cells and the dose further decreased when treated with TSA loaded in the fused nanosystem + lapatinib (**Figure 3.3.6**) as compared to uninduced cells (**Figure 3.3.5)**, thereby indicating that our loaded system has a better efficiency in metastatic TNBCs. The IC_{50} of the treatment modules is mentioned in **Table 3.3.2** and **Table 3.3.3.**

Sample	IC_{50}
Free TSA	402.6 nM
Lapatinib	13.31 μM
Nanosystem loaded TSA	95.57 nM
Free TSA+ Lapatinib	6.004 μM
Nanosystem loaded TSA+ Lapatinib	2.974 μM

Table 3.3.2. IC_{50} values of the inhibitors following treatment of MDA MB-231 cells for 48 h.

Sample	IC_{50}
Free TSA	134.7 nM
Lapatinib	5.116 μM
Nanosystem loaded TSA	127.7 nM
Free TSA+ Lapatinib	67.35 nM+ 3.499 μM
Nanosystem loaded TSA+ Lapatinib	63.85 nM+ 1.542 μM

Table 3.3.3. IC_{50} values of EMT induced inhibitor treated MDA MB-231 cells after 48 h.

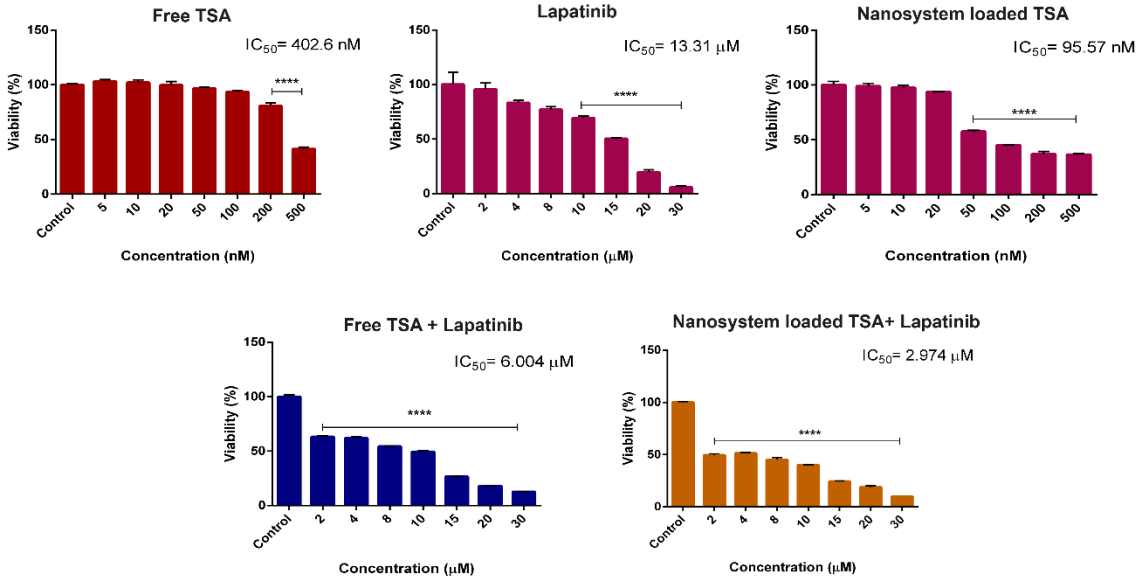

Figure 3.3.5. Assessment of cell viability upon treatment of MDA MB-231 cells with inhibitors and in combination.

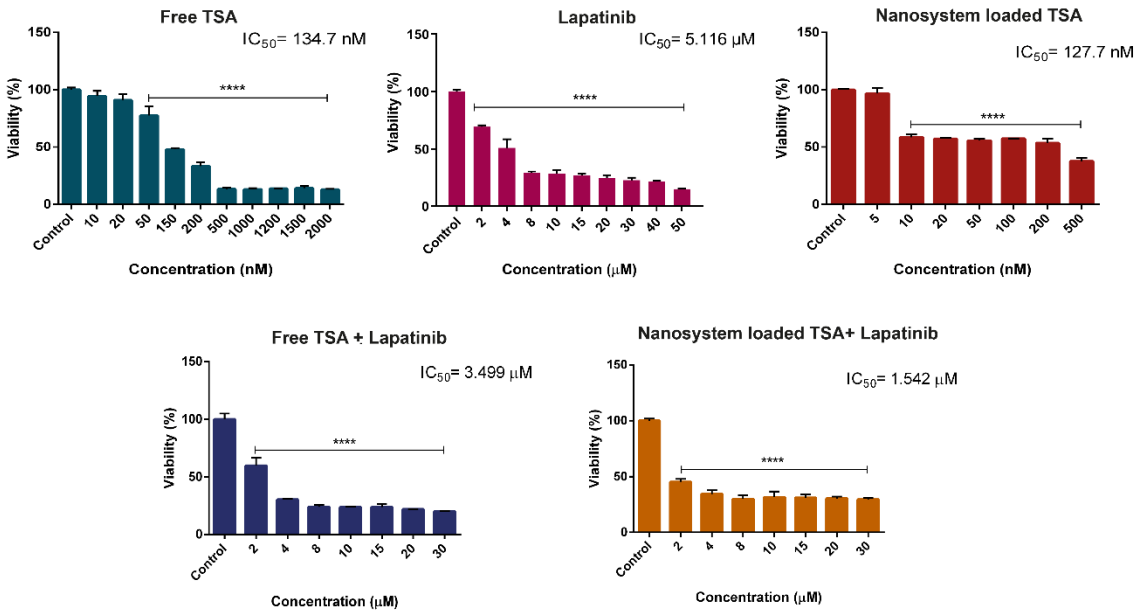

Figure 3.3.6. Assessment of cell viability upon treatment of EMT induced MDA MB-231 cells with inhibitors and in combination reveals an efficient induction of cell death with a much lower concentration of inhibitors required in targeted co-therapy, as indicated by the IC_{50} values.

Following treatment, live–dead cell imaging analysis of MDA MB-231 cells and EMT induced MDA MB-231 cells showed decrease in green fluorescence by Calcein AM thereby, confirming increase in cell death after treatment for 48 h (**Figure 3.3.7** and **Figure 3.3.8**) which was more efficient in targeted co-therapy module (**Figure 3.3.7 (vi) and 3.3.8 (vi)**) with a much lower concentration of inhibitors.

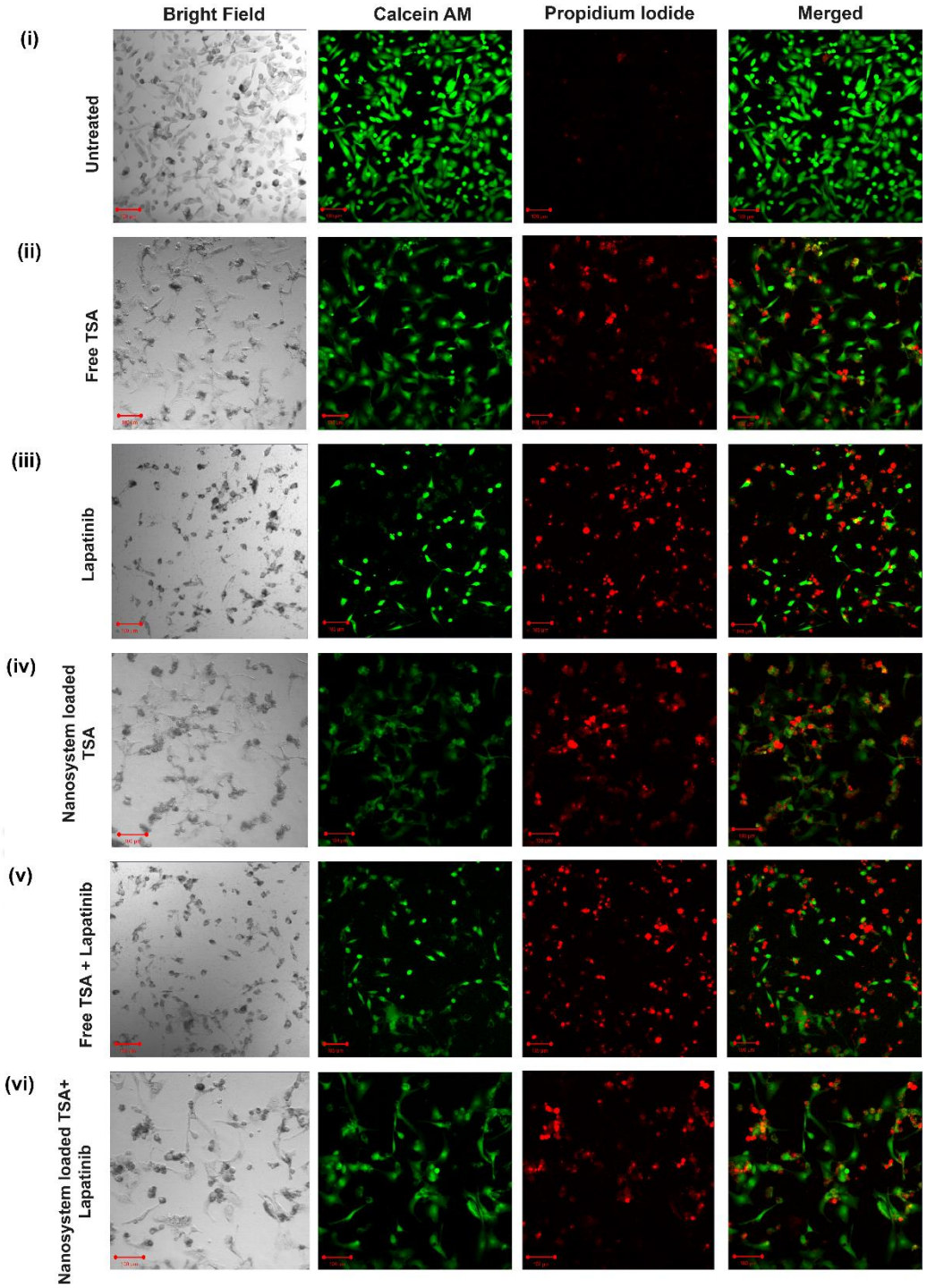

Figure 3.3.7: Induction of cell death by inhibitor treatment in monolayer cells. Live-dead cell imaging of MDA MB-231 monolayer employing Calcein AM/PI dual staining. Green fluorescence depicts live cells stained by Calcein AM and the red fluorescence indicate dead cells by PI after treatment with IC_{50} values of free TSA (ii) , lapatinib (iii), nano-system loaded TSA(iv), free TSA+ lapatinib (v) and nano-system loaded TSA+ lapatinib (vi) for 48 h.

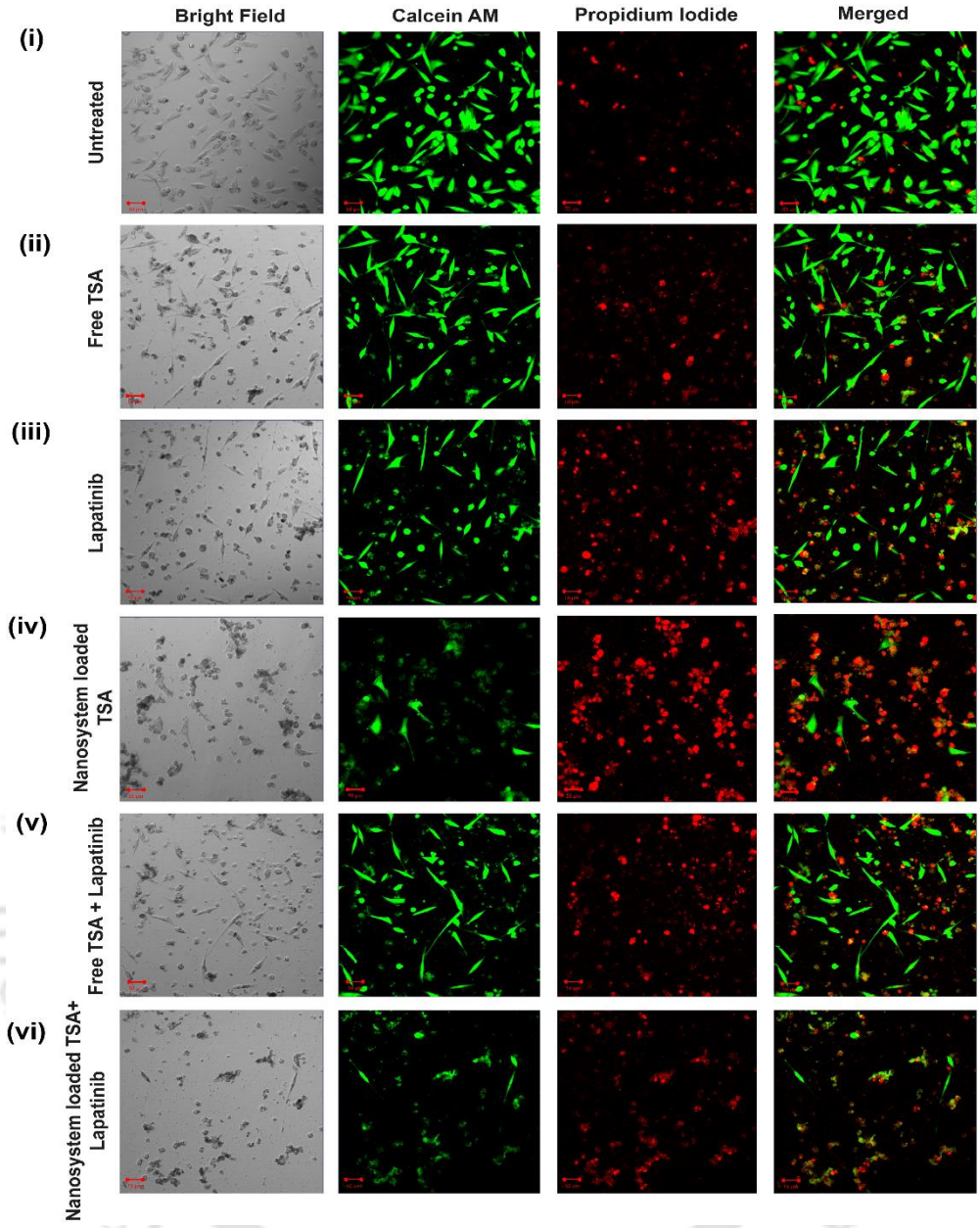

Figure 3.3.8. Induction of cell death by inhibitor treatment in monolayer cells. Live–dead cell imaging of EMT induced TNBC monolayer employing Calcein AM/PI dual staining. Green fluorescence depicts live cells stained by Calcein AM and the red fluorescence indicates dead cells by PI after treatment with IC_{50} values of free TSA (ii), lapatinib (iii), nanosystem loaded TSA (iv), free TSA+ lapatinib (v), and nanosystem loaded TSA + lapatinib (vi) for 48 h. Decreased green fluorescence and increased red fluorescence in nanosystem loaded TSA+ lapatinib at a much lower concentration explicates the efficient induction of cytotoxicity by targeted co-therapy.

Due to interference between the HDACi, Trichostatin A, and AlamarBlue, it was unfeasible to deduce the IC_{50} of MDA MB- 231 spheroids. Thus, the EMT uninduced and induced spheroids of MDA MB-231 cells were treated with increasing doses of the combination of inhibitors and imaged in confocal microscope. It was found that with increasing concentration, there was a decrease in the fluorescence of Calcein AM (green fluorescence), indicating cell death, and thus the approximate IC_{50} was deduced from the intensity of fluorescence and treated the cells with free TSA (2 μM), lapatinib (30 μM), nanosystem loaded TSA (800 nM), free TSA + lapatinib (20 μM), and nanosystem loaded TSA + lapatinib (10 μM) (**Figure 3.3.9 (i)-(vi)**) for uninduced MDA MB-231 cells and free TSA (1 μM), lapatinib (20 μM), nanosystem loaded TSA (800 nM), free TSA + lapatinib (10 μM), and nanosystem loaded TSA + lapatinib (8 μM) for 72 h (**Figure 3.3.10 (i)-(vi)**) for EMT induced cells.

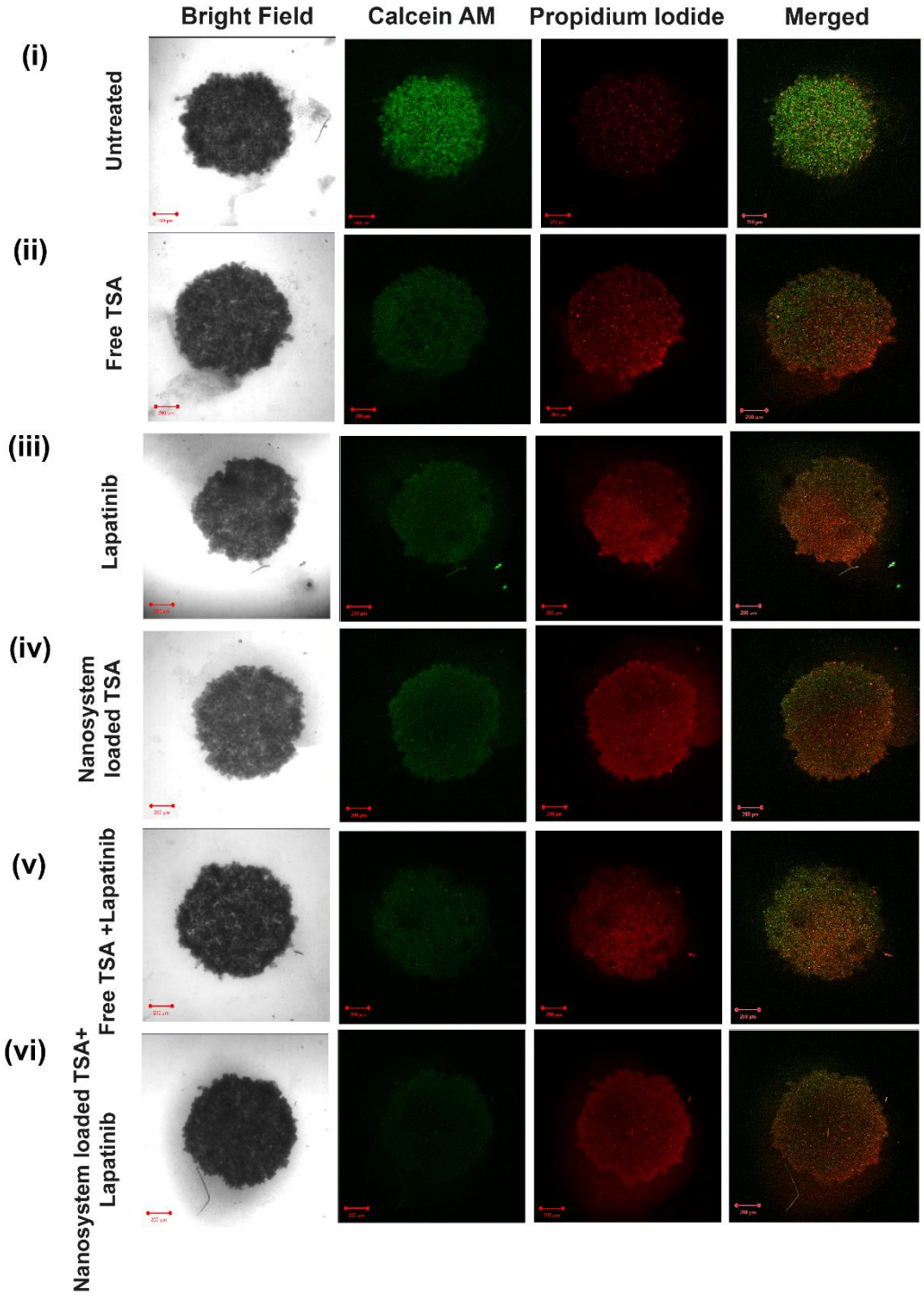

Figure 3.3.9. Induction of cell death by inhibitor treatment in spheroids. Live- dead cell imaging of MDA MB-231 spheroids employing Calcein AM/PI dual staining. Green fluorescence depicts live cells stained by Calcein AM and the red cells indicate dead cells by PI after treatment with free TSA (2 μM) (ii), lapatinib (30 μM) (iii), nano-system loaded TSA (800 nM) (iv), free TSA+ lapatinib (20 μM) (v) and nano-system loaded TSA+ lapatinib (10 μM) (vi) for 72 h.

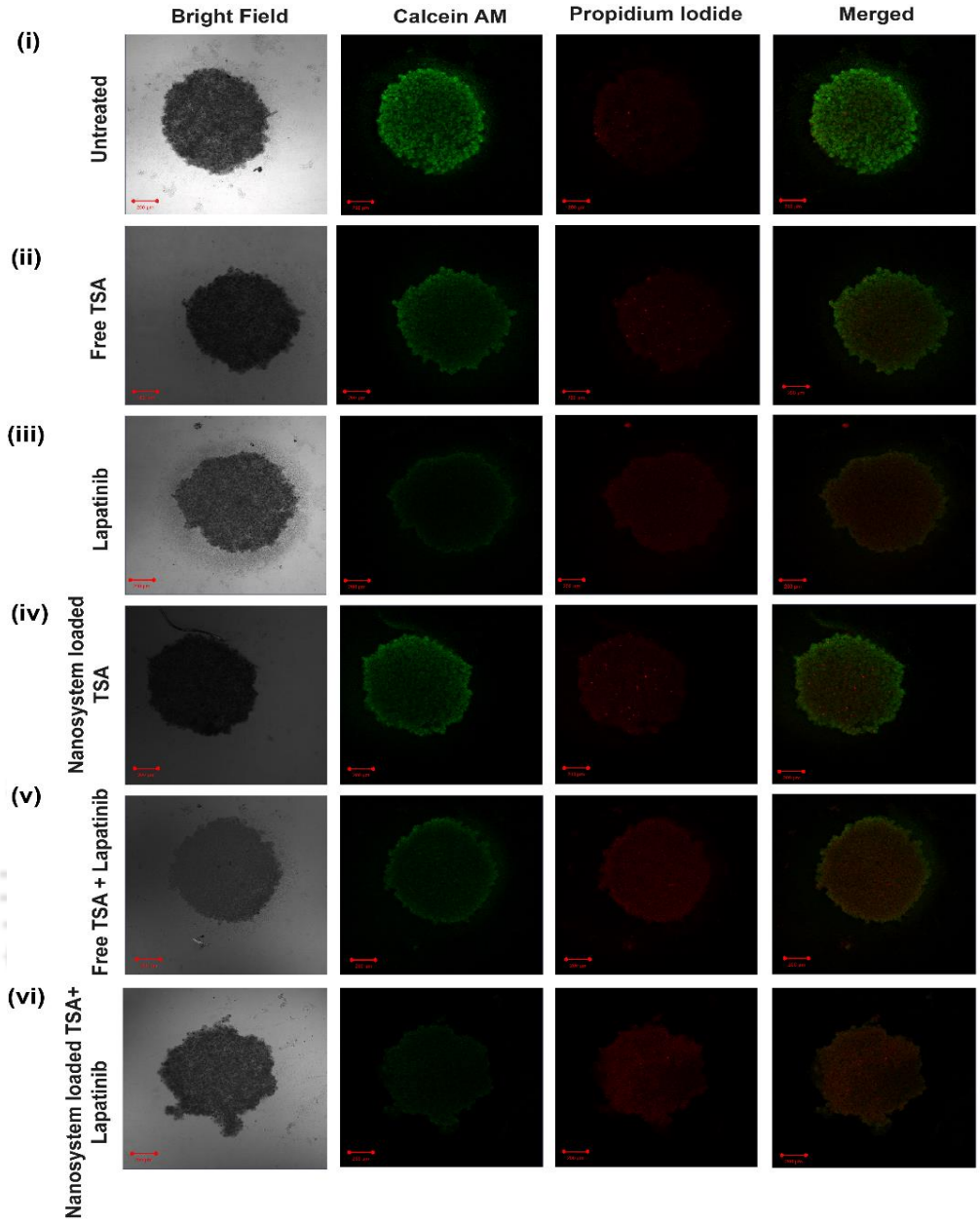

Figure 3.3.10. Induction of cell death by inhibitor treatment in spheroids. Live–dead cell imaging of EMT induced TNBC spheroids employing Calcein AM/PI dual staining. Green fluorescence depicts live cells stained by Calcein AM and the red fluorescence indicates dead cells by PI after treatment with (ii) free TSA (1 μM), (iii) lapatinib (20 μM), (iv) nanosystem loaded TSA (800 nM), (v) free TSA+ lapatinib (10 μM), and (vi) nanosystem loaded TSA+ lapatinib (8 μM) for 72 h. The increase in red fluorescence and decrease in green fluorescence after treatment with nanosystem loaded TSA + lapatinib at a much lower concentration indicates the increased efficiency of targeted co-therapy in a 3D tumor model.

3.3.1.5. Induction of Apoptosis by Combination Treatment with Tyrosine Kinase Inhibitor, Lapatinib, and Nanosystem Loaded HDAC Inhibitor, TSA: The viability study showed that the combination therapy when lapatinib is treated along with TSA loaded in the nanosystem had better efficacy in the reduction of cell viability. Following this, in order to explore the immensity of apoptosis in uninduced as well as EMT induced MDA MB-231 cells, an Annexin V-FITC assay was performed; it showed an efficient induction of apoptosis, as shown in **Figure 3.3.11 and 3.3.12**, with a very low necrotic population indicating an effective module for cancer therapy. The percentage of apoptosis in uninduced and EMT induced MDA MB-231 cells is summarized in **Table 3.3.4 and 3.3.5**.

Sample	% of Apoptosis
Free TSA	41.78
Lapatinib	10.91
Nanosystem loaded TSA	51.58
Free TSA+ Lapatinib	25.57
Nanosystem loaded TSA+ Lapatinib	45.62

Table 3.3.4. Percentage of apoptosis of MDA MB-231 cells following treatment with inhibitors after 48 h.

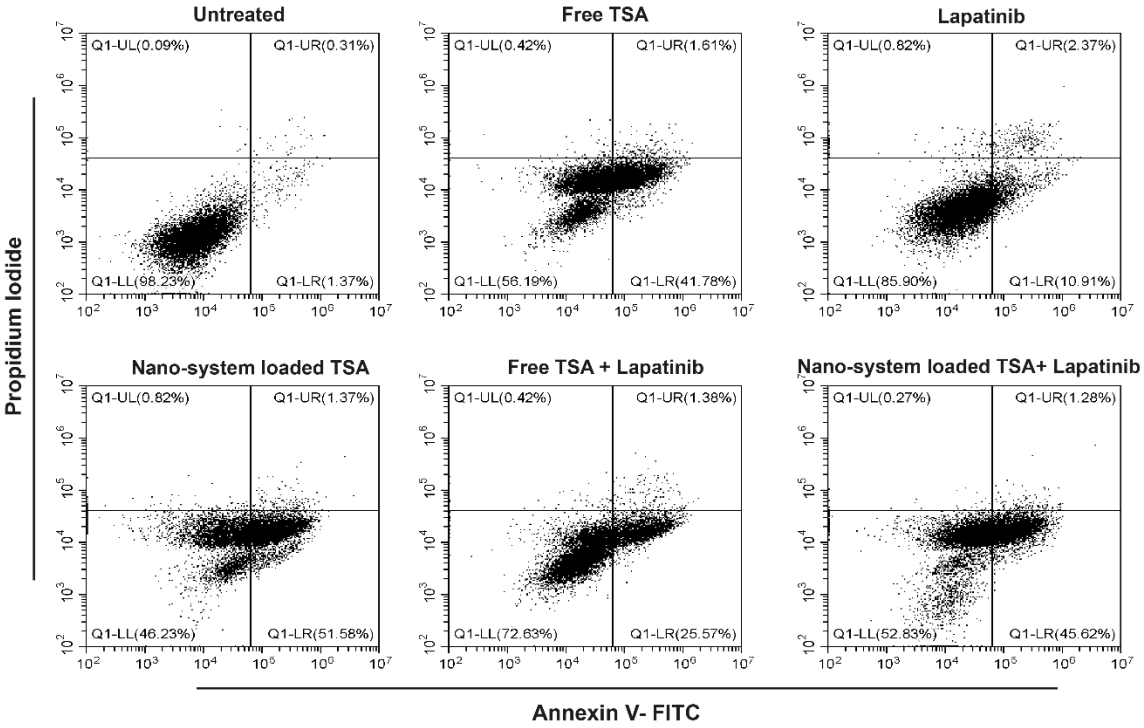

Figure 3.3.11. Evaluation of apoptosis in MDA MB-231 treated cells. Flow cytometric evaluation of apoptosis in treated cells. Annexin V–FITC–PI-based flow cytometric determination of apoptosis in MDA MB-231 cells treated with IC_{50} doses of free and targeted inhibitors singly and in co-therapy module.

Sample	% of Apoptosis
Free TSA	14.43
Lapatinib	16.29
Nanosystem loaded TSA	49.45
Free TSA+ Lapatinib	13.82
Nanosystem loaded TSA+ Lapatinib	66.03

Table 3.3.5. Percentage of apoptosis of EMT induced MDA MB-231 cells following treatment with inhibitors after 48 h.

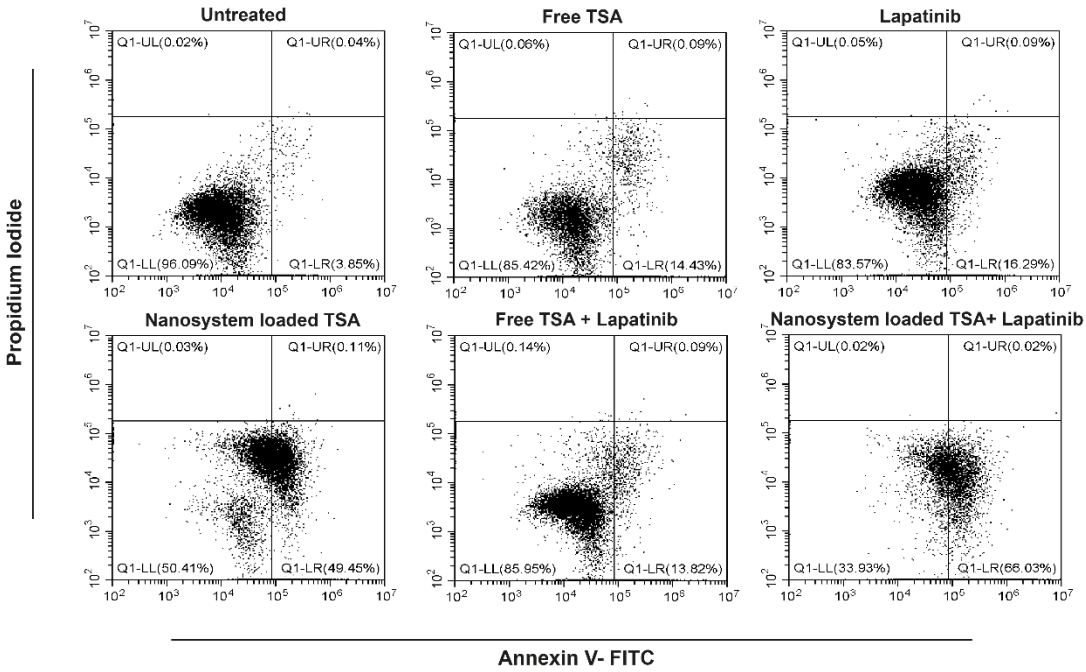

Figure 3.3.12. Evaluation of apoptosis in EMT induced TNBC treated cells. Evaluation of treated cells for apoptosis by flow cytometry. Annexin V–FITC–PI-based flow cytometric detection of apoptosis in MDA MB-231 cells treated with IC_{50} doses of free and targeted inhibitors singly and in the co-therapy module reveals more efficient apoptosis when treated with targeted combination of inhibitors.

3.3.1.6. Generation of Reactive Oxygen Species (ROS): Flow cytometric analysis of treated MDA MB-231 cells showed upregulation in the generation of ROS when treated in the combination module. The fold increase was equal in uninduced MDA MB-231 cells when treated with the targeted combination of inhibitors with much lower concentrations of inhibitors (**Figure 3.3.13**). The fold increase in the ROS generation in EMT induced MDA MB-231 cells was almost similar in nanosystem loaded TSA + lapatinib and free TSA + lapatinib with

comparatively lower concentration of inhibitors used in targeted co-therapy (**Figure 3.3.14**). The percentage of ROS generation in uninduced and EMT induced cells have been summarized in **Table 3.3.6** and **3.3.7** respectively.

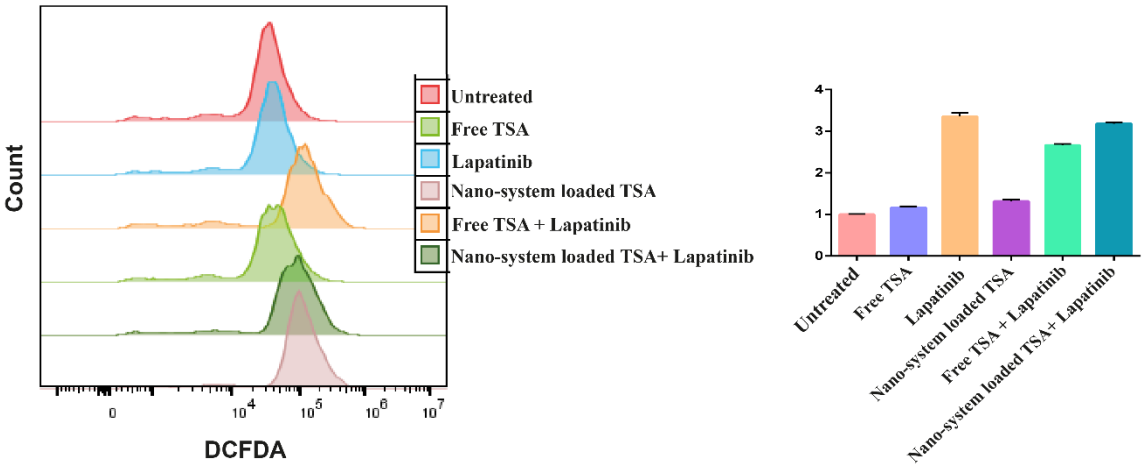

Figure 3.3.13. DCF-DA assay to sense ROS generation following treatment of MDA MB-231 cells with IC_{50} of the inhibitors after 6 h.

Sample	Fold change
Free TSA	1.2
Lapatinib	3.3
Nanosystem loaded TSA	1.3
Free TSA+ Lapatinib	2.7
Nanosystem loaded TSA+ Lapatinib	3.2

Table 3.3.6. Generation of ROS following treatment with inhibitors and in combination.

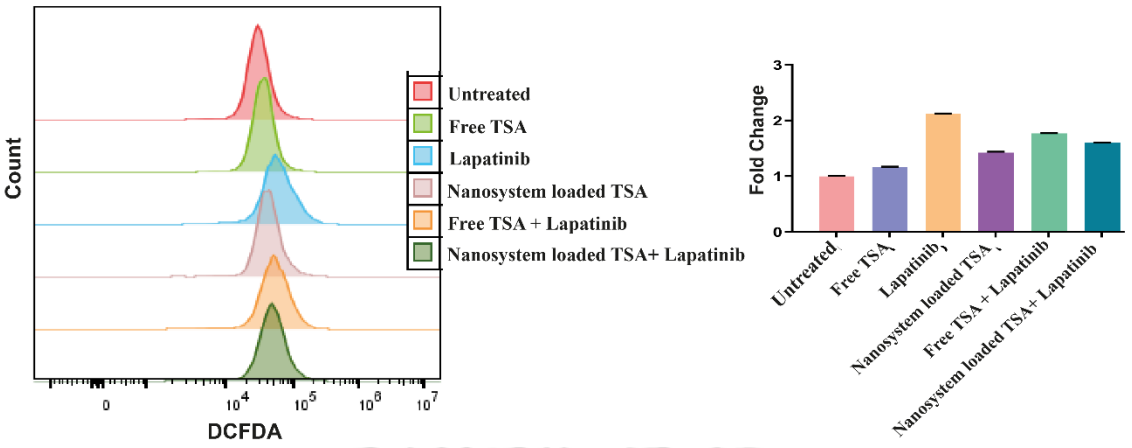

Figure 3.3.14. DCF-DA assay to sense ROS generation following treatment of EMT induced MDA MB-231 cells with IC_{50} reveals almost similar generation of ROS in targeted co-therapy with a comparatively lower concentration of inhibitors in comparison with untargeted co-therapy after 6 h.

Sample	Fold change
Free TSA	1.2
Lapatinib	2.1
Nanosystem loaded TSA	1.4
Free TSA+ Lapatinib	1.8
Nanosystem loaded TSA+ Lapatinib	1.6

Table 3.3.7. Representation of fold change in ROS generation after treatment of EMT induced MDA MB-231 cells with inhibitors and in combination with respect to untreated samples.

3.3.1.7. Depolarization of Mitochondrial Membrane after Combination Treatment with Lapatinib and Nanosystem Loaded TSA: In an endeavor to elucidate the mechanics of cell death, mitochondrial membrane integrity was analyzed. The consequence of ROS aggregation on the mitochondrial membrane integrity was estimated. Cyanine dye JC-1 (5,5′,6,6′-tetrachloro-1,1′,3,3′-tetraethylbenzimidazolylcarbocyanine iodide) builds red conglomerates in polarized mitochondria; on the other hand, it stays a monomer (emitting green fluorescence) in depolarized mitochondria. A prominent red fluorescence from untreated cells of healthy mitochondria and increase in green fluorescence from treated cells which was significantly higher in free TSA and nanosystem loaded TSA (~60% and ~51% respectively) was observed in uninduced MDA MB-231 cells, however, there was minimal depolarization when treated with lapatinib (~16%). This might have resulted in the decrease in depolarization when the HDAC inhibitor was treated in combination with lapatinib **(Figure 3.3.15).** The percentage of cells undergoing mitochondrial membrane depolarization in treated uninduced cells has been summarized in **Table 3.3.8**.

Sample	Mitochondrial Depolarization (%)
Control	4.02
Free TSA	60.17
Free Lapatinib	16.18
Nano-system loaded TSA	50.73
Free TSA+ Lapatinib	35.21
Nano-system loaded TSA+Lapatinib	37.64

Table 3.3.8. Percentage of mitochondrial depolarization following treatment of MDA MB-231 cells.

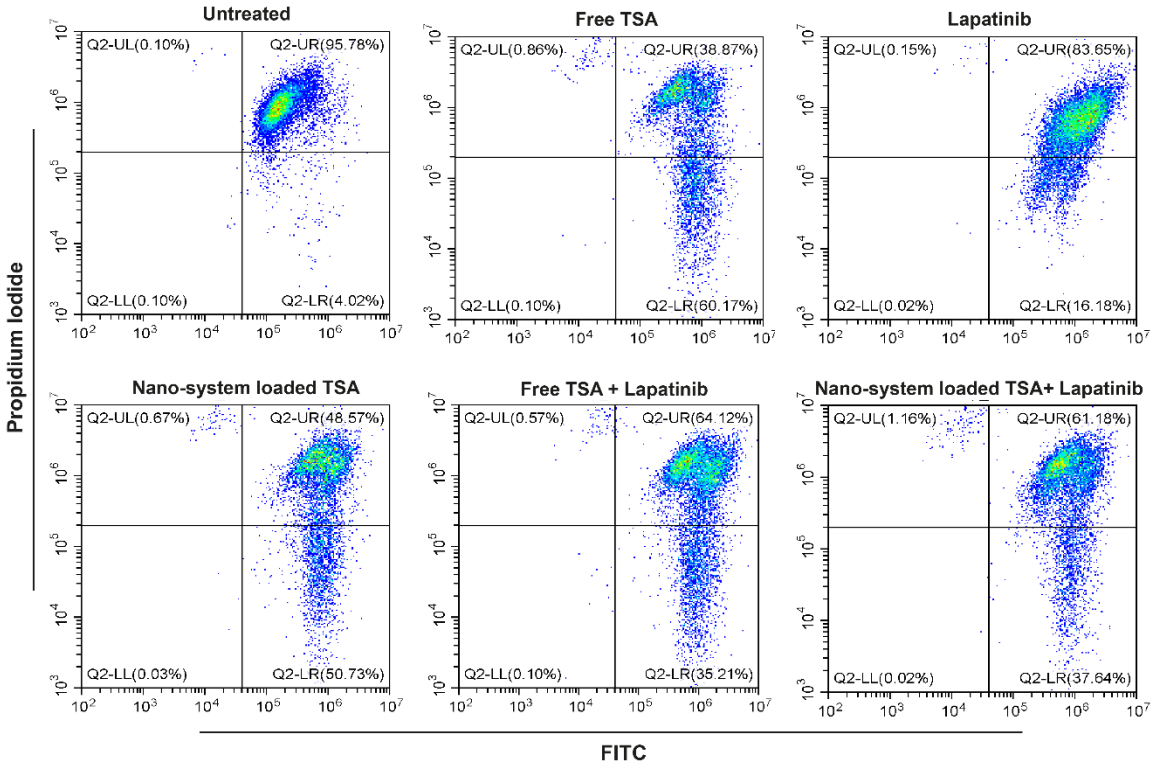

Figure 3.3.15. Flow cytometric evaluation of mitochondrial membrane potential using JC-1 staining of MDA MB-231 cells.

In EMT induced MDA MB-231 cells, a salient red fluorescence from untreated cells of healthy mitochondria and an increase in green fluorescence from treated cells was detected, which was significantly higher in nanosystem loaded TSA and nanosystem loaded TSA in combination with lapatinib (~62% and ~58%, respectively), suggesting mitochondrial membrane depolarization after treatment for 48 h (**Figure 3.3.16**). The percentage of cells undergoing mitochondrial membrane depolarization in treated EMT induced cells has been summarized in **Table 3.3.9**.

Sample	Mitochondrial Depolarization (%)
Control	23.94
Free TSA	26.68
Free Lapatinib	26.48
Nanosystem loaded TSA	61.98
Free TSA+ Lapatinib	32.02
Nanosystem loaded TSA+ Lapatinib	58.30

Table 3.3.9. Percentage of mitochondrial depolarization following treatment of EMT induced MDA MB-231 cells.

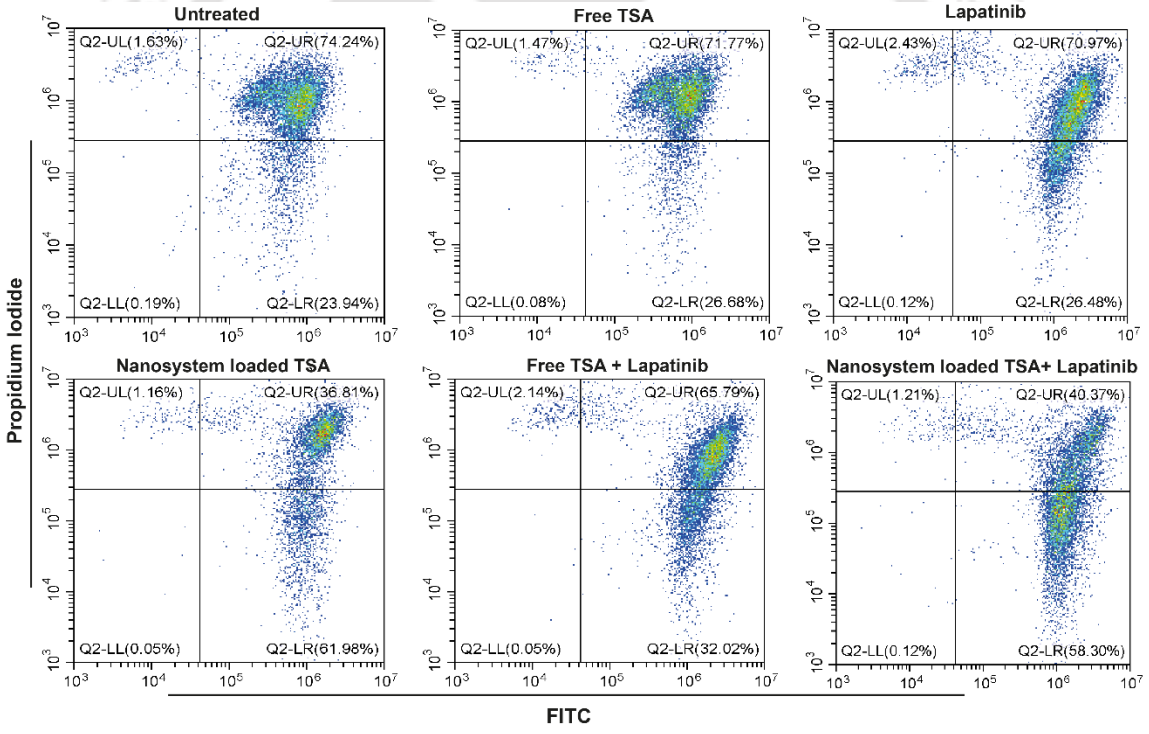

Figure 3.3.16. Flow cytometric evaluation of mitochondrial membrane potential employing JC-1 staining of EMT induced MDA MB-231 cells indicates higher concentration of cells undergoing mitochondrial depolarization in targeted co-therapy.

3.3.1.8. Cell Cycle Analysis: In order to observe the outcome of the inhibitors and combination treatment, cell cycle ontogeny was supervised during the course of 48 h of treatment. An S-phase arrest in the case of uninduced MDA MB-231 cells was detected (**Figure 3.3.17**). The percentage of S-phase increased to 55.4% in nanosystem loaded TSA + Lapatinib treated MDA MB-231 cells.

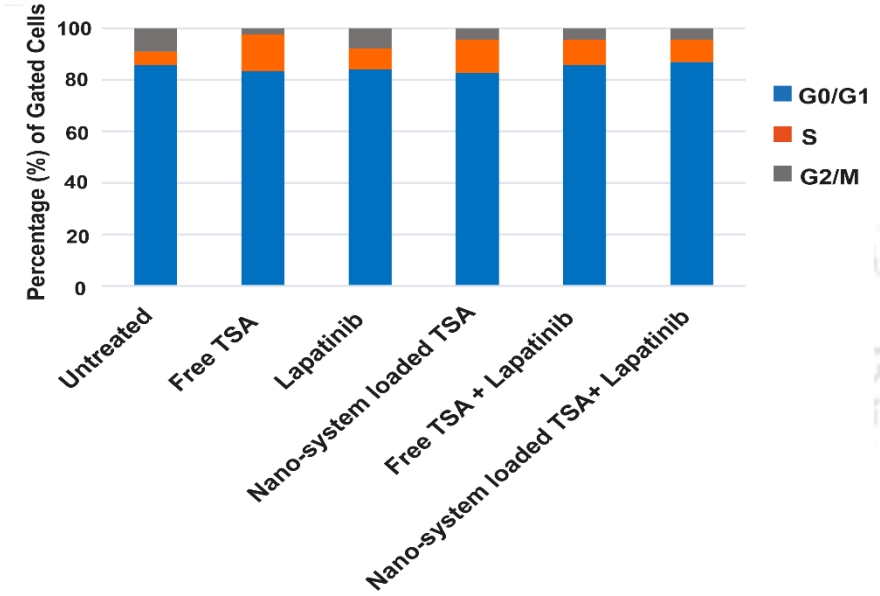

Figure 3.3.17. Analysis of cell cycle of MDA MB-231 cells following 48 h treatment with inhibitors,

However, there was a G2/ M phase arrest in the case of EMT induced MDA MB-231 cells (**Figure 3.3.18**). The G2/ M arrest percentage in EMT induced MDA MB-231 cells was found to be 26.6% when treated with nanosystem loaded TSA + Lapatinib. There was also an increase in the sub-G1 population, which is considered to be an apoptotic cell population. Therefore, it can be stated that there is a modulation in the cell cycle progression in metastatic TNBCs after treatment with the targeted combination module leading to apoptosis.

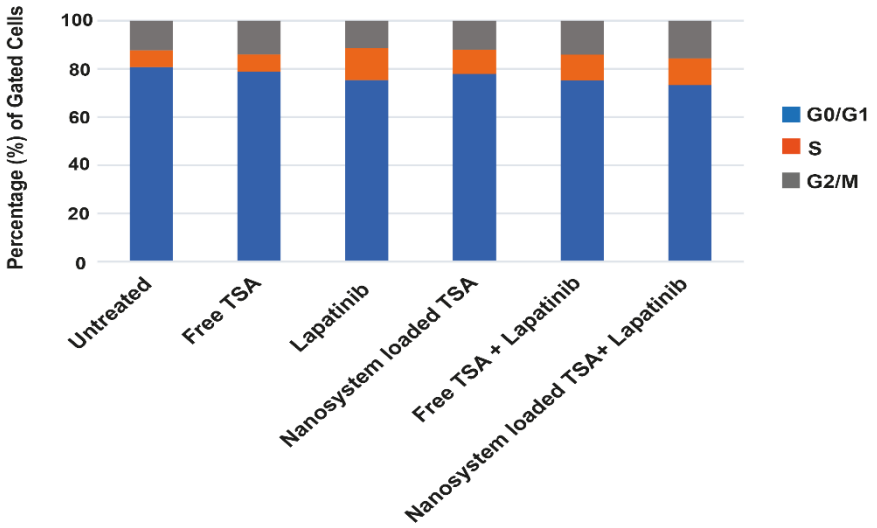

Figure 3.3.18. Analysis of cell cycle of EMT induced MDA MB-231 cells following 48 h of treatment with inhibitors indicating an increase in S-phase.

3.3.1.9. Co-targeting EMT Significantly Alters the Expression of EMT Markers: The EGF receptor are often overexpressed in malignant tumors and are acknowledged for their involvement in tumor growth and progression [119]. Several studies have conceded that epigenetic factors like histone modifications are involved in the regulation of EGF induced EMT. Many studies have reported that HDAC inhibitors abate EMT by upregulating E-cadherin in various solid tumors like ovarian cancer, breast cancer, esophageal cancer, etc., thus suggesting the role of HDAC inhibitors in the therapeutic reduction of EMT. Overexpression of EGFR is associated with poor prognosis, cell proliferation, tumor progression, and subsequently leading to metastasis thereby resulting in lowered survival rate in patients with advanced cancer. Several tyrosine kinase inhibitors (TKIs) targeting EGFR have been successfully developed for treatment of cancer patients; however, they displayed prominent activity only in heavy doses [120].

Our mRNA expression studies of uninduced MDA MB-231 cells after co-therapy with targeted TSA and lapatinib revealed increment in the expression of E-cadherin and depletion in N-cadherin expression by ~8 fold and ~0.8 fold respectively, at a much lower concentration compared to the singly or untargeted inhibitors treatment, thereby suggesting the suppression of EMT in TNBC. Subsequently, it was also observed that there was significant reduction in the expression of TWIST1 by ~0.4 fold as well, however, no noticeable change in the expression of SNAI1 was observed after the homologous co-targeted therapy (**Figure 3.3.19**). The fold change in uninduced MDA MB-231 cells has been summarized in **Table 3.3.10.**

Sample	E-cadherin	N-cadherin	TWIST1
Free TSA	4.7	0.82	0.25
Free Lapatinib	2.2	0.2	0.3
Nano-system loaded TSA	7.6	0.5	0.3
Free TSA+ Lapatinib	1.3	0.9	0.12
Nano-system loaded TSA+Lapatinib	8.3	0.84	0.4

Table 3.3.10. Fold change in the expression of EMT markers following treatment of MDA MB-231 cells with the different inhibitors.

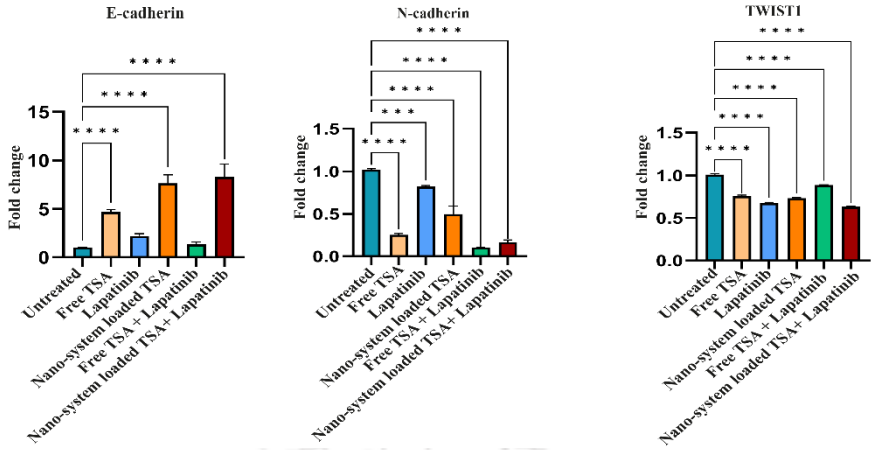

Figure 3.3.19. Graphical elucidations of alterations in gene expression conforming to treatment with inhibitors quantitated by qRT-PCR analysis. Findings are represented as mean of relative gene expression level w.r.t β-actin ± SEM of three autonomous trials.

The mRNA expression studies of EMT induced MDA MB-231 cells after co-therapy with targeted TSA and lapatinib revealed an increment in the expression of E-cadherin and depletion in N-cadherin expression by ~5.6 fold and ~0.8 fold, respectively, at a much lower concentration compared to the singly or untargeted inhibitors treatment, thereby suggesting the suppression of EGF induced EMT in TNBC. Subsequently, it was detected that there was significant reduction in the expression of TWIST1 by ~0.6 fold as well; however, no noticeable change in the expression of SNAI1 was observed after the homologous co-targeted therapy (**Figure 3.3.20**). The fold change in the expression of EMT markers of induced MDA MB-231 cells have been summarised in **Table 3.3.11**.

Sample	E-cadherin	N-cadherin	TWIST1
Free TSA	5.07	0.43	-
Free Lapatinib	4.2	0.78	0.2
Nano-system loaded TSA	5.3	0.6	-
Free TSA+ Lapatinib	3.9	0.66	-
Nano-system loaded TSA+Lapatinib	5.6	0.75	0.55

Table 3.3.11. Fold change in the expression of EMT markers following treatment of induced MDA MB-231 cells with the different inhibitors.

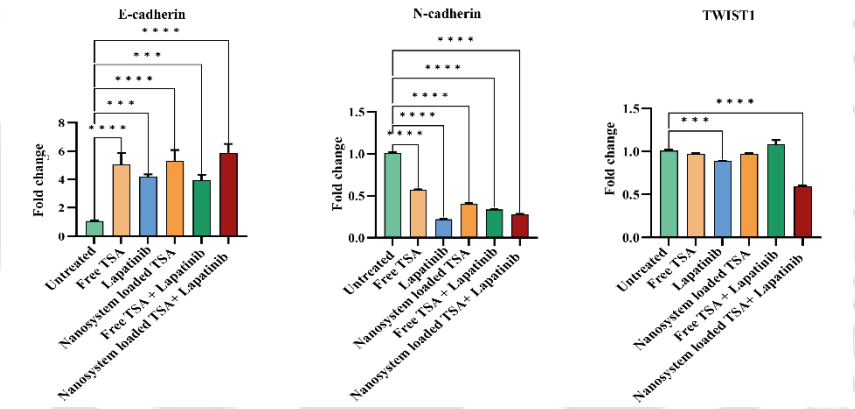

Figure 3.3.20. Graphical elucidation of alterations in gene expression conforming to treatment with free and loaded inhibitors and in the combination module quantitated by qRT-PCR. Findings reveal an increase in epithelial markers and a decrease in mesenchymal markers and are represented as mean of relative gene expression w.r.t. β-actin ± SEM of three autonomous trials.

3.3.1.10. Homologous Targeting Results in Significant Inactivation of the Non-canonical Wnt/*β*-Catenin Signaling Pathway: Studies have indicated the involvement of histone modifications and tyrosine kinases in the development and progression of EMT. Since the HDACi TSA was found to be toxic *in vivo* and require high doses of TKI lapatinib for an effective outcome, the MDA MB-231 cells were treated by homologous co-targeting.

After treatment of the uninduced MDA MB-231 cells with the inhibitors, a downregulation in the EMT markers, Vimentin and ZEB1 by ~0.5 fold each was observed in targeted co-therapy. It was also seen that there was no significant change in the expression of Sp1 after treatment with the lapatinib and in combination with lapatinib. The downstream molecule, *β*-catenin, was also significantly downregulated by ~0.5 fold following treatment with targeted co-therapy. The fold change alteration in the expression of *β*-Catenin, ZEB1, Vimentin and Sp1 following treatment with the different inhibitors singly and in combination have been summarised in **Table 3.3.12.** C-myc and Akt was significantly downregulated when treated in combination in targeted combination module by ~0.4 and ~0.7 fold each. There was also a significant lowered expression in Gsk3β and HDAC4 by ~0.3 fold and ~0.8 fold respectively, following treatment with targeted combination therapy (**Figure 3.3.21**). The fold change alteration in the expression of c-myc, Akt, Gsk3β and HDAC4 following treatment with the different inhibitors singly and in combination have been summarised in **Table 3.3.13.**

Sample	β-Catenin	ZEB1	Vimentin	Sp1
Free TSA	0.7	0.6	-	0.6
Free Lapatinib	0.4	0.32	-	0.1
Nano-system loaded TSA	0.9	0.6	0.56	0.8
Free TSA+ Lapatinib	0.5	0.3	0.43	-
Nano-system loaded TSA+Lapatinib	0.5	0.55	0.5	-

Table 3.3.12. The fold change alteration in the expression of β-Catenin, ZEB1, Vimentin and Sp1 following treatment with inhibitors.

Sample	c-myc	Akt	Gsk3β	HDAC4
Free TSA	0.1	0.4	0.5	0.82
Free Lapatinib	0.2	-	0.4	0.74
Nano-system loaded TSA	-	-	0.5	0.74
Free TSA+ Lapatinib	-	0.64	0.3	0.78
Nano-system loaded TSA+Lapatinib	0.43	0.66	0.3	0.8

Table 3.3.13. The fold change alteration in the expression of c-myc, Akt, Gsk3β and HDAC4 following treatment with inhibitors.

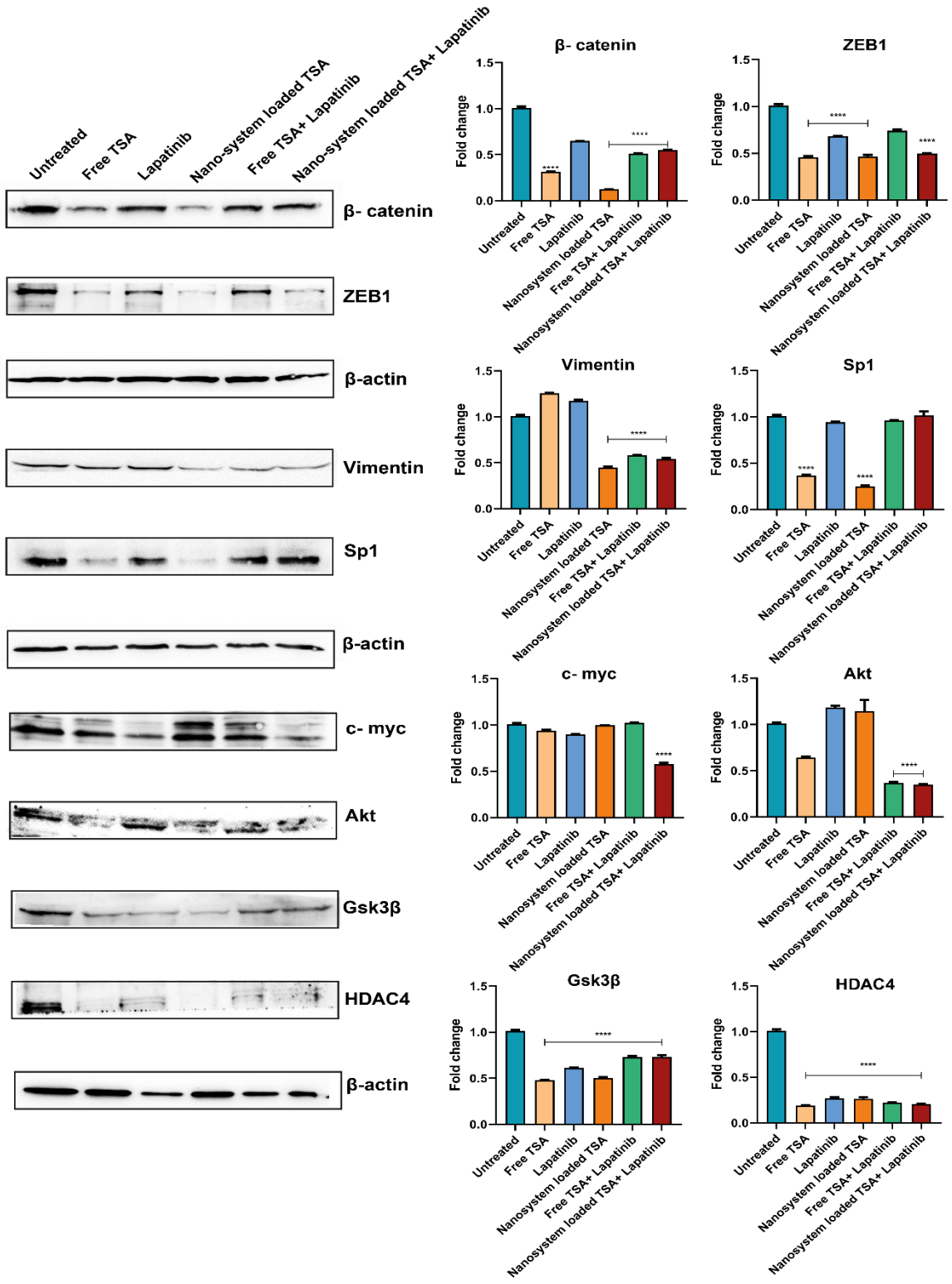

Figure 3.3.21 Western Blot representatives showing levels of β- catenin, ZEB1, Vimentin, Sp1, c-myc, Akt, Gsk3β, HDAC4 and β-actin in MDA MB- 231 cell extracts which were treated with IC_{50} values of the inhibitors for 48 h. β-actin acts as a loading check.

Protein expression analysis of EMT induced MDA MB-231 cells revealed the downregulation of EMT markers, Vimentin by ~0.6 fold and ZEB1 and Slug by ~0.5 fold each, after targeted co-therapy module (**Figure 3.3.22**). It was found that HDAC4, which effectively regulates EMT by upregulation of the expression of Vimentin and reduction in E-cadherin expression in an esophageal carcinoma, was also down-regulated when treated with the homologous targeting by co-therapy by ~0.6 fold in the case of metastatic breast cancer. Although free TSA, nanosystem loaded TSA, and free TSA + lapatinib exhibited similar effect on the expression profile following treatment, a similar extent of down-regulation in the expression of HDAC4 was attained with a much lower concentration when the EMT induced TNBC cells were treated with the combination module (**Figure 3.3.22**). Specificity protein 1 (Sp1), which is a transcription factor and has a key role in tumor ontogeny in breast cancer, was detected to be upregulated in EMT induced MDA MB-231 cells. Though, there was no significant alteration in expression upon treatment with the inhibitors treated singly, however, upon treatment in combination module, there was a decrease in its expression that was significantly lowered by ~0.5 fold when treated with nanosystem loaded TSA + lapatinib.

Subsequently, the protein expression profiling of the EMT induced MDA MB-231 cells upon co-therapy resulted in the alteration of the Wnt/β-catenin signaling pathway by the downregulation of the expression of β-catenin by ~0.7 fold, c-myc by ~0.8 fold, Gsk-3β by ~0.4 fold and pGsk-3β by ~0.3 fold, thereby affecting the progression of EMT. Reports have shown that Akt signaling pathway interacts with Wnt/β-catenin signaling pathway resulting in drug resistance. Akt was most effectively downregulated when the TNBC cells were treated with lapatinib by ~0.8 fold; however, the change in expression was not highly modulated (~0.2 fold) when the cells were treated with targeted co-therapy (**Figure 3.3.22**). The alteration in the expression of the above mentioned proteins have been summarised in **Table 3.3.14, 3.3.15, 3.3.16 and 3.3.17.**

Sample	*β*-Catenin	ZEB1	Akt
Free TSA	0.45	-	0.3
Free Lapatinib	0.5	0.5	0.8
Nano-system loaded TSA	0.8	0.54	0.2
Free TSA+ Lapatinib	0.7	0.4	0.2
Nano-system loaded TSA+Lapatinib	0.7	0.54	0.2

Table 3.3.14. Fold change in the expression of β-catenin, ZEB1 and Akt following treatment of induced MDA MB-231 cells with different inhibitors.

Sample	Gsk-3*β*	pGsk-3*β*
Free TSA	0.1	-
Free Lapatinib	-	-
Nano-system loaded TSA	-	-
Free TSA+ Lapatinib	0.2	-
Nano-system loaded TSA+Lapatinib	0.4	0.3

Table 3.3.15. Fold change in the expression of Gsk-3β and pGsk-3β following treatment of induced MDA MB-231 cells with different inhibitors.

Sample	Slug	Vimentin
Free TSA	0.3	0.45
Free Lapatinib	0.2	0.3
Nano-system loaded TSA	0.46	0.6
Free TSA+ Lapatinib	0.48	0.55
Nano-system loaded TSA+Lapatinib	0.5	0.55

Table 3.3.16. Fold change in the expression of Slug and Vimentin following treatment of induced MDA MB-231 cells with different inhibitors.

Sample	c-myc	HDAC4	Sp1
Free TSA	-	0.7	0.1
Free Lapatinib	0.6	-	-
Nano-system loaded TSA	-	0.7	-
Free TSA+ Lapatinib	0.4	0.7	0.23
Nano-system loaded TSA+Lapatinib	0.84	0.6	0.53

Table 3.3.17. Fold change in the expression of c-myc, HDAC4 and Sp1 following treatment of induced MDA MB-231 cells with different inhibitors.

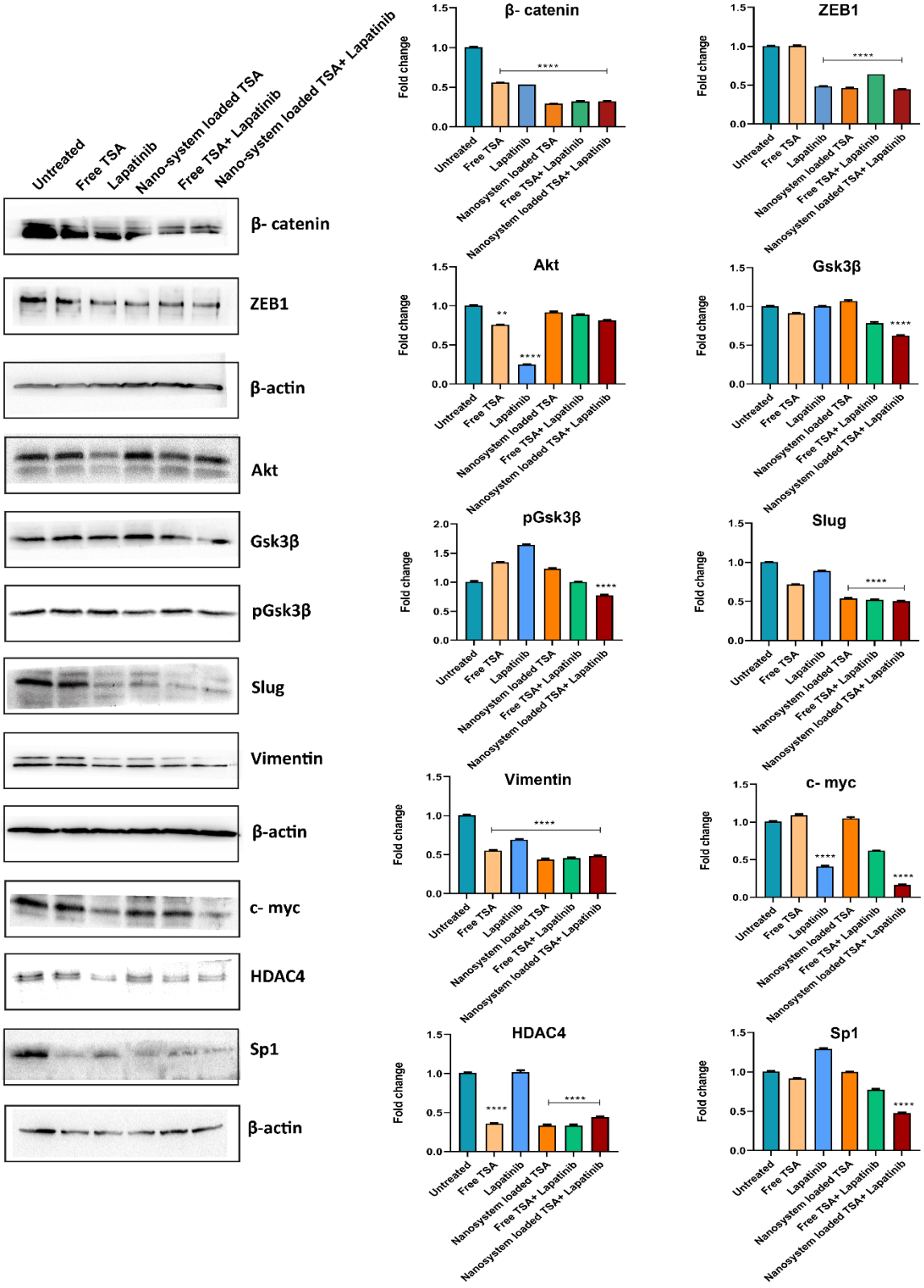

Figure 3.3.22. Western blot representatives showing levels of *β*-catenin, ZEB1, Akt, Gsk3*β*, pGsk3*β*, Slug, Vimentin, c-myc, HDAC4, Sp1, and *β*-actin in EMT induced MDA MB-231 cell extracts that were treated with IC_{50} values of the inhibitors for 48 h. *β*-actin acts as a loading check.

3.3.2. Discussion: Breast cancer has been ranked as the leading cause for the increase in mortality rate in women with poor prognosis and lack of targeted therapeutics. Based on the receptors present, TNBC is the most metastatic and resistant to therapies and drugs. Chemotherapy and radiotherapy are the most commonly accepted therapies for successful treatment [121]. The absence of receptors on the surface of TNBC cells and a multitude of crosstalk, makes it a challenging process to target and prevent EMT [122] [123]. Though single therapy treatment shows effective results in preclinical studies, it fails to display promising results in clinical models [69]. Multiple signaling networks have been detected to be involved in enduring the EMT and stemness of TNBC cells, which are governed by a cascade of events; however, very few pathways are efficacious for effective therapy for TNBC.

Wnt/β-catenin signaling has a crucial part in the development of embryos and tumors by influencing cell proliferation, differentiation, and survival [69]. Krejci *et al*. showed that RTK signaling mediated by EGFR kinases actuates Wnt/β-catenin signaling by phosphorylation of LRP6 [124]. Epigenetic therapy is an emerging field for cancer therapy, as it has been observed that HDACi and DNMTi have the ability to reverse immune escape via several mechanisms, thereby leading to an increase in the expression of immune related genes [125]. Although the use of histone modulators like HDACi and DNMTi has been clinically limited to hematological malignancies, their usage has not been extensively studied in breast cancers [121].

The important challenge in present day cancer therapy is to develop targeted anticancer drugs for site specific delivery for effective treatment and minimal toxicity. Thereby, in order to develop a more targeted and efficient therapy, fused nanosystems was developed by fusing nano-vesicles from MDA MB-231 cells and exosomes from MCF-7 cell lines to target EMT induced TNBC. The pan HDACi, Trichostatin A (TSA), and a tyrosine kinase inhibitor, lapatinib were chosen for co-

targeting and found that the targeted co-therapy resulted in an enhanced cytotoxic effect and suppressed metastatic behavior. This is due to decreased cell proliferation, migration, and induction of apoptosis by causing an increment in the generation of ROS in the TNBC cells, MDA MB-231. Cell cycle progression is a very highly regulated mechanism whose imbalance results in uncontrolled growth and proliferation of cells resulting in metastasis and several other irregularities. Our targeted co-therapy resulted in an increased S-phase arrest and increased sub-G1 population, depicting cell shrinkage and DNA fragmentation, which are the markers of programmed cell death.

Considering the crosstalk among several signaling pathways involved in the metastasis of EMT, the contributions of Wnt/β-catenin signaling and histone modifications in TNBC progression was endeavoured to be elucidated. The expression profiles of the downstream signaling pathways were investigated that might play a major role in this critical transition. The study showed that SNAI2, a transcriptional repressor of E-cadherin, was downregulated by the targeted co-treatment. This resulted in an increment of E-cadherin expression but reduction in N-Cadherin expression, thereby reversing EMT phenotype.

Myc, a transcription factor, activation results in the recruitment of an array of coactivators to E-box elements, thereby resulting in the regularization of several biological processes [126]. The c-myc gene is a majorly amplified oncogene in human breast cancer [127]. Yin *et al*. showed that overexpression of myc resulted in higher levels of Vimentin and Zeb-1, two ingrained markers of EMT, and did not express perceptible E-cadherin in MDA MB-231 cells [128]. After the treatment of EGF induced MDA MB-231 cells with our targeted co-therapeutic drugs, it was observed that there was an effective decrease in the expression of c-myc. The targeted therapy also resulted in increased efficiency in the decreased expression of Vimentin and ZEB1 (Zinc Finger E-box binding homeobox) and Slug, the phenotypical markers of EMT as compared to single agent therapy or untargeted

co-treatment, thereby inhibiting metastasis in TNBC. Nam *et al*. showed that ZEB2 activated the EMT marker vimentin by activating the transcriptional activity of Sp1 and subsequently interacting with it, thereby upregulating mesenchymal gene expression and repressors of E-cadherin [129]. Sp1 is a transcription factor that is found to be required in the progression of breast cancer [130]. Our results show that Sp1 was significantly downregulated when treated with targeted inhibitors in combination, resulting in the repressing of EMT markers and contributing to its reversal.

TWIST1 is a transcription factor that is involved in a signaling cascade responsible for the initiation of mesoderm development, resulting in the loss of expression of epithelial characteristics and an increase in the mesenchymal properties [131]. A significant decrease in the expression of TWIST1 was observed by the targeted co-treatment which eventually decrease the efficiency of metastasis in TNBC cells.

Tzeng *et al*. showed that WNT signals crosstalk with Akt signaling pathway by enhancing phosphorylation of Gsk3β, which acts as a bridge between the two pathways, thereby resulting in resistance to pan inhibitors in TNBC [132]. In the downstream regulator genes such as β-catenin and Akt was significantly lowered after targeted co-therapy, suggesting that this co-treatment can positively regulate TNBC suppression in a more efficacious manner. GSK3β is a multifaceted kinase that acts as a major factor in regulating a number of cellular processes and participates in several different pathways but is broadly studied owing to its indispensable involvement in the Wnt/β-catenin signaling pathway [133]. Vijay *et al*. observed that there was significant inhibition in sphere formation when treated with Gsk3β inhibitors, thereby targeting stem cell-like properties that are promoted by EMT [133]. Our studies resulted in the inhibited expression of Gsk3β, which contributed to a decrease in the expression of mesenchymal phenotypic markers, designating its ability to suppress the progress of EMT.

Collectively, the fusion of exosomes and membrane derived nano-vesicles from breast cancer cells can serve as an efficient targeted delivery system by efficient homing to the parental cells that reduces the laborious engineering of nanoparticles for specific delivery. The inhibitor loaded nanosystem also resulted in an increased effect over the regulatory pathways with respect to the free components, resulting in more efficacious anticancer activities.

3.3.3. Conclusion: Considering the resistance of metastatic TNBC toward various anticancer drugs and therapies due to unregulated expression of proliferative genes and proteins, a homologous and multitargeted therapy by aiming two pathways, namely, Wnt/β-catenin signaling and histone modification was ventured upon. Both these pathways have been found to be independently responsible in augmenting the metastatic behavior of TNBC. The present study showed that targeted cotherapy using fused exosomes and nano-vesicles from breast cancer cells resulted in an efficient subduing of EGF induced triple negative breast cancer that not only resulted in apoptosis of the MDA MB-231 cells, but also affected the regulatory pathways at the genetic and proteomic levels in a synergistic manner. The targeted therapy using a hybrid fusion of exosomes and membrane derived nano-vesicles played a very substantial role in the site specific delivery of the drugs for a more effective outcome for the curtailment of metastatic TNBC

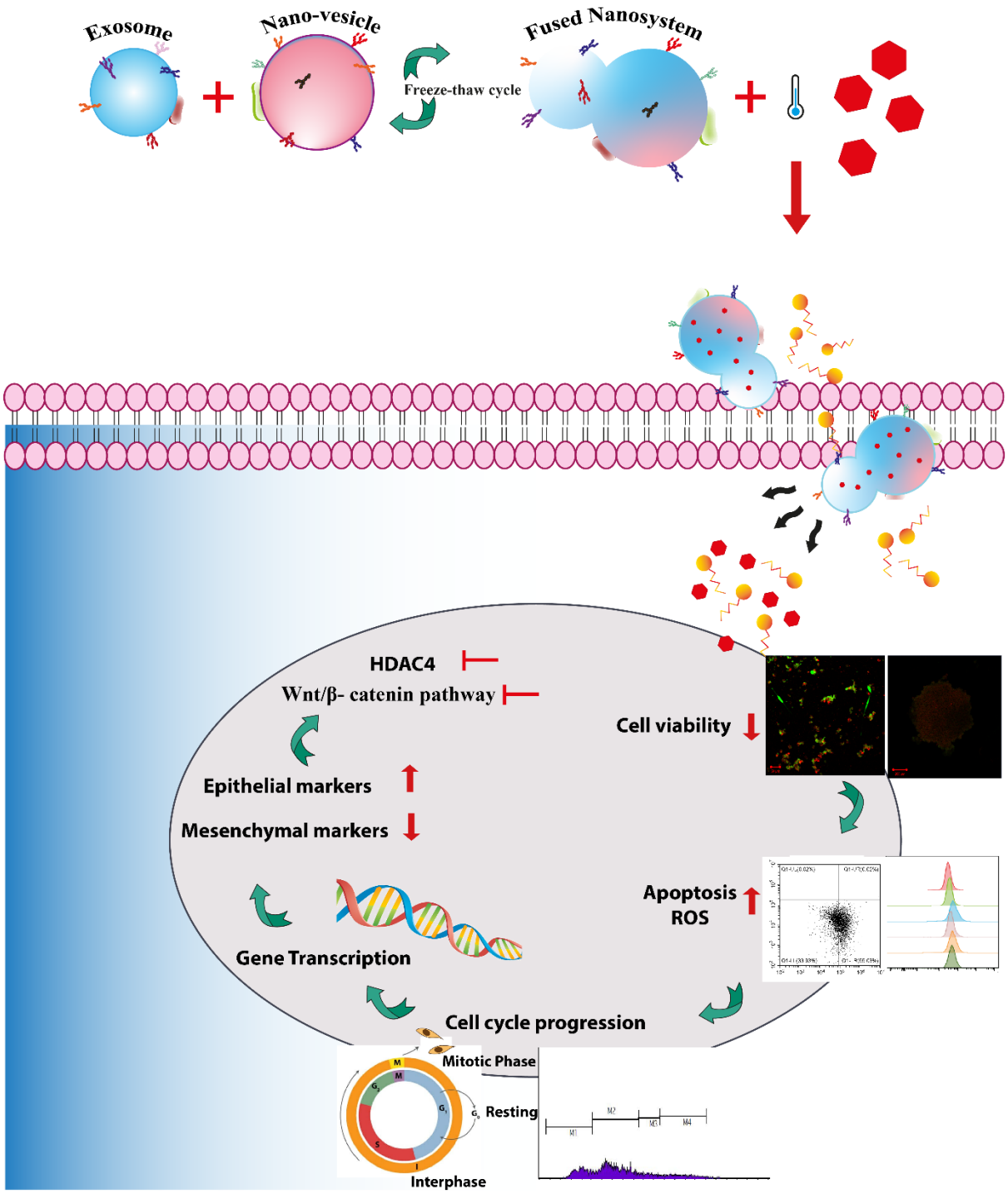

Schematic 3.3: Formulation of a hybrid nanosystem for homologous co-targeted therapy of triple negative breast cancer [***ACS Applied Bio Materials***, 6(2), 681-693, 2023].

Section 4

Conclusion and Future Prospects

Conclusion and Future Prospects

TNBC is regulated by several interdependent signaling pathways, contributing to the activation of EMT and subsequently resulting in enhanced invasive and migration abilities. The heterogeneous nature, negative expression of hormone receptors on the surface and cross-talks among multiple pathways make it arduous to target TNBC and suppress the progression of EMT. In spite of the discovery and development of several therapeutic strategies to curb TNBC, failing to achieve targeted delivery of the therapeutic drugs have resulted in its ineffectiveness. The current thesis work has focused on the development of a site directed delivery system and targeting the pathways which are significantly involved in the advancement of TNBC.

The salient conclusions of the work have been categorized under three major subheadings and delineated below:

Development of a biomimetic nanocarriers for specific homologous targeting of breast cancer.

- Nano-vesicles were synthesised from breast cancer cells for site-directed delivery.
- They were substantially hemo-compatible and biocompatible which would contribute to avoid evasion by the immune system.
- The nano-vesicles retained its inherent properties like surface receptors even after downstream processing.
- The high uptake of the nano-vesicles and excellent internalization by their parent cells suggested the successful homologous targeting by the nano-vesicles.
- Evaluation of cellular uptake mechanism indicated that the nano-vesicles were primarily taken up by the clathrin-mediated pathway.

- Additionally, loading of a drug in the nano-vesicles exhibited efficient cytotoxic ability by apoptosis at lower dosage as compared to treatment with free drugs.
- Employing multicellular tumor spheroids, which mimicked tumor microenvironment, to evaluate the cytotoxic ability of drug loaded nano-vesicles helped to understand and study the effect of our system on the tumor models for better interpretation.
- The generation of ROS following treatment with nano-vesicle loaded drug implied regulated cell death *via* nucleic acid damage or membrane disruption of the cancer cells.
- Taking into consideration the findings, it may be stated that the use of cell membranes as biological nano-carrier, demonstrating impressive self-homing capabilities, might lead to the development of a potential nano-delivery system for cancer therapy *in vivo* as they can be derived from the patient's own cells.

Targeting tumor micro-environment of metastatic TNBC cells via exosomes derived from non-invasive breast cancer cells for MDR inhibition and enhancing drug susceptibility.

- Exosomes were successfully isolated from non-invasive breast cancer cell line by polymer- precipitation method.
- Though the exosomes did not show significant cytotoxicity against the metastatic TNBC cell line, however, the increase in the generation of ROS indicated induction of DNA damage.
- Changes in the cell cycle progression with an S-phase arrest was observed in metastatic TNBC cell line following treatment with exosomes implying suppression of proliferation.
- Immunocytochemistry revealed a decrement in the expression of MDR1/ABCB1 and EGFR after exosome treatment.

- Gene expression analysis exhibited alteration in the expression of ABC transporters by the downregulation of ABCB1, ABCG2 and ABCC1 responsible for multi-drug resistance following treatment of metastatic TNBC cells with exosomes.
- The expression of EMT markers were also found to be significantly lowered confirming the ability of exosomes from non-invasive breast cancer cell line in modulation of the tumor niche of TNBC cells by the induction of phase transition from mesenchymal phenotype (EMT) to epithelial phenotype (MET).
- The cytotoxic study of an inhibitor in combination with exosomes showed an increased effect in TNBC cells towards anti-cancerous drugs demonstrating an effective increment in drug sensitivity.
- In conclusion, the findings delineated the effect of exosomes in the modification of the tumor niche thereby lowering the drug resistance ability and making it susceptible towards targeted and efficient anti-cancer therapy.

Engineering hybrid nanosystem for homologous targeting of EMT induced triple negative breast cancer cells.

- A hybrid nanosystem was synthesised by fusing exosomes from non-invasive breast cancer cell line and nano-vesicles from the cells to be targeted.
- The hybrid nanosystem was loaded with an HDAC inhibitor and employed to target epigenetic modulation in combination with Wnt/β-catenin pathway by combination treatment with tyrosine kinase inhibitor.
- The targeted co-therapy exhibited better anti-proliferative effect by the induction of apoptosis at a much lower dosage as compared to freely available inhibitors.

- The targeted co-therapy resulted in the lowering of the migration potential of TNBC in a more efficient mode.
- The Calcein AM/PI dual staining assay reveal efficient apoptosis mediated cell death in spheroids following treatment with targeted co-therapy.
- Co-targeting Wnt/β-catenin pathway and histone deacetylation induced the phase transition from epithelial to mesenchymal transition (EMT) to mesenchymal to epithelial transition (MET).
- Proteomic analysis of the metastatic TNBC cells exhibited downregulation in the expression of the downstream molecules of Wnt/β-catenin pathway and HDAC implying suppression of mesenchymal differentiation and stemness of TNBC.
- In conclusion, the findings of the study demonstrated targeted co-therapy resulted in an efficient subduing of EGF induced triple negative breast cancer by affecting the regulatory pathways at the genetic and proteomic levels in a synergistic manner.
- The targeted therapy using a hybrid fusion of exosomes and membrane derived nano-vesicles played a very substantial role in the site specific delivery of the drugs for a more effective outcome for the curtailment of metastatic TNBC.

Future prospects:

The future scope of the work based on current investigations include

- the development of a specified nano-delivery system for the cells or diseases to be targeted by synthesising nano-carriers from the parent cells.
- using exosomes to modulate microenvironment of the diseased area thereby making it susceptible to resistant drugs and having an enhanced therapeutic effect.

- The corroborations of this research might open up new horizons for the curtailment of metastatic TNBC with further validations in *in vivo* system

References

[1] Sung H, Ferlay J, Siegel RL, Laversanne M, Soerjomataram I, Jemal A, Bray F. Global cancer statistics 2020: GLOBOCAN estimates of incidence and mortality worldwide for 36 cancers in 185 countries. *CA. Cancer J. Clin.* 2021; 71(3): 209-249.

[2] J. S. Reis-filho and D. Ph, "Triple-Negative Breast Cancer, *New England journal of medicine,* 2010; 363(20):1938-48.

[3] Wang DY, Jiang Z, Ben-David Y, Woodgett JR, Zacksenhaus E. Molecular stratification within triple-negative breast cancer subtypes. *Scientific reports*. 2019; 9(1):19107.

[4] Ensenyat-Mendez M, Llinàs-Arias P, Orozco JI, Íñiguez-Muñoz S, Salomon MP, Sesé B, DiNome ML, Marzese DM. Current triple-negative breast cancer subtypes: dissecting the most aggressive form of breast cancer. *Frontiers in oncology*. 2021; 11:681476.

[5] Dass SA, Tan KL, Selva Rajan R, Mokhtar NF, Mohd Adzmi ER, Wan Abdul Rahman WF, Tengku Din TA, Balakrishnan V. Triple negative breast cancer: A review of present and future diagnostic modalities. *Medicina*. 2021; 57(1):62.

[6] Lehmann BD, Pietenpol JA. Clinical implications of molecular heterogeneity in triple negative breast cancer. *The Breast*. 2015; 24:S36-40.

[7] Bianchini G, Balko JM, Mayer IA, Sanders ME, Gianni L. Triple-negative breast cancer: challenges and opportunities of a heterogeneous disease. *Nature reviews Clinical oncology*. 2016; 13(11):674-90.

[8] Jang MH, Kim HJ, Kim EJ, Chung YR, Park SY. Expression of epithelial-mesenchymal transition–related markers in triple-negative breast cancer: ZEB1 as a potential biomarker for poor clinical outcome. *Human pathology*. 2015; 46(9):1267-74.

[9] Kalluri R, Weinberg RA. The basics of epithelial-mesenchymal transition. *The Journal of clinical investigation*. 2009; 119(6):1420-8.

[10] Gonzalez DM, Medici D. Signaling mechanisms of the epithelial-mesenchymal transition. *Science signaling*. 2014; 7(344):re8-.

[11] Telli ML, Carlson RW. First-line chemotherapy for metastatic breast cancer. *Clinical breast cancer*. 2009; 9:S66-72.

[12] Coley HM. Mechanisms and strategies to overcome chemotherapy resistance in metastatic breast cancer. *Cancer treatment reviews*. 2008; 34(4):378-90.

[13] Gottesman MM, Fojo T, Bates SE. Multidrug resistance in cancer: role of ATP–dependent transporters. *Nature reviews cancer*. 2002; 2(1):48-58.

[14] Simon SM, Schindler M. Cell biological mechanisms of multidrug resistance in tumors. Proceedings of the National Academy of Sciences. 1994; 91(9):3497-3504.

[15] Gottesman MM. Mechanisms of cancer drug resistance. *Annual review of medicine*. 2002; 53(1):615-627..

[16] Larsen AK, Escargueil AE, Skladanowski A. Resistance mechanisms associated with altered intracellular distribution of anticancer agents. *Pharmacology & therapeutics*. 2000; 85(3):217-229.

[17] Chikazawa N, Tanaka H, Tasaka T, Nakamura M, Tanaka M, Onishi H, Katano M. Inhibition of Wnt signaling pathway decreases chemotherapy-resistant side-population colon cancer cells. *Anticancer research*. 2010; 30(6):2041-2048..

[18] Wang Z, Li Y, Kong D, Banerjee S, Ahmad A, Azmi AS, Ali S, Abbruzzese JL, Gallick GE, Sarkar FH. Acquisition of epithelial-mesenchymal transition phenotype of gemcitabine-resistant pancreatic cancer cells is linked with activation of the notch signaling pathway. *Cancer research*. 2009; 69(6):2400-2407.

[19] Sissung TM, Baum CE, Kirkland CT, Gao R, Gardner ER, Figg WD. Pharmacogenetics of membrane transporters: an update on current approaches. *Molecular biotechnology*. 2010; 44:152-67.

[20] M. Dean, Y. Hamon, and G. Chimini, "The human ATP-binding cassette (ABC) transporter superfamily," *Journal of Lipid Research*. 2001; 42(7):1007-17

[21] C. H. Choi, "ABC transporters as multidrug resistance mechanisms and the development of chemosensitizers for their reversal," *Cancer Cell International*. 200; 5:1-3.

[22] F. J. Sharom, "ABC multidrug transporters: Structure, function and role in chemoresistance," *Pharmacogenomics*. 2008; 105-127.

[23] H. Lage, "An overview of cancer multidrug resistance: A still unsolved problem," *Cellular and Molecular Life Sciences*. 2008; 65:3145-67.

[24] K. M. Britton *et al.*, "Breast cancer, side population cells and ABCG2 expression," *Cancer*

Lett., 2012; 323(1):97-105.

[25] F. Guestini *et al.*, "Impact of Topoisomerase IIα, PTEN, ABCC1/MRP1, and KI67 on triple-negative breast cancer patients treated with neoadjuvant chemotherapy," *Breast Cancer Research and Treatment*, 2019; 173:275-88.

[26] B. G. Hollier, K. Evans, and S. A. Mani, "The epithelial-to-mesenchymal transition and cancer stem cells: A coalition against cancer therapies," *Journal of Mammary Gland Biology and Neoplasia*. 2009; 14:29-43.

[27] A. Singh and J. Settleman, "EMT, cancer stem cells and drug resistance: An emerging axis of evil in the war on cancer," *Oncogene*. 2010; 29(34):4741-51.

[28] Y. Li, M. Y. Maitah, A. Ahmad, D. Kong, B. Bao, and F. H. Sarkar, "Targeting the Hedgehog signaling pathway for cancer therapy," *Expert Opinion on Therapeutic Targets*. 2012; 16(1):49-66.

[29] N. Yang *et al.*, "Inhibition of sonic hedgehog signaling pathway by Thiazole Antibiotic Thiostrepton Attenuates the CD44+/CD24-stem-like population and sphere-forming capacity in triple-negative breast cancer," *Cell. Physiol. Biochem.*, 2016; 38(3):1157-70.

[30] M. Garg, "Epithelial-mesenchymal transition - activating transcription factors - multifunctional regulators in cancer," *World J. Stem Cells*, 2013; 5(4):188.

[31] J. M. Bailey, P. K. Singh, and M. A. Hollingsworth, "Cancer metastasis facilitated by developmental pathways: Sonic hedgehog, notch, and bone morphogenic proteins," *Journal of Cellular Biochemistry*. 2007; 102(4):829-39.

[32] T. Palomero *et al.*, "CUTLL1, a novel human T-cell lymphoma cell line with t(7;9) rearrangement, aberrant NOTCH1 activation and high sensitivity to γ-secretase inhibitors," *Leukemia*, 2006; 20(7):1279-87.

[33] J. J. Speiser, Ç. Erşahin, and C. Osipo, "The functional role of notch signaling in triple-negative breast cancer," in *Vitamins and Hormones*, 2013; 93:277-306.

[34] R. Soares, G. Balogh, S. Guo, F. Gärtner, J. Russo, and F. Schmitt, "Evidence for the notch signaling pathway on the role of estrogen in angiogenesis," *Mol. Endocrinol.*, 2004; 1;18(9):2333-43.

[35] A. Sharma, A. N. Paranjape, A. Rangarajan, and R. R. Dighe, "A monoclonal antibody against human notch1 ligand-binding domain depletes subpopulation of putative breast

cancer stem-like cells," *Mol. Cancer Ther.*, 2012; 11(1):77-86.

[36] R. Benedito *et al.*, "The Notch Ligands Dll4 and Jagged1 Have Opposing Effects on Angiogenesis," *Cell*, 2009; 137(6):1124-35.

[37] L. Sun and J. Fang, "Epigenetic regulation of epithelial–mesenchymal transition," *Cellular and Molecular Life Sciences*. 2016; 73:4493-515.

[38] A. Nickel and S. C. Stadler, "Role of epigenetic mechanisms in epithelial-to-mesenchymal transition of breast cancer cells," *Translational Research*. 2015; 165(1):126-42.

[39] S. J. Serrano-Gomez, M. Maziveyi, and S. K. Alahari, "Regulation of epithelial-mesenchymal transition through epigenetic and post-translational modifications," *Molecular Cancer*. 2016; 5(1):1-4.

[40] P. Fedele, L. Orlando, and S. Cinieri, "Targeting triple negative breast cancer with histone deacetylase inhibitors," *Expert Opinion on Investigational Drugs*. 2017; 26(11):1199-206.

[41] K. K. Wong, "DNMT1: A key drug target in triple-negative breast cancer," *Seminars in Cancer Biology*. 2021; 72: 198-213 (Academic Press).

[42] E. Martin-Orozco, A. Sanchez-Fernandez, I. Ortiz-Parra, and M. Ayala-San Nicolas, "WNT Signaling in Tumors: The Way to Evade Drugs and Immunity," *Front. Immunol.* 2019; 10:2854.

[43] L. Farahmand, B. Darvishi, K. Majidzadeh-A, and A. Madjid Ansari, "Naturally occurring compounds acting as potent anti-metastatic agents and their suppressing effects on Hedgehog and WNT/β-catenin signalling pathways," *Cell Proliferation*. 2017; 50(1):e12299.

[44] X. Xu, M. Zhang, F. Xu, and S. Jiang, "Wnt signaling in breast cancer: biological mechanisms, challenges and opportunities," *Molecular Cancer*. 2020; 19:1-35.

[45] W. Wang, Q. Pan, G. M. Fuhler, R. Smits, and M. P. Peppelenbosch, "Action and function of Wnt/β-catenin signaling in the progression from chronic hepatitis C to hepatocellular carcinoma," *Journal of Gastroenterology*. 2017; 52:419-31.

[46] S. Moradi-Kalbolandi, A. Hosseinzade, M. Salehi, P. Merikhian, and L. Farahmand, "Monoclonal antibody-based therapeutics, targeting the epidermal growth factor receptor family: from herceptin to Pan HER," *Journal of Pharmacy and Pharmacology*. 2018; 70(7):841-54.

[47] J. A. Mccubrey *et al.*, "GSK-3 as potential target for therapeutic irvention in cancer,"

Oncotarget 2014; 5(10):2881.

[48] M. A. Medina *et al.*, "Triple-negative breast cancer: A review of conventional and advanced therapeutic strategies," *International Journal of Environmental Research and Public Health*. 2020; 17(6):2078.

[49] P. Lopez-Bergami and G. Barbero, "The emerging role of Wnt5a in the promotion of a pro-inflammatory and immunosuppressive tumor microenvironment," *Cancer and Metastasis Reviews*. 2020; 39:933-52.

[50] R. Butti, S. Das, V. P. Gunasekaran, A. S. Yadav, D. Kumar, and G. C. Kundu, "Receptor tyrosine kinases (RTKs) in breast cancer: Signaling, therapeutic implications and challenges," *Molecular Cancer*. 2018; 17(1):1-8.

[51] F. Khodabakhsh, P. Merikhian, M. R. Eisavand, and L. Farahmand, "Crosstalk between MUC1 and VEGF in angiogenesis and metastasis: a review highlighting roles of the MUC1 with an emphasis on metastatic and angiogenic signaling," *Cancer Cell International*. 2021; 21:1-1.

[52] J. Xu, J. R. Prosperi, N. Choudhury, O. I. Olopade, and K. H. Goss, "β-catenin is required for the tumorigenic behavior of triple-negative breast cancer cells," *PLoS One*, 2015; 10(2):e0117097.

[53] W. Xu *et al.*, "Hypoxia activates Wnt/β-catenin signaling by regulating the expression of BCL9 in human hepatocellular carcinoma," *Sci. Rep.*, 2017; 7(1):1-3.

[54] A. S. Zimmer, M. Gillard, S. Lipkowitz, and J. M. Lee, "Update on PARP Inhibitors in Breast Cancer," *Current Treatment Options in Oncology*. 2018; 19:1-9.

[55] A. A. Turk and K. B. Wisinski, "PARP inhibitors in breast cancer: Bringing synthetic lethality to the bedside," *Cancer*. 2018; 124(12):2498-506.

[56] P. García-Teijido, M. L. Cabal, I. P. Fernández, and Y. F. Pérez, "Tumor-infiltrating lymphocytes in triple negative breast cancer: The future of immune targeting," *Clinical Medicine Insights: Oncology*. 2016; CMO-S34540.

[57] E. Dai, Z. Zhu, S. Wahed, Z. Qu, W. J. Storkus, and Z. S. Guo, "Epigenetic modulation of antitumor immunity for improved cancer immunotherapy," *Molecular Cancer*. 2021; 20:1-27.

[58] M. Maio *et al.*, "Molecular pathways: At the crossroads of cancer epigenetics and immunotherapy," *Clin. Cancer Res.*, 2015; 21(18):4040-7.

[59] M. Conte, R. De Palma, and L. Altucci, "HDAC inhibitors as epigenetic regulators for cancer immunotherapy," *International Journal of Biochemistry and Cell Biology*. 2018; 98:65-74.

[60] P. Schmid *et al.*, "Atezolizumab and Nab-Paclitaxel in Advanced Triple-Negative Breast Cancer," *N. Engl. J. Med.*, 2018; 379(22):2108-21.

[61] N. Garmpis *et al.*, "Histone deacetylases as new therapeutic targets in triple-negative breast cancer: Progress and promises," *Cancer Genomics and Proteomics*. 2017; 14(5):299-313.

[62] M. J. Ramaiah, A. D. Tangutur, and R. R. Manyam, "Epigenetic modulation and understanding of HDAC inhibitors in cancer therapy," *Life Sciences*. 2021; 277:119504.

[63] M. Terranova-Barberio *et al.*, "HDAC inhibition potentiates immunotherapy in triple negative breast cancer," *Oncotarget*, 2017; 8(69):114156.

[64] A. Maiti, Q. Qi, X. Peng, L. Yan, K. Takabe, and N. C. Hait, "Class I histone deacetylase inhibitor suppresses vasculogenic mimicry by enhancing the expression of tumor suppressor and anti-angiogenesis genes in aggressive human TNBC cells," *Int. J. Oncol.*, 2019; 55(1):116-30.

[65] Y. M. Woo, "Epigenetic regulation in cystogenesis," in *Advances in Experimental Medicine and Biology*, 2016; 59-68.

[66] S. Wu, Z. Luo, P. J. Yu, H. Xie, and Y. W. He, "Suberoylanilide hydroxamic acid (SAHA) promotes the epithelial mesenchymal transition of triple negative breast cancer cells via HDAC8/FOXA1 signals," *Biol. Chem.*, 2016; 397(1):75-83.

[67] S. Vinayak *et al.*, "Open-label Clinical Trial of Niraparib Combined with Pembrolizumab for Treatment of Advanced or Metastatic Triple-Negative Breast Cancer," *JAMA Oncol.*, 2019; 5(8):1132-40.

[68] A. Lee and M. B. A. Djamgoz, "Triple negative breast cancer: Emerging therapeutic modalities and novel combination therapies," *Cancer Treatment Reviews*. 2018; 62:110-22.

[69] N. K. R. Chalakur-Ramireddy and S. B. Pakala, "Combined drug therapeutic strategies for the effective treatment of Triple Negative Breast Cancer," *Bioscience Reports*. 2018; 38(1).

[70] D. Rosenblum, N. Joshi, W. Tao, J. M. Karp, and D. Peer, "Progress and challenges towards targeted delivery of cancer therapeutics," *Nature Communications*. 2018; 9(1):1410.

[71] D. E. Owens and N. A. Peppas, "Opsonization, biodistribution, and pharmacokinetics of polymeric nanoparticles," *Int. J. Pharm.*, vol. 307, no. 1, pp. 93–102, 2006; 307(1):93-102.

[72] A. Aghebati-Maleki *et al.*, "Nanoparticles and cancer therapy: Perspectives for application of nanoparticles in the treatment of cancers," *Journal of Cellular Physiology*. 2020; 235(3):1962-72.

[73] Z. Chen *et al.*, "Cancer Cell Membrane-Biomimetic Nanoparticles for Homologous-Targeting Dual-Modal Imaging and Photothermal Therapy," *ACS Nano*, 2016; 10(11):10049-57.

[74] R. Li, Y. He, S. Zhang, J. Qin, and J. Wang, "Cell membrane-based nanoparticles: a new biomimetic platform for tumor diagnosis and treatment," *Acta Pharm. Sin., B* 2018; 8(1):14-22.

[75] J. Y. Zhu *et al.*, "Preferential Cancer Cell Self-Recognition and Tumor Self-Targeting by Coating Nanoparticles with Homotypic Cancer Cell Membranes," *Nano Lett.*, 2016; 16(9): 5895-901.

[76] D. M. Zhu *et al.*, "Engineered red blood cells for capturing circulating tumor cells with high performance," *Nanoscale*, 2018; 10(13):6014-23.

[77] C. M. J. Hu, L. Zhang, S. Aryal, C. Cheung, R. H. Fang, and L. Zhang, "Erythrocyte membrane-camouflaged polymeric nanoparticles as a biomimetic delivery platform," *Proc. Natl. Acad. Sci. U. S. A.*, 2011; 108(27):10980-5.

[78] C. M. J. Hu *et al.*, "Nanoparticle biointerfacing by platelet membrane cloaking," *Natu* , 2015; 526(7571):118-21.

[79] J. Jin and Z. M. Bhujwalla, "Biomimetic Nanoparticles Camouflaged in Cancer Cell Membranes and Their Applications in Cancer Theranostics," *Front. Oncol.*, 2020; 9:1560.

[80] B. Huppertz, C. Bartz, and M. Kokozidou, "Trophoblast fusion: Fusogenic proteins, syncytins and ADAMs, and other prerequisites for syncytial fusion," *Micron*, 2006; 37(6):509-17.

[81] P. S. Aguilar *et al.*, "Genetic basis of cell-cell fusion mechanisms," *Trends Genet.*, 2013; 29(7):427-37.

[82] L. I. Larsson, B. Bjerregaard, and J. F. Talts, "Cell fusions in mammals," *Histochem. Cell Biol.*, 2008, 129:551-61.

[83] B. Bjerregaard, S. Holck, I. J. Christensen, and L. I. Larsson, "Syncytin is involved in breast cancer-endothelial cell fusions," *Cell. Mol. Life Sci.*, 2006; 63:1906-11.

[84] C. F. Ruivo, B. Adem, M. Silva, and S. A. Melo, "The biology of cancer exosomes: Insights and new perspectives," *Cancer Research*. 2017; 77(23):6480-8.

[85] B. Février and G. Raposo, "Exosomes: Endosomal-derived vesicles shipping extracellular messages," *Current Opinion in Cell Biology*. 2004; 16(4):415-21.

[86] L. T. Brinton, H. S. Sloane, M. Kester, and K. A. Kelly, "Formation and role of exosomes in cancer," *Cellular and Molecular Life Sciences*. 2015; 72:659-71.

[87] L. J. Vella, "The emerging role of exosomes in epithelial-mesenchymal-transition in cancer," *Frontiers in Oncology*. 2014; 4:361.

[88] P. Sen, M. Saha, and S. S. Ghosh, "Nanoparticle mediated alteration of EMT dynamics: an approach to modulate cancer therapeutics," *Mater. Adv.*, 2020; 1(8):2614-30.

[89] E. V. Batrakova and M. S. Kim, "Using exosomes, naturally-equipped nanocarriers, for drug delivery," *J. Control. Release*, 2015; 219:396-405.

[90] S. EL Andaloussi, S. Lakhal, I. Mäger, and M. J. A. Wood, "Exosomes for targeted siRNA delivery across biological barriers," *Advanced Drug Delivery Reviews*. 2013; 65(3):391-7.

[91] D. Ha, N. Yang, and V. Nadithe, "Exosomes as therapeutic drug carriers and delivery vehicles across biological membranes: current perspectives and future challenges," *Acta Pharmaceutica Sinica B*. 2016; 6(4):287-96.

[92] K. B. Johnsen, J. M. Gudbergsson, M. N. Skov, L. Pilgaard, T. Moos, and M. Duroux, "A comprehensive overview of exosomes as drug delivery vehicles - Endogenous nanocarriers for targeted cancer therapy," *Biochimica et Biophysica Acta - Reviews on Cancer*. 2014; 1846(1):75-87.

[93] S. Gurunathan, M. H. Kang, and J. H. Kim, "A comprehensive review on factors influences biogenesis, functions, therapeutic and clinical implications of Exosomes," *International Journal of Nanomedicine*. 2021; 16:1281.

[94] S. Mathivanan, H. Ji, and R. J. Simpson, "Exosomes: Extracellular organelles important in intercellular communication," *Journal of Proteomics*. 2010; 73(10):1907-20.

[95] R. J. Simpson, J. W. E. Lim, R. L. Moritz, and S. Mathivanan, "Exosomes: Proteomic insights and diagnostic potential," *Expert Review of Proteomics*. 2009; 6(3):267-83.

[96] T. Kobayashi, F. Gu, and J. Gruenberg, "Lipids, lipid domains and lipid-protein interactions in endocytic membrane traffic," *Semin. Cell Dev. Biol.*, 1998; 9(5): 517-526. Academic Press

[97] Z. Qian, Q. Shen, X. Yang, Y. Qiu, and W. Zhang, "The role of extracellular vesicles: An epigenetic view of the cancer microenvironment," *BioMed Research International*. 2015.

[98] P. Guo, J. Huang, Y. Zhao, C. R. Martin, R. N. Zare, and M. A. Moses, "Nanomaterial Preparation by Extrusion through Nanoporous Membranes," *Small*. 2018; 14(18):1703493.

[99] B. T. Luk *et al.*, "Safe and Immunocompatible Nanocarriers Cloaked in RBC Membranes for Drug Delivery to Treat Solid Tumors," *Theranostics*, 2016; 6(7):1004.

[100] A. P. Bidkar, P. Sanpui, and S. S. Ghosh, "Red Blood Cell-Membrane-Coated Poly(Lactic-co-glycolic Acid) Nanoparticles for Enhanced Chemo- A nd Hypoxia-Activated Therapy," *ACS Appl. Bio Mater.*, 2019; 2(9):4077-86.

[101] L. Rao *et al.*, "Red Blood Cell Membrane as a Biomimetic Nanocoating for Prolonged Circulation Time and Reduced Accelerated Blood Clearance," *Small*, 2015; 11(46):6225-36.

[102] K. M. de la Harpe, P. P. D. Kondiah, Y. E. Choonara, T. Marimuthu, L. C. du Toit, and V. Pillay, "The Hemocompatibility of Nanoparticles: A Review of Cell-Nanoparticle Interactions and Hemostasis," *Cells*. 2019; 8(10):1209.

[103] K. S. Park *et al.*, "Mesenchymal stromal cell-derived nanovesicles ameliorate bacterial outer membrane vesicle-induced sepsis via IL-10," *Stem Cell Res. Ther.*, 2019; 10(1):1-14.

[104] I. S. Mohammad, B. Chaurasiya, X. Yang, C. Lin, H. Rong, and W. He, "Homotype-targeted biogenic nanoparticles to kill multidrug-resistant cancer cells," *Pharmaceutics*, 2020; 12(10):950.

[105] E. C. Costa, A. F. Moreira, D. de Melo-Diogo, V. M. Gaspar, M. P. Carvalho, and I. J. Correia, "3D tumor spheroids: an overview on the tools and techniques used for their analysis," *Biotechnol. Adv.*, 2016; 34(8):1427-41.

[106] K. C. Chung *et al.*, "Novel biphasic effect of pyrrolidine dithiocarbamate on neuronal cell viability is mediated by the differential regulation of intracellular zinc and copper ion levels, NF-κB, and MAP kinases," *Journal of Neuroscience Research*, 2000; 59(1):117-25.

[107] H. U. Simon, A. Haj-Yehia, and F. Levi-Schaffer, "Role of reactive oxygen species (ROS) in apoptosis induction," *Apoptosis*, 2000; 5:415-8.

[108] M. Redza-Dutordoir and D. A. Averill-Bates, "Activation of apoptosis signalling pathways by reactive oxygen species," *Biochim. Biophys. Acta - Mol. Cell Res.*, 2016; 1863(12):2977-92.

[109] V. A. Da Silva, K. A. E. P. Da Silva, J. M. A. Delou, L. M. Da Fonseca, A. G. Lopes, and M.

A. M. Capella, "Modulation of ABCC1 and ABCG2 proteins by ouabain in human breast cancer cells," *Anticancer Res.*, 2014; 34(3):1441-8.

[110] A. Sharma, "Role of stem cell derived exosomes in tumor biology," *International Journal of Cancer*. 2018; 142(6):1086-92.

[111] R. Kalluri, "The biology and function of exosomes in cancer," *Journal of Clinical Investigation*. 2016; 126(4):1208-15.

[112] S. Dutta, C. Warshall, C. Bandyopadhyay, D. Dutta, and B. Chandran, "Interactions between exosomes from breast cancer cells and primary mammary epithelial cells leads to generation of reactive oxygen species which induce DNA damage response, stabilization of p53 and autophagy in epithelial cells," *PLoS One*, 2014; 9(5):e97580.

[113] J. C. Akers, D. Gonda, R. Kim, B. S. Carter, and C. C. Chen, "Biogenesis of extracellular vesicles (EV): Exosomes, microvesicles, retrovirus-like vesicles, and apoptotic bodies," *Journal of Neuro-Oncology*. 2013; 113:1-1.

[114] M. Colombo, G. Raposo, and C. Théry, "Biogenesis, secretion, and intercellular interactions of exosomes and other extracellular vesicles," *Annual review of cell and developmental biology*. 2014; 30:255-89.

[115] W. M. Henne, N. J. Buchkovich, and S. D. Emr, "The ESCRT Pathway," *Developmental Cell*. 2011; 21(1):77-91.

[116] K. L. Thu, I. Soria-Bretones, T. W. Mak, and D. W. Cescon, "Targeting the cell cycle in breast cancer: towards the next phase," *Cell Cycle*. 2018; 17(15):1871-85.

[117] A. Marra, D. Trapani, G. Viale, C. Criscitiello, and G. Curigliano, "Practical classification of triple-negative breast cancer: intratumoral heterogeneity, mechanisms of drug resistance, and novel therapies," *npj Breast Cancer*. 2020; 6(1):54.

[118] M. Nedeljković and A. Damjanović, "Mechanisms of chemotherapy resistance in triple-negative breast cancer-how we can rise to the challenge," *Cells*, 2019; 8(9):957.

[119] G. Iancu *et al.*, "Tyrosine kinase inhibitors in breast cancer (Review)," *Exp. Ther. Med.*, 2021; 23(2):1-10.

[120] D. Zhang *et al.*, "Epidermal growth factor receptor tyrosine kinase inhibitor reverses mesenchymal to epithelial phenotype and inhibits metastasis in inflammatory breast cancer," *Clin. Cancer Res.*, 2009; 15(21):6639-48.

[121] M. K. Ediriweera, K. H. Tennekoon, and S. R. Samarakoon, "Emerging role of histone deacetylase inhibitors as anti-breast-cancer agents," *Drug Discovery Today*. 2019; 24(3):685-702.

[122] F. Podo *et al.*, "Triple-negative breast cancer: Present challenges and new perspectives," *Molecular Oncology*. 2010; 4(3):209-29.

[123] S. Al-Mahmood, J. Sapiezynski, O. B. Garbuzenko, and T. Minko, "Metastatic and triple-negative breast cancer: challenges and treatment options," *Drug Delivery and Translational Research*. 2018; 1483-507.

[124] P. Krejci *et al.*, "Receptor tyrosine kinases activate canonical WNT/β-catenin signaling via MAP kinase/LRP6 pathway and direct β-catenin phosphorylation," *PLoS One*, 2012; 7(4):e35826.

[125] A. Roberti, A. F. Valdes, R. Torrecillas, M. F. Fraga, and A. F. Fernandez, "Epigenetics in cancer therapy and nanomedicine," *Clinical Epigenetics*. 2019; 11(1):1-8.

[126] L. García-Gutiérrez, M. D. Delgado, and J. León, "Myc oncogene contributions to release of cell cycle brakes," *Genes*. 2019; 10(3):244.

[127] J. Xu, Y. Chen, and O. I. Olopade, "MYC and Breast Cancer," *Genes Cancer*, 2010; 1(6):629-40.

[128] S. Yin, V. T. Cheryan, L. Xu, A. K. Rishi, and K. B. Reddy, "Myc mediates cancer stem-like cells and EMT changes in triple negative breast cancers cells," *PLoS One*, 2017; 12(8):e0183578.

[129] E. H. Nam, Y. Lee, Y. K. Park, J. W. Lee, and S. Kim, "Zeb2 upregulates integrin α5 expression through cooperation with sp1 to induce invasion during epithelial-mesenchymal transition of human cancer cells," *Carcinogenesis*, 2012; 33(3):563-71.

[130] L. Yue *et al.*, "The oncoprotein HBXIP activates transcriptional coregulatory protein LMO4 via sp1 to promote proliferation of breast cancer cells," *Carcinogenesis*, 2013; 34(4):927-35.

[131] Y. Kang and J. Massagué, "Epithelial-mesenchymal transitions: Twist in development and metastasis," *Cell*. 2004; 118(3):277-9.

[132] H. E. Tzeng *et al.*, "The pan-PI3K inhibitor GDC-0941 activates canonical WNT signaling to confer resistance in TNBC cells: Resistance reversal with WNT inhibitor," *Oncotarget*, 2015; 6(13):11061.

[133] G. V. Vijay *et al.*, "GSK3β regulates epithelial-mesenchymal transition and cancer stem cell properties in triple-negative breast cancer," *Breast Cancer Res.*, 2019; 21(1):1-4.

Publications and Conferences

Journal Publications:

From Thesis Work-

1. **Saha, M.**, Bidkar, A.P. and Ghosh, S.S. Developing membrane-derived nanocarriers for ex vivo therapy of homologous breast cancer cells. ***Nanomedicine***, *16*(21), 1843-1856 (2021). https://doi.org/10.2217/nnm-2021-0153
2. **Saha, M**. and Ghosh, S.S. Engineered Hybrid Nanosystem for Homologous Targeting of EMT Induced Triple Negative Breast Cancer Cells. ***ACS Applied Bio Materials***, 6(2), 681-693 (2023). https://doi.org/10.1021/acsabm.2c00925
3. **Saha, M**. and Ghosh, S.S. Targeting tumor micro-environment of metastatic TNBC cells via exosomes derived from non-invasive breast cancer cells for MDR inhibition and enhancing drug susceptibility. **(Manuscript under Revision)**

From Collaborative Work-

1. Sen, P., **Saha, M**. and Ghosh, S.S. Nanoparticle mediated alteration of EMT dynamics: an approach to modulate cancer therapeutics. ***Materials Advances***, *1*(8), 2614-2630 (2020).
2. Mallik, R., **Saha, M**. and Mukherjee, C. Porous Silica Nanospheres with a Confined Mono (aquated) Mn (II)-Complex: A Potential T 1–T 2 Dual Contrast Agent for Magnetic Resonance Imaging. ***ACS Applied Bio Materials***, *4*(12), 8356-8367 (2021).
3. Horo, H., **Saha, M**., Das, H., Mandal, B. and Kundu, L.M. Synthesis of highly fluorescent, amine-functionalized carbon dots from biotin-modified

chitosan and silk-fibroin blend for target-specific delivery of antitumor agents. ***Carbohydrate Polymers***, *277*, 118862 (2022).

4. Sarkar, P., **Saha, M.**, Nandi, N., Sahu, D.K. and Sahu, K. Red-Emitting Silver Nanoclusters for Dual-Mode Detection of Cu2+ and Vitamin B12 in Living Cells. ***ACS Applied Nano Materials***, *5*(6), 7670-7678 (2022).
5. Mallik, R., Khannam, M., **Saha, M.**, Marandi, S., Kumar, S. and Mukherjee, C., 2022. The electrostatic confinement of aquated monocationic Gd (iii) complex-molecules within the inner core of porous silica nanoparticles creates a highly efficient T 1 contrast agent for magnetic resonance imaging. ***Dalton Transactions***, *51*(37), 14138-14149 (2022).

Workshops/ Conferences Attended:

1. Seminar on 'Translational Research & Biomarker Discovery' organized by Indian Institute of Technology, Guwahati.

2. National conference on 'New trends in multi modal molecular imaging applications for animal studies in drug discovery' organized by National Institute of Pharmaceutical Education and Research, Guwahati.

3. 5th National workshop on 'NEMS/MEMS & Theranostics Devices' organized by Indian Institute of Technology, Guwahati

4. National Conference on "Chemistry of Chalcogenides" (NC3-2021) organized by Department of Applied Chemistry, Defense Institute of Advanced Technology, Pune- 411025, India.

5. 7th International Conference on Advanced Nanomaterials and Nanotechnology (ICANN2021) organized by Centre for Nanotechnology, Indian Institute of Technology Guwahati.

6. 42nd Annual Conference of the Indian Association of Cancer Research "Bringing basic and translational research to the clinic: Challenges and

Opportunities" organized by (ACTREC), Tata Memorial Centre, Navi Mumbai, India.

भारतीय प्रौद्योगिकी संस्थान गुवाहाटी
Indian Institute of Technology Guwahati

Appendix

Buffers and their composition:

4 X protein loading dye (for 10 ml)	2 ml 1M Tris-HCl (pH 6.8), 0.8 g SDS, 4.0 ml 100 % glycerol, 0.4 ml 14.7 M β- mercaptoethanol, 8 mg bromophenol blue in water
6 X DNA loading dye	0.25 (%) (w/v) bromophenol blue, 0.25 % (w/v) xylene cyanol FF, 30 % (v/v) glycerol in water
30% Acrylamide solution	29.2 % (w/w) Acrylamide, 0.8 % (w/w) N, N' - methylenebisacrylamide.
Blocking buffer for western blot	4 % (w/v) BSA in PBST/ TBST
Gel running buffer(10x)	250 mM Tris base, 1.92 M glycine, and 1 % SDS
Phosphate buffer saline	137 mM NaCl, 2.68 mM KCl, 7.98 mM Na_2HPO_4, 1.4 mM KH_2PO_4, pH 7.4
Tris buffered saline	Tris-HCl (50Mm), NaCl (150 mM), pH 7.5
Tris buffered saline Tween -20 (TBST)	Tris-HCl (50Mm), NaCl (150 mM), Tween 20 (0.1% v/v) pH 7.5
Tris acetate EDTA(TAE) 50 X, (100 ml)	24.2 g Tris base, 5.71 ml of glacial acetic acid, 10 ml of 0.5 EDTA (pH 8)
Towbin Buffer (5X)	25 mM Tris base, 192 mM glycine, and 20 % methanol

भारतीय प्रौद्योगिकी संस्थान गुवाहाटी
Indian Institute of Technology Guwahati